Assessment of Hip Fracture Risk by a Two-Level Subject-Specific Biomechanical Model

By

Masoud Nasiri Sarvi

A thesis submitted to
the Faculty of Graduate Studies
in partial fulfilment of
the requirements for the degree of
Doctor of Philosophy

Department of Mechanical Engineering
Faculty of Engineering
University of Manitoba
Winnipeg, Manitoba

December 2015

Abstract

Sideways fall-induced hip fracture is a major worldwide health problem among the elderly population. Biomechanical modeling is a practical way to study hip fracture risk. However, all existing biomechanical models for assessing hip fracture risk mainly consider the femur-related parameters. Their accuracy is limited as hip fracture is significantly affected by loading conditions as well. The objective of this study is to introduce a two-level subject-specific model to improve the assessment of hip fracture risk.

The proposed biomechanical model consists of a whole-body dynamics model and a proximal femur finite element model, which are constructed from the subject's whole-body and hip DXA (dual energy X-ray absorptiometry) scan. The whole-body dynamics model is used to determine the impact force onto the hip during a sideways fall. Obtained load/constraint conditions are applied to the finite element model in order to determine the stress/strain distribution in the proximal femur. Fracture risk index is then defined over the critical locations of the femur using the finite element solutions.

It is found that hip fracture risk is significantly affected by the subject's body configuration during the fall, body anthropometric parameters, trochanteric soft tissue thickness, load/constraint conditions, and bone mineral density, which are not effectively taken into account by currently available hip fracture discriminatory tools. Predicted hip fracture risk of 130 clinical cases, including 80 females and 50 males, by the proposed model re-

veals that biomechanical determinants of hip fracture differ widely from individual to individual. This study presents the first in-depth subject-specific model that provides a comprehensive, fast, accurate, and non-expensive method for assessing the hip fracture risk. The proposed model can be easily adopted in clinical centers to identify patients at high risk of hip fracture who may benefit from the in-time treatment to reduce the fracture risk.

Acknowledgments

I would like to take this opportunity to express my sincerest thanks to my supervisor, Professor Yunhua Luo, for his teaching and guidance through this work. Professor Luo has been so influential in ensuring my academic, professional, financial, and moral well-being ever since I started to work with him. Without his constant support, this work would not have been possibly done. Many thanks are also directed to the advisory committee members, Professors Stephen Robinovitch, Shaahin Filizadeh, Qingjin Peng, and Quan (Abraham) Wang for their constructive advice.

The reported research has been supported by the Natural Sciences and Engineering Council (NSERC), Research Manitoba and Manitoba Centre for Health Policy in Canada, which are gratefully acknowledged. I also gratefully acknowledge the Department of Anatomy in Southern Medical University, Guangzhou, China, for the collaboration in conducting the experiments in this study.

I would also like to thank my dear friends in Winnipeg as well as my colleagues in the Computational Biomechanics Group for all the academic discussion, mutual support, encouragement, and happy time working together.

Above all, I am deeply indebted to my parents, brothers, and sisters for their unconditional love and support to overcome all the challenges I went through during my entire life.

Dedication

To my parents

Contents

List of Tables

List of Figures

List of Copyrighted Material

Figure 1.3 was cited from "http://advancedortho.net/info/hipfractureinfo.php". Copyright was obtained on February 5, 2014.

Figure 1.4 was cited from "J. A. Kanis, A. Oden, E. V. McCloskey, H. Johansson, D. A. Wahl, and C. Cooper, "A systematic review of hip fracture incidence and probability of fracture worldwide", *Osteoporosis International*, 23(9), pp. 2239-2256, 2012". Copyright was obtained on July 08, 2014.

Figure 1.5 was cited from "A.A. Fisher, E.D. O'Brien, and M.W. Davis, "Trends in hip fracture epidemiology in Australia: Possible impact of bisphosphonates and hormone replacement therapy", *Bone*, 45(2), pp. 246-253, 2009". Copyright was obtained on July 08, 2014.

Figure 1.6 was cited from "B. Gullberg, O. Johnell, and J. A. Kanis, "World-wide Projections for Hip Fracture", *Osteoporosis International*, 7, pp. 407-413, 1997". Copyright was obtained on July 08, 2014.

Figures 1.1(a) and 3.2(b) were cited from "http://stpetehipandknee.com/anatomy-hip-joint/". Copyright was obtained on August 22, 2014.

Figure 3.3 (b) was cited from "http://www.gettyimages.ca/detail/illustration/coronal-section-through-female-pelvis-stock-graphic/74062134?Language=en-GB". Copyright

List of Abbreviations

aBMD	areal Bone Mineral Density
BH	Body Height
BMI	Body Mass Index
BW	Body Weight
CSA	Cross-Sectional Area
CSMI	Cross-Sectional Moment of Inertia
CT	Computed Tomography
DE	Distortion Energy
DoF	Degree of Freedom
DXA	Dual Energy X-ray Absorptiometry
FE	Finite Element
FOS	Factor Of Safety
FRAX	Fracture Risk Assessment Tool
FRI	Fracture Risk Index
HR-pQCT	High Resolution peripheral QCT
HSA	Hip Structural Analysis
HU	Hounsfield Unit
ISCD	International Society for Clinical Densitometry
QCT	Quantitative Computed Tomography
RF	Risk Factor
ROI	Region of Interest
SD	Standard Deviation
STT	Soft Tissue Thickness

vBMD	volumetric Bone Mineral Density
vQCT	volumetric Quantitative Computed Tomography
WHO	World Health Organization
2D	Two Dimension
3D	Three Dimension

Nomenclature

CC	Correlation between pixel intensity and tissue mass density
W	Body mass
P_i	Pixel intensity
ρ_i	Mass of pixel i
m_k	Mass of body segment k
r_k	Mass center of body segment k
I_k	Mass moment of inertia of body segment k
r_i	Distance of pixel i from the distal end of the link
N_k	Number of pixels enclosed in the contour of body segment k
T	Kinetic energy
V	Potential energy
q_i	Degree of freedom i
τ_i	Generalized moment of degree of freedom i
α	Angle between the shank and the z-axis in coronal plane
β	Angle between the shank and the z-axis in sagittal plane
γ	Angle between the trunk and the z-axis in coronal plane
κ	Angle between the trunk and the z-axis in sagittal plane
φ	Angle between the link and z-axis in determining the effective mass
$\dot{\alpha}$	Velocity of the angle α
$\dot{\beta}$	Velocity of the angle β
$\dot{\gamma}$	Velocity of the angle γ
l_i	Length of body segment i
l'_i	Distance of the mass center of body segment i from the distal end

K	Stiffness of the impact model
C	Damping coefficient of the impact model
δ	Logarithmic decrement
z_i	Amplitude of the vibration
ξ	Damping ratio
τ_d	The period of the damped vibration
ω_d	The frequency of the damped vibration
ω_n	Natural frequency
z	Hip vertical position
$\dot{z}$	Hip vertical velocity
G_1	Linear momentum before the impact
G_2	Linear momentum after the impact
F_{impact}	Impact force
F_{joint}	Joint (internal) force
$EM_{lower\ extremity}$	Effective mass of lower extremity
Δt	Time interval
g	Acceleration of gravity
P	Mass center of the shank divided by the shank length
Q	Mass center of the thigh divided by the thigh length
R	Mass center of the trunk divided by the trunk length
B	Deformation matrix
D	Material property matrix
E	Young's modulus
$k^{(e)}$	Element stiffness matrix
$N^{(e)}$	Shape function matrix
R^2	Coefficient of determination
r	Correlation coefficient
$u^{(e)}$	Displacement vector
$U^{(e)}$	Nodal displacement
σ_Y	Yield strength

σ	Stress vector
σ_x	Normal stress in x-direction
σ_y	Normal stress in y-direction
τ_{xy}	Shear stress on xy-plane
ε	Nodal strain
ε_x	Normal strain in x-direction
ε_y	Normal strain in y-direction
γ_{xy}	Shear strain in xy-plane
η_{ROI}	Fracture risk index over a region of interest
$\sigma_{von-Mises}$	von-Mises Stress
A_i	Area of the finite element i

List of Appendices

Chapter 1

Introduction

Low-trauma hip fracture has become a common health problem among the elderly all over the world [1-10], mainly due to the population aging and the prevalence of osteoporosis. Of all osteoporotic fractures, hip fracture has the highest morbidity and mortality rate [11]. Approximately 50% of patients have permanent functional disability greater than that before fracture [12, 13]. The incidence of hip fracture appears to be increasing in many countries [10] and the total number of hip fractures is estimated to be more than 5 million by 2050 [14]. Socioeconomic impacts of hip fracture are twofold. On the one hand, hip fracture increases the morbidity and mortality in the elderly [15-17]; on the other hand, it is a substantial source of health care expenditure [18, 19]. Therefore, there is an urgent need to accurately assess hip fracture risk and then develop preventive and protective measures. In this chapter, hip anatomy is first reviewed and hip fractures are classified by anatomic location. Then, prevalence of hip fracture is presented, followed by a description of the significance of accurately assessing hip fracture risk. The objectives of the present study and the layout of the dissertation are described at the end of this chapter.

1.1 Hip Fracture: Anatomy, Causes, and Consequences

Hip fracture is a medical condition in which there is a break in the continuity of the femoral bone. Hip fracture is generally affected by hip anatomy [20], the applied forces to the hip [21], and bone mechanical properties [22]. In this section, hip anatomy is explained to show why the hip is likely to experience fracture in a fall, followed by an analysis of hip fracture causes and consequences.

1.1.1 Hip Anatomy

The hip joint is one of the most important joints in the human body. It is also one of the most flexible joints allowing a great range of motions. To better understand hip fracture, it helps to know the anatomy of the hip joint. The hip is a joint formed by the ball-shape head of the femur and the socket of the pelvis. The femurs are the longest and the strongest bones in the human body, extending from the hip to the knee. Important geometric features of femur bones include the head, neck, greater and lesser trochanters, as shown in Figure 1.1 (a). A femur is composed of two types of bones, cortical and cancellous. The cortical bone forms the outer layer of the femur and withstands most of the forces and moments. Cancellous bone is mostly enclosed by the cortical bone and mainly absorbs the shock energy produced in walking and running [23]. The hip joint is a stable ball and socket joint, much more stable than the shoulder joint. The stability in the hip mainly attributes to the deep socket, i.e., the acetabulum. Additional stability is provided by the strong joint capsule and its surrounding muscles and ligaments. The high level of stability of the hip joint is required to support the upper body [23].

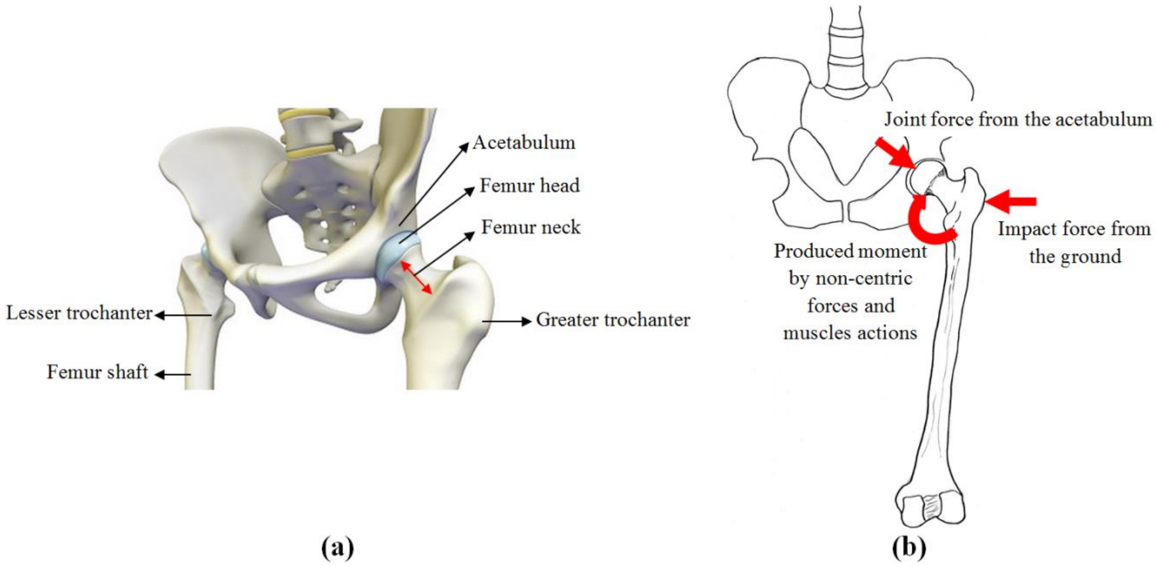

Figure 1.1. (a) Anatomic structure of the hip [24]. (b) Concentration of applied forces on the proximal femur in a lateral fall which increases the risk of fracture.

More than 90% of all hip fractures occur in falls [25] as the femur is subjected to a high level impact force. As shown in Figure 1.1 (b), in a sideways fall, the greater trochanter and the femoral head are subjected to the impact and the joint force respectively from the ground and the acetabulum. The forces produce a moment at the intersection of the neck-shaft axes. Muscles that are attached to the femur also produce forces during the fall. As it is shown in Figure 1.1 (b), the applied forces in a fall are mainly on the proximal femur and it may explain why the majority of fall-induced hip fractures occur at the proximal femur [26]. A hip fracture refers to any fracture of the proximal femur down to a level of approximately five centimeters below the lower border of the lesser trochanter [27]. The extent of the break depends on the forces that are involved.

1.1.2 Causes of Hip Fracture

Hip fracture is usually caused by an applied force that exceeds the strength of the femur bone [28]. Therefore, any situation that either induces a high level of force on the femur bone or decreases the bone strength should be considered as a hip fracture cause.

The main cause of hip fracture is falling (90-92%) [25, 29-31], in particular falling in sideways direction (63-69% in fall-related fractures) [8, 32], as it induces a high level of force on the femur. Parameters that increase the risk of fall and apply a high level of force on the femur, especially in the elderly, are

- mental impairment and confusion
- impaired vision
- impaired muscles reactions
- slow reflex response
- inability to effectively use the arms to reduce the energy of the fall
- impaired neuromuscular coordination and neurological diseases (e.g. hemiplegia, Parkinson's disease)
- reduced soft tissue padding over the hip [33, 34]

In the elderly, most fractures occur after a low-trauma fall, which would not cause any severe injury to a healthy individual. Therefore, low bone strength is another main cause of hip fracture. Osteoporosis as a progressive bone disease, which is characterized by decreases in bone mass and density, has been identified as one of the main contributors of hip fracture [35, 36]. Osteoporosis advances when bone resorption exceeds bone formation and therefore it is more common among the elderly [37]. Approximately three to four out of ten women over the age of 50, and one in eight men, suffer osteoporotic fracture in their lifetime [38].

Apart from the osteoporosis, several other causes may reduce the strength of the bone such as bone cancer and medical side effects [27]. Other factors associated with reduction in bone strength include [27]

- genetic and family history
- sedentary life style
- impaired nutrition
- smoking
- excess alcohol
- medications (including tranquillizers, hypnotics, anticonvulsant drugs and steroids)
- osteomalacia from vitamin D deficiency, malabsorption, liver or renal disease,
- cardiovascular disease and cardiac arrhythmias
- underlying bone disease (e.g. Paget’s disease, bone tumours and secondary bone tumours)
- endocrine abnormalities: hyperthyroidism, hyperparathyroidism or hypercortisolism

In addition to the mentioned causes, high-trauma falls and accidents such as car and motorcycle accidents can lead to hip fracture [39]. But they are not studied in this dissertation. Figure 1.2 shows how different factors contribute to the hip fracture [6, 27].

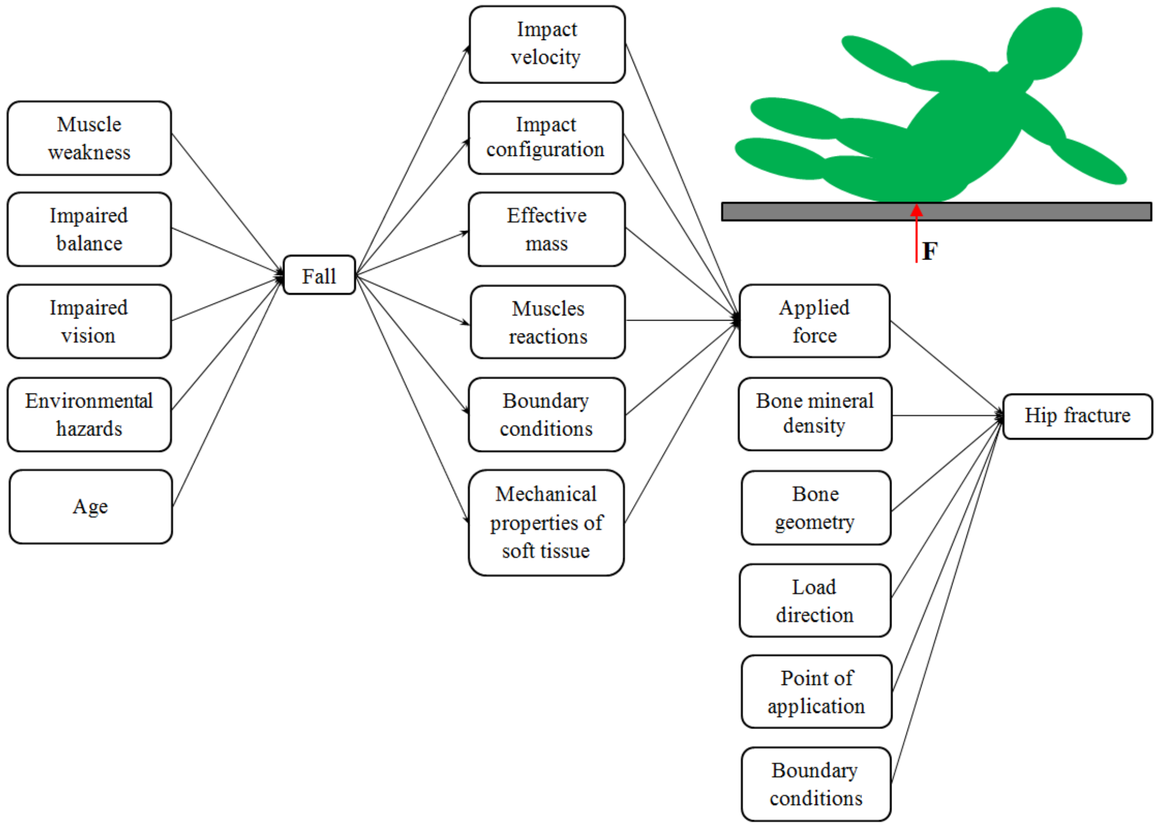

Figure 1.2. Conceptual model of the fall-induced hip fracture procedure and associated effective factors

1.1.3 Hip Fracture Consequences

Hip fractures are associated with significant morbidity, mortality, loss of independence, and financial burden [3, 9, 14, 31, 40-42]. It has been reported that approximately 20 percent of hip fracture patients died within one year of the fracture [43]. Generally, the first year after hip fracture appears to be the most critical time. A recent meta-analysis revealed that women sustaining a hip fracture had a 5-fold increase and men almost an 8-fold increase in relative likelihood of death within the first 3 months compared with age- and sex-matched controls [18]. The relative death risk decreases substantially over the second year but still much higher than that of the controls [44]. Many lose their ability to walk mainly due to the pain caused by the hip fracture. In fact, only 40–79 percent of patients regain their previous ambulatory function a year after the fracture, and less than half return to their pre-fracture status of daily activities [45].

In addition to functional impairments, hip fracture can have a negative impact on self-esteem, body image, and mood [46], which may lead to psychological problems [47]. Individuals who suffer fractures may be immobilized by a fear of falling again and suffering more fractures. They may feel isolated and helpless. The National Osteoporosis Foundation conducted a survey [48] among 1000 women with osteoporotic fracture in the United States to investigate the psychological effects of the fracture on the patients. 89 percent of said they feared breaking another bone; 80 percent were afraid that they would be less able to perform their daily activities and lose their independence; 73 percent worried that they would have to reduce activities with family and friends; and 68 percent were concerned that another fracture would result in their having to enter a nursing home [48]. If not addressed, fear about the future and a sense of helplessness can produce significant anxiety and depression. These problems may be compounded by an inability to fulfill occupational, domestic, or social duties, thus leading to further social isolation.

The disability, reduced functional status, and poor mental health caused by hip fracture can have a profound impact on the quality of the individual’s life. Survivors of hip fracture reported a 52 percent reduction in quality of life in the first 12 months and a 21 percent reduction after two years [49].

Also, hip fracture is a major cause of the need for long-term nursing home care and a major contributor to health care costs [19, 50, 51]. There are approximately 23,000 cases of hip fracture every year in Canada with associated treatment costs of about $1 billion

[52]. In the United States, 310,000 hip fractures occurred in 2003 and the total medicare cost was estimated between $10.3 and $15.2 billion, including acute medical care and nursing home services [42, 53, 54]. As the population of the elderly is still continuously increasing, the number of hip fractures is expected to rise dramatically and it will put more burdens on the community health care system [2, 55].

1.1.4 Classification of Hip Fractures

In general, there are three types of hip fractures, depending on what region of the proximal femur is involved [56]:

1. Femoral neck fractures occur in the narrow section of the proximal femur that lies between the femoral head and the intertrochanteric cross-section. Most femoral neck fractures occur within the capsule surrounding the hip joint and are, therefore, termed intracapsular fracture. The blood supply to the femoral head is carried by a number of arteries that pass through the femoral neck region. Therefore, femoral neck fractures may disrupt the blood supply to the femoral head, causing death of the femoral head bone tissues, called osteonecrosis or avascular necrosis. Femoral neck fractures are further grouped into nondisplaced and displaced fractures by the alignment of the fractured segments in relation to the original anatomic position of the femur [57].
2. Intertrochanteric fractures occur at a lower location than femoral neck fractures, in the area between the greater and lesser trochanters. The trochanters are bony projections where major hip muscles are attached. Intertrochanteric hip fractures occur outside of the joint capsule and are therefore also called extracapsular frac-

ture in the literature. Intertrochanteric fractures are complicated by the pull of the hip muscles on the bony muscle attachments, which can exert competing forces against fractured bone segments and pull them out of alignment. Thus, healing of the fracture in a misaligned position is considered as a complication for intertrochanteric fractures. Intertrochanteric fractures may be further grouped into stable and unstable fractures, depending on the location, number, and size of the fractured bony segments [57].

3. Subtrochanteric fractures occur in the zone about 5 cm below the lesser trochanter of the proximal femur. The blood supply to the bone of the subtrochanteric region is not as good as the blood supply to the bone of the intertrochanteric region and thus heals more slowly [57]. Similar to the intertrochanteric fractures, subtrochanteric fractures are likely to cause femur misalignment [57].

In more complicated cases, the fracture of the bone can involve more than one of these zones. Figure 1.3 shows different types of proximal femur fracture.

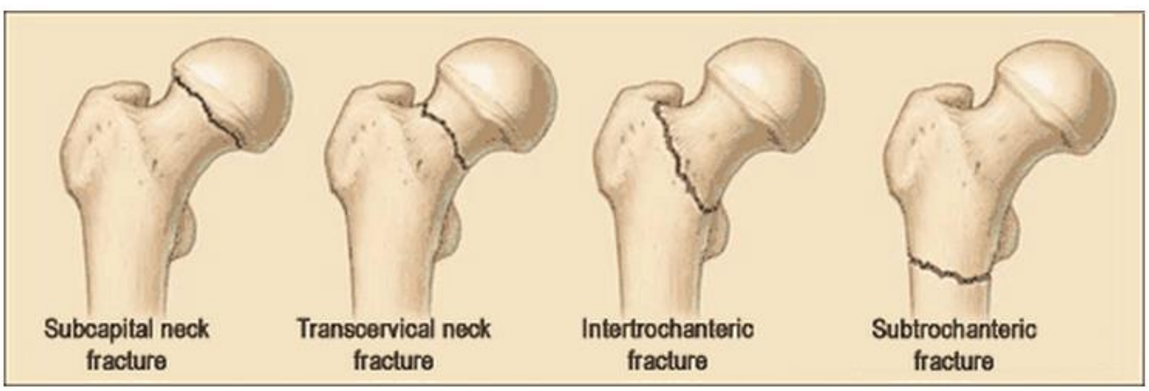

Figure 1.3. Three main types of hip fractures: femoral neck fracture (subcapital and transcervical fractures), intertrochanteric fracture, and subtrochanteric fracture [58]

1.2 Demographic Feature of Hip Fractures

A variety of studies have examined hip fracture rates in different regions of the world [10, 40, 41, 59]. Greater than 10-fold differences have been found on the basis of studies undertaken at a regional or national level for different calendar years. The studies show that the main demographic risk factors for hip fractures include increased age and female gender [10, 14]. The geographic distribution by fracture risk is shown for men and women combined in Figure 1.4. Heterogeneity in hip fracture risk in countries can be seen in this figure. Based on statistical results [10], for women, the lowest annual incidences are found in Nigeria (2/100,000), South Africa (20), Tunisia (58), and Ecuador (73). The highest rates were observed in Denmark (574/100,000), Norway (563), Sweden (539), and Austria (501). The incidence of hip fracture in men is approximately half of that noted in women. The highest annual incidence in men has been found in Denmark (290/ 100,000) and the lowest in Ecuador (35/100,000) [10].

As it is shown in Figure 1.4, the high-risk countries are Iceland, UK, Ireland, Denmark, Sweden, and Norway in north western Europe; Belgium, Germany, Austria, Switzerland, and Italy in central Europe; Greece, Hungary, Czech Republic, Slovakia, and Slovenia in south western Europe; Lebanon, Oman, Iran, Hong Kong, Singapore, Malta and Taiwan in Asia; and Argentina in south America. Regions of moderate risk include North America, Oceania, the Russian Federation, and southern countries of Latin America. Low-risk regions include the northern regions of Latin America, Africa, Jordan, Saudi Arabia, India, China, Indonesia and the Philippines. It is notable that in Europe, the majority of countries are categorized as high or moderate risk. Low risk is identified only in Croatia and Romania [10].

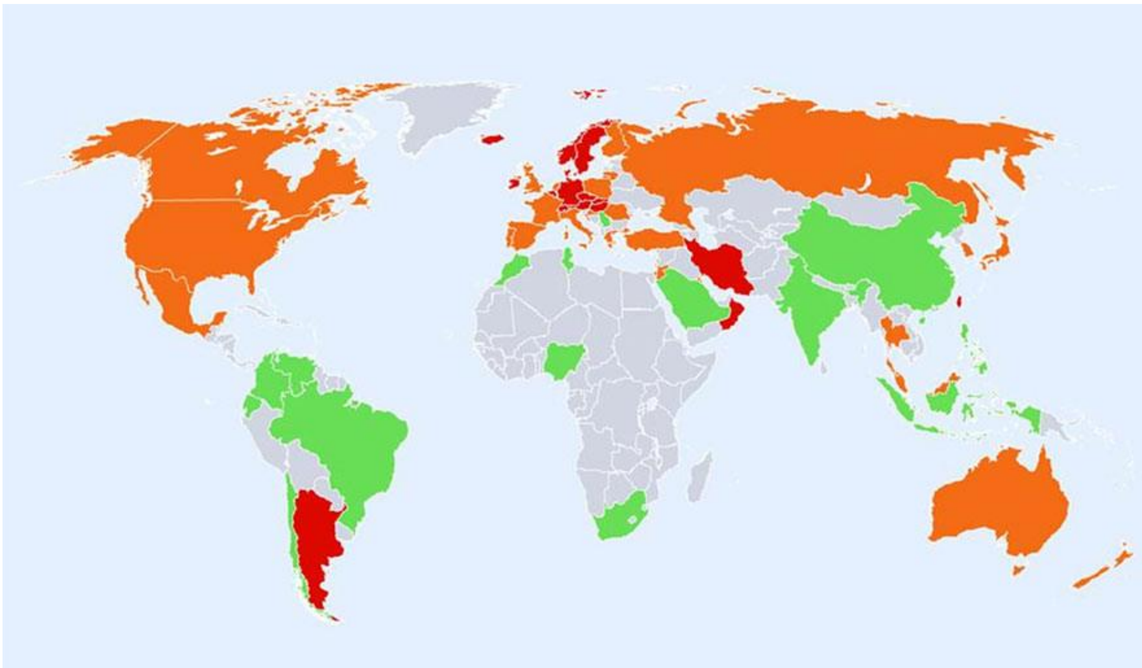

Figure 1.4. Hip fracture rates (men and women combined) in different countries of the world categorized by risk. Where estimates are available, countries are color coded red (annual incidence >250/100,000), orange (150–250/100,000) or green (<150/100,000) [10].

Hip fracture incidence rates are known to increase exponentially with age in both men and women for the most regions of the world [60-63]. Figure 1.5 reveals the variation trends of hip fracture incidents with age in both genders in Australia, where there is an exponential increase in hip fracture incidence with increasing age [40]. The increasing rate of hip fracture in the elderly is mainly associated with their slower reflex response and the inability to effectively use their arms to reduce the energy of the fall, and low bone density of the proximal femur [33, 34].

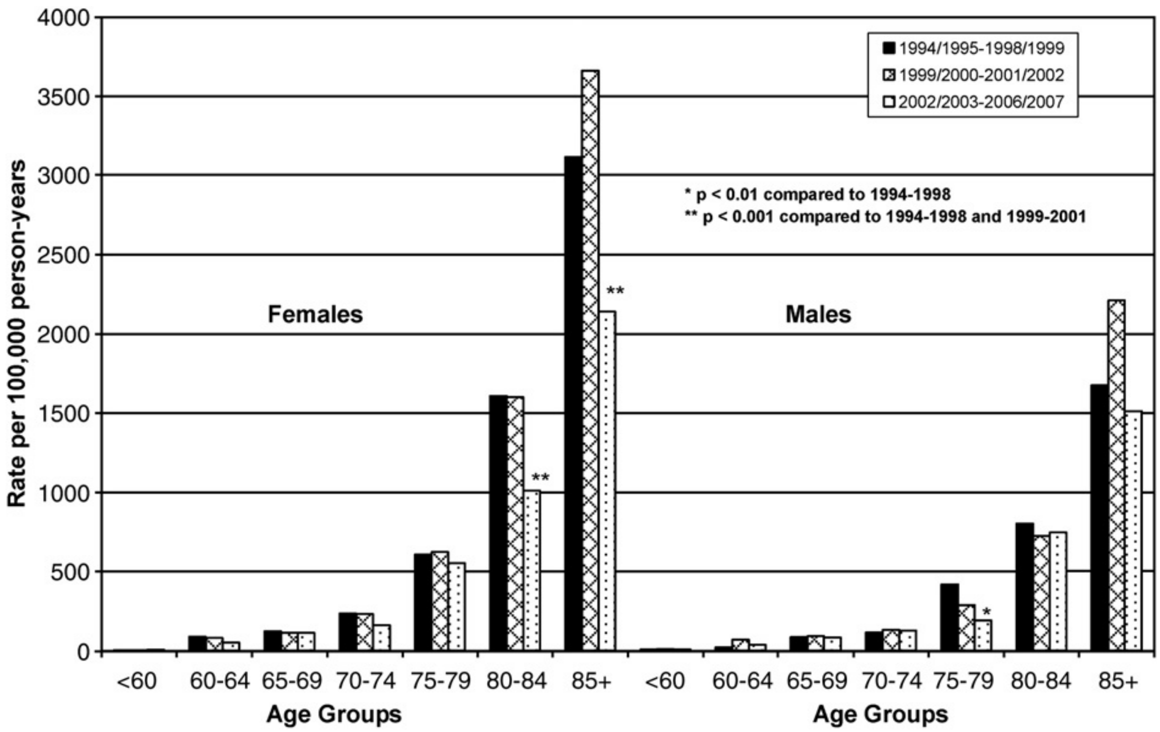

Figure 1.5. Secular trends in age- and gender-specific incidence rates of hip fractures in Australia between 1994/1995 and 2006/2007 [40]

Epidemiological studies show that the number of hip fractures will rise from 1.66 million in 1990 to 4.5~21.3 million by 2050 (Figure 1.6) depending on the underlying assumptions about age and gender specific incidence trends [9, 14, 40, 64].

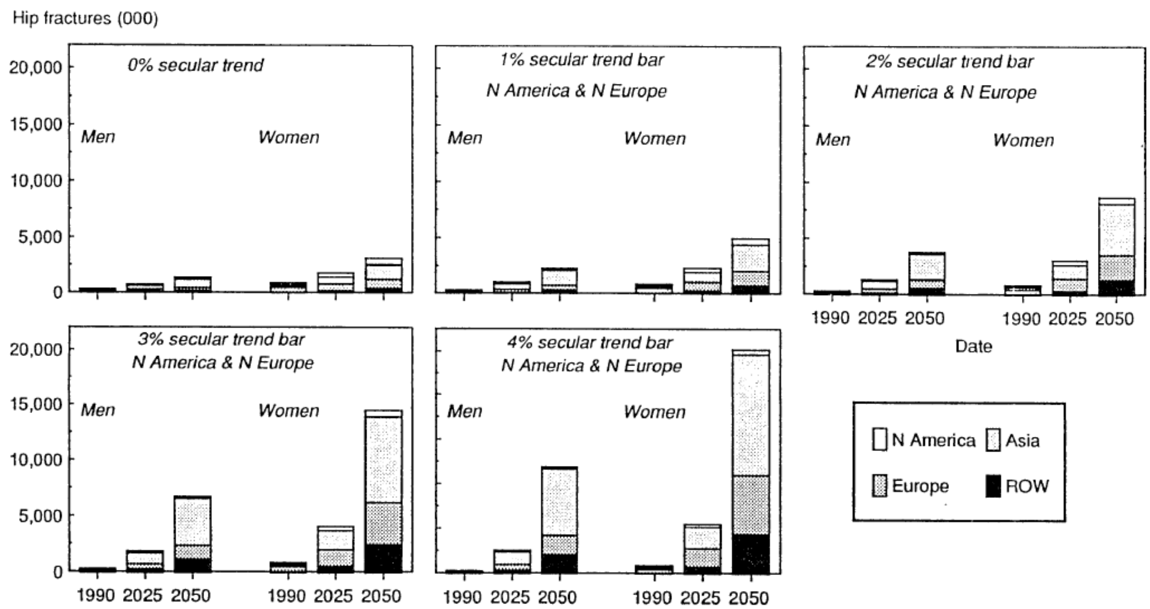

Figure 1.6. Estimated number of hip fractures by sex in the year 1990 and the number expected in 2025 and 2050 by region assuming: no increase in age- and sex-specific rates, or a 1% annual increase world-wide, or no increase in North America and Northern Europe but an increase in age- and sex-specific incidence elsewhere of 2%, 3% or 4%. (ROW is rest of world) [14]

1.3 Significance of Accurately Assessing Hip Fracture Risk

The aim of accurately assessing hip fracture risk is to identify patients at high risk of hip fracture and to start in-time prevention and protection measures to reduce the number of hip fractures. These measures are accepted by the patients only after they are accurately diagnosed with the high fracture risk. Also, accurate assessment of hip fracture risk is the prerequisite step before starting a therapy. For example, during the process of osteoporosis treatment, it is required to monitor the change of fracture risk and subsequently track the effectiveness of the therapy. By knowing the risk of fracture, people can improve their bone health and change their environment to reduce the likelihood of the fall.

Patients diagnosed with high fracture risk may consider the following prevention measurements:

- individualized exercise programs:
    - ❖ muscle-strengthening exercises [65]
    - ❖ practicing balance exercises [66]
    - ❖ increasing the lower extremity joint function [21]
- management of visual impairment:
    - ❖ obtaining maximum vision correction [6, 67]
- examination of basic neurological function, including mental status, muscle strength, lower extremity peripheral nerves and reflexes [68]
- using mobility assisting devices (e.g., walking stick, frames)
- implementing surveillance and observation strategies

Protection measurements must be provided to patients with high fracture risk, for example:

- remembering that sideways falling is more likely to result in a hip fracture than falling in other directions [8]:
    - ❖ trying to fall forward or backward not from sides
- taking steps to reduce the potential energy and subsequently decrease the risk of fracture [69]
- landing with the aid of hands or reachable objects around to break the fall [70]
- using hip protectors [71-76]
- environmental modification (e.g., flooring) [20]

- medication and nutritional improvement:
  - consuming a calcium-rich diet that provides between 1,000 mg (milligrams) daily for men and women up to age 50 [77]. Women over age 50 and men over age 70 should increase their intake to 1,200 mg daily from a combination of foods and supplements.
  - obtaining 600 IU (International Units $\approx 0.025\mu g$) of vitamin D daily up to age 70 [77]. Men and women over age 70 should increase their uptake to 800 IU daily.
  - 5-15 minutes exposure to sunlight 4-6 times per week [78]

1.4 Objectives and Scopes of the Study

The objective of this study is to develop a two-level subject-specific biomechanical model for improving assessment of hip fracture risk. The expected outcomes of the research are twofold: (a) provide a more accurate hip fracture risk predictor than the currently existing techniques; (b) increase the applicability of the model in clinics.

To achieve the objective, a dynamics model at the musculoskeletal level is integrated with a finite element model at the femur level. The scopes of the study are (a) modeling of the human body to simulate the sideways fall and to determine the impact and internal forces applied to the proximal femur; and (b) applying the obtained loading condition to the proximal femur finite element model to determine hip fracture risk indices. By implementing the models into computer codes with well-designed user interface, it is expected that the models will be able to help clinicians to more accurately assess the hip fracture risk.

1.5 Organization of the Dissertation

This dissertation is organized into seven chapters. Chapter 1 introduces the background and justifies the significance of the present study by looking into the prevalence, causes, and consequences of the hip fracture.

Chapter 2 reviews the existing approaches for assessing hip fracture risk. Their advantages and limitations are discussed.

Chapter 3 starts with a general description of the two-level subject-specific biomechanical model, followed by a description of the need for developing a whole-body dynamics model and a proximal femur finite element model for assessing the risk of hip fracture.

In chapter 4, the whole-body dynamics model, the impact model and their application in determining the loading condition in a lateral fall are described in detail.

Chapter 5 presents the construction of the proximal femur finite element model, load application, boundary conditions, and material properties assignment. At the end of this chapter, the method for calculating fracture risk indices (FRI) at critical regions of interest is introduced.

Chapter 6 presents results of the dynamics model in predicting the impact force in a sideways fall that are validated using experiment data. Also, results of the proposed two-level subject-specific biomechanical model in assessing the hip fracture risk indices of 130 clinical cases are included in this chapter.

Chapter 7 summarizes the findings in this research and outlines some possible extensions for further studies.

Chapter 2

Literature Review

High incidence and serious consequences of hip fracture have urged researchers from different communities to develop more effective techniques for predicting and preventing hip fractures. For example, nutritionists and pharmacologists have worked to reduce the risk of hip fracture by increasing bone mineral density (BMD) and preventing bone loss [15] [79]. Radiologists proposed different methods to measure the BMD by exposing patients to the X-ray beams and clinicians have used the results of BMD testing as a tool for predicting hip fracture [80, 81]. Biomechanical engineers have contributed in developing mechanical tools such as Finite Element Models (FEM) and structural analysis to accurately assess hip fracture risk. The present chapter reviews currently available approaches for evaluating hip fracture risk.

2.1 Available Methods for Evaluating Hip Fracture Risk, Their Advantages and Limitations

The World Health Organization (WHO) recommended BMD testing for diagnosing osteoporosis, due to its reliable performance in measuring bone mineral content. Currently, the measurement of areal bone mineral density (aBMD) by DXA is a commonly used non–invasive hip fracture risk assessment tool. Hip Structural Analysis (HAS) evaluates femur strength using equivalent cross-section parameters. Fracture Risk Assessment Tool (FRAX) uses population-based statistical databases to predict ten-year hip fracture risk in a patient. Finite element analysis is another tool for predicting hip fracture risk, which is recently well established and developed in simulating the femoral bone under fall loading conditions. A review of tools for assessing hip fracture risk is presented in the following sections and their advantages and limitations are discussed.

2.1.1 DXA Imaging, Areal BMD and T-score

Bone densitometry based on hip DXA is now a well-established method in clinical centers for monitoring osteoporosis. This method evaluates the bone mineral densities at critical locations and compares the measured BMD with that of healthy young persons. DXA is the most widely used method for measuring BMD due to its low dosage of radiation, high measurement precision, easy calibration, and short scan time [82]. It is, therefore, referred to as the “gold standard” by the WHO [83].

The fundamental principle used in DXA scanning is to measure the transmission of X-rays of two different energy levels through the body [84]. DXA scanning enables estimating the ‘areal’ densities, i.e., the mass in grams over the unit projected area (cm^2). The obtained bone mineral density is thus called areal BMD. Areal BMD is usually measured at the narrowest femoral neck, the inter-trochanter, and over the whole proximal femur. Bone densitometry using DXA images is a sensitive technique and can detect changes in bone density 6 to 12 months after an effective osteoporosis therapy [85]. It is also currently used as an indicator of fracture risk [86]. The severity of osteoporosis and the fracture risk of a patient are measured by the so-called T-score [87]. The T-score is calculated as

$$\text{T-score} = \frac{Measured\ BMD - Young\ adult\ mean\ BMD}{Young\ adult\ standard\ deviation}. \tag{2.1}$$

The T-score, therefore, indicates the difference between the patient’s BMD and the mean peak bone mass achieved in healthy young adults.

According to the WHO report [88], osteoporosis and fracture risk are defined by bone density levels as follows:

- A T-score within 1 Standard Deviation (SD) ($-1 <$T-score< 1) of the young adult mean indicates normal bone density (low fracture risk).
- A T-score of 1 to 2.5 SD below the young adult mean ($-2.5 <$T-score< -1) indicates low bone mass (intermediate fracture risk).
- A T-score of 2.5 SD or more below the young adult mean (T-score< -2.5) indicates the presence of osteoporosis (high fracture risk).

In general, the risk for bone fracture doubles with every SD below normal. Thus, a person with a BMD of 1 SD below normal (T-score of -1) has twice the risk for bone fracture as a person with a normal BMD. A person with a T-score of -2 has four times the risk for bone fracture as a person with a normal BMD [35].

In addition to the T-score, Z-score is another way of measuring osteoporosis and assessing fracture risk [89]. Similar to the T-score, the Z-score is expressed in units of the population SD. However, instead of comparing the patient's BMD with those of young adults, it is compared with the mean BMD expected for the patient's peers. The Z-score is defined as

$$\text{Z-score} = \frac{Measured\ BMD - Age\ matched\ mean\ BMD}{Age\ matched\ standard\ deviation}. \tag{2.2}$$

Although not as widely used as T-score, Z-score nevertheless remains a useful measurement because it expresses the patient's risk of fracture relative to their peers. Z-score is a more appropriate method for assessing the hip fracture risk in elderly compared to T-score. Based on the T-score criterion, a large proportion of old people are classified in the osteoporotic category, even if the BMD is normal for their age [90]. It means T-score is not a proper fracture risk evaluator for the elderly. This deficiency does not appear in Z-score measurement since the patient's BMD is compared with the mean value of peers with matched age.

The radiation dosage used in DXA scanning is about 1 to 10 μSv, which is comparable to the average daily dose from natural background radiation (7μSv) [91, 92]. Therefore, DXA has been widely adopted in osteoporosis monitoring centers. Nevertheless, bone densitometry based on DXA scanning has a number of limitations. A DXA image tells nothing about how the mineral is distributed along the projection path; thus, it cannot be used to draw conclusions about tissue mineralization or porosity [93]. The use of T-scores is inappropriate in children and young adults [94], as their bone density has not yet reached the peak value. Also, there is less evidence for establishing a valid diagnostic threshold for men [95]. The International Society for Clinical Densitometry (ISCD) recommended the use of the Caucasian male normalized database and a T-score of -2.5 as a diagnostic threshold [96]. However, the WHO recommended using the same value as used to define osteoporosis in women [95]. This requires further investigation in order to standardize the approach used in different clinical services. It can also be argued that the WHO definition of intermediate fracture risk ($-2.5 <$T-score< -1) covers too large a percentage of women under the category of osteopenia. Furthermore, the WHO definition of high risk of fracture (T-score< -2.5) only covers too small a percentage of the severe osteoporosis patients while the majority of fractures occur in patients with T-score above the threshold [95, 97]. This criterion is thus not effective, particularly for making remedial decisions.

2.1.2 Computed Tomography and Volumetric BMD

Computed Tomography (CT) is a powerful non-destructive evaluation technique for producing three-dimensional (3D) images of an object. It is presently the accepted method for the measurement of volumetric Bone Mineral Density (vBMD), expressed in units of mg/cm^3. Contrary to the projection used in DXA scanning, CT uses X-rays from multiple angles to generate and reconstruct 3D-image datasets of the scanned object. Volumetric quantitative CT (vQCT) also provides detailed 3D information of bones. Materials with large atomic numbers and higher densities have higher X-ray attenuation. The level of X-ray attenuation is expressed as CT numbers, measured in Hounsfield units (HU). After being calibrated with scan phantoms, HU is used to calculate the bone mineral density.

Information of the internal structure of an object such as dimensions, shape, and internal defects are readily available from CT images. Although DXA still remains the predominant screening tool for evaluating the fracture risk because of its lower radiation dosage and cost, the use of quantitative CT has increased recently due to its ability to separate cortical and trabecular bone and ability to provide true volumetric density [98]. Areal bone mineral density measured from the DXA image has a strong correlation with hip fracture risk [99, 100], but it is not able to provide detailed anatomic information of the pathophysiology of hip fracture [101].

Quantitative CT provides information on bone size such as tissue volume and cross-sectional thickness along with the trabecular volumetric BMD [98]. Trabecular bone has a higher turnover rate than cortical bone due to its greater surface area. That is the reason why QCT is known as a very useful technique to monitor bone turnover and assess the efficacy of a treatment. Despite of the high dosage of radiation required for preparing a QCT image, it has become a clinical research tool in analyzing hip fracture risk [102].

2.1.3 Hip Structural Analysis (HSA)

Beck and Ruff [103] developed a hip structural analysis method to measure proximal femur geometry and strength using hip DXA scans [93]. HSA program is now commercially available and is used to automatically assess the geometric and structural parameters of the femur. The method is based on the principle that a line of pixel values across the bone is summed up in the projected DXA image [103]. The program analyzes the proximal femur at three locations: the narrowest femoral neck, the intertrochanteric cross-section along the bisector of the neck-shaft angle, and the sub-trochanteric cross-section that is approximately five centimeters below the lesser trochanter. For each region, the distribution of the bone mass across the bone is extracted and then equivalent geometry properties are derived [104]. The output of the HSA program includes the following parameters:

- Areal BMD (g/cm^2): mean values of BMD in the critical cross-sections [10].
- Outer diameter (cm): the distance between outer margins of the cross-section.
- Cross-sectional area (CSA,cm^2): this is defined as the surface area of bone tissue in the cross-section after excluding soft tissue spaces. CSA is an index of resistance to the axial force.
- Cross-sectional moment of inertia (CSMI, cm^4): index of structural rigidity; reflects distribution of mass over the cross-section.
- Section modulus (cm^3): this is an index of the resistance to bending forces and is calculated as $CSMI/d_{max}$ where d_{max} is the maximum distance from either bone edge to the centroid of the profile [105].

HSA has been used to measure effects of osteoporosis treatment, as well as to analyze age-related differences in structural geometry and femoral strength [106].

The main limitation of HAS is that DXA scanners are not designed or optimized for structural analysis. DXA scanners have excellent precision when used for measuring

BMD, but they are not designed to measure geometry [107]. The dimensional information presented in a single projection image can only reveal bending properties in the image plane. Small femur axial rotation may change the projected dimensions from which the geometry is measured. Although HSA provides critical insights into the bone fragility, it is not superior to BMD measurement in hip fracture predicting [108]. The reproducibility of HSA is not as good as that of conventional DXA analysis and the results are more operator-dependent [109]. Precision in measuring structural parameters of paired images using HSA is worse than conventional BMD due to the positioning inconsistence [110]. HSA is not able to distinguish mineralization contributed by different bone types, for example cortical and cancellous bone, and it thus measures average tissue mineralization which may introduce error into the output parameters [107].

2.1.4 FRAX

FRAX® is a 10-year fracture risk assessment tool, adopted by the WHO. The FRAX® model has been developed from studying population-based cohorts in Europe, North America, Asia and Australia [111]. It has been developed as a tool for helping healthcare providers to identify and proactively treat patients with a high risk of bone fractures due to low bone mass and other significant risk factors.

The significant contributors to the osteoporotic fracture risk are BMD, age, sex, ethnicity, body mass index (BMI), prior fracture, parental history of hip fracture, current smoking, and daily alcohol consumption [111]. Population-based statistical databases are used in the fracture risk assessment tool. FRAX® models were internally and externally validated [112, 113]. If a model is validated from a stratum of the same population, then it is called internal validation. The external validity concerns the extent to which the results are true for new cases, for example different populations.

The FRAX tool has limitations in predicting bone fracture:

- Not all risk factors are considered properly in the FRAX® tool such as the effect of osteoporosis therapy; therefore, the actual risk may be considerably over- or underestimated [114].
- Although fall history is a well-recognized risk factor for fracture, this is not included in the FRAX® [114].
- The main limitation of the FRAX® is that it does not take the accurate fall-induced impact force into account that is critically important in hip fracture risk assessment [30, 115]. Fall-related parameters may be included in FRAX®, but data needs to be collected in a systematic way and results must be validated for optimal performances.

2.1.5 Proximal Femur Finite Element Models Constructed from QCT or DXA Images

The finite element method, an advanced computational method for structural stress analysis developed in engineering mechanics, was introduced to orthopedic biomechanics in 1970s to evaluate stresses in human bones [116]. Since then, this method has been increasingly applied in stress analyses of bones and bone-prosthesis structures [117]. From a biomechanics viewpoint, an approach that is able to consider complex geometries and to accurately represent the heterogeneous distribution of material properties of bone may provide more accurate estimation of bone strength, compared to the BMD-based methods. In this regard, there is an increasing interest in the use of FE analysis to assess bone biomechanical behavior. For the FE simulations, different commercially available softwares such as ANSYS and ABAQUS or in-house computer codes developed by MATLAB, C, etc. are usually used.

Since 1970s, the finite element method, along with digital imaging techniques, has been used to investigate bone strength and to screen osteoporosis. Generally, the biomechanical FE models can be classified into two groups, i.e., three-dimensional (QCT-based) and two-dimensional (2D) (DXA-based), which are described in the following.

DXA-based finite element modeling:

The general procedure of the DXA-based FE method is that the two-dimensional geometry of the femur is extracted from the hip DXA image using image processing algorithms [118]. The segmented proximal femur from the DXA image is meshed and the inhomogeneous material properties are assigned. Load/constraint conditions are then applied to the constructed model to calculate the strain and stress distribution in the proximal femur.

The DXA-based FE models have limitations in predicting hip fracture. As the DXA is a 2D image, the overlapped part of the femur with pelvis interferes model construction and the BMD of the femoral head is overestimated from the DXA image. It means that the actual fracture risk is higher than what is calculated by the DXA-based FE models. The other issue in estimating the overall fracture risk is that a high stress is generated on the shaft due to the applied boundary conditions on the distal end of the femur. These stresses interfere the calculation of fracture risk, but they are not realistic as the applied constraint conditions do not accurately simulate the real boundary conditions. The mentioned limitations should be removed to improve the DXA-based FE models. Although a 2D DXA-based FE model is not a realistic representation of the real femur as the geometric and material information in depth is missing, it can determine the fall-induced stress and strain distribution in the femur with a reasonable accuracy [119]. The validity of using a 2D DXA-based FE model to predict strength and fracture of a 3D femur bone has been established by experimental efforts [119, 120]. Also, DXA imaging requires lower dosage of radiation compared to QCT imaging, which makes the 2D FE models more suitable for clinical application.

QCT-based finite element modeling:

DXA scanning technique has certain limitations, namely, a 3D object is projected onto a 2D plane and the depth information is lost, while this issue does not appear in computed tomography. For the complex geometry of bones, a QCT-based finite element model [47] is in principle more accurate in evaluating bone strength and fracture risk. One group of the finite element models have been constructed directly from voxels of QCT scans. The main advantage of voxel-based FE models is that they can be generated extremely fast. However, voxel elements lead to jagged edges due to protruding vertices of the cubes at the surface, which results in errors in the computed local stresses and strains [56]. More recently, volumetric modeling of trabecular bone has been accomplished using tetrahedral elements [56]. By using this technique the bone surface can be represented more accurately; however, the mesh generation requires much longer time [56, 121-126].

High-resolution peripheral QCT (HR-pQCT) is a newly developed in vivo clinical imaging modality. It can assess the 3D microstructure of cortical and trabecular bone and is suitable as an input for microstructural finite element analysis to evaluate bone's mechanical properties [127-129].

Although QCT scans contain all required information to construct a 3D finite element model, it has a number of limitations mainly due to its high dosage of radiation [130], which may introduce several side effects to the patient [131], and long computational time. Also, the high cost of scans and limited access to scanners prevent the potential applications of QCT-based finite element models in clinical environment.

Considering the advantages of the FE analysis over the statistical methods in predicting the hip fracture risk and the ability of constructing a subject-specific model, we selected image-based FE modeling in this research. Due to the mentioned limitations in QCT imaging, in particular the high dosage of radiation and the fact that fewer people are willing to do QCT scanning, we chose the DXA-based finite element modeling to assess hip fracture risk, as it will increase the applicability of the model in clinics.

All existing finite element models developed for studying hip fracture risk are of single-level; i.e., they do not consider how the impact force is affected by the whole body dynamics in fall. Since the impact force is one of the major contributors to hip fracture, it definitely affects the predicted fracture risk. Previously, simple empirical functions were adopted to estimate the impact force by considering the body weight and height [21, 132-134]. However, the impact force is affected by many anthropometric and kinematic parameters including body weight, body height, velocities of body segments, body configuration before the impact, etc. All the mentioned parameters are subject specific and must be determined by a subject-specific dynamics model.

2.2 Bone Fracture Criterion and Hip Fracture Risk Measurement

Assessment of hip fracture under stance loading or lateral impact force is usually performed using three criteria: factor of safety (FOS) [135], risk factor (RF) [59], and fracture risk index (FRI) [136]. In this section a review is performed on previously adopted bone fracture criteria and introduced hip fracture risk measurements, in both 2D and 3D FE models.

Keyak et al. [135] assessed FOS under two loading conditions; one representing loading during the stance phase of gait, the other simulating the impact from a fall. Their study was based on a 3D FE model generated from CT data of the patient. They calculated FOS to compare the actual element strength with the applied von Mises stress.

Schileo et al. [137] applied maximum principle strain, von Mises stress, and maximum principle stress criteria to calculate Risk Factor and to predict fracture location of the femur. RF compares the applied stress/strain with the yield one to predict the bone fracture. Lotz et al. [138, 139] also used von Mises stress yield criterion for cortical bone and crushing-cracking stress criterion for trabecular bone. The performance of nine stress- and strain-based failure theories in assessment of hip fracture is investigated by Keyak and Rossi [140]. They evaluated the distortion energy (DE), maximum normal stress, maximum normal strain, maximum shear strain, maximum shear stress, Coulomb-Mohr, modified Mohr, Hoffman and a strain-based Hoffman failure theories, using CT-based FE models of the femur [140].

The above mentioned fracture risk measurements are all derived from CT-images. The most recent DXA-based fracture risk criterion is proposed by Luo et al. [136]. They calculated the averaged FRI as a ratio between the effective stress (von Mises stress) by applied forces and the allowable stress (yield stress) of the bone over a region of interest (ROI). FRI is a local fracture risk measurement while FOS and RF are global ones. As it is aimed to determine the fracture risk in critical locations of the proximal femur using DXA images, the FRI is adopted in this study.

Chapter 3

A Two-Level Biomechanical Model for Assessing Hip Fracture Risk

Hip fracture risk in a sideways fall is affected by a number of factors, for example, the impact force and the strength of the femur. The impact force acting on the greater trochanter depends, in turn, on the velocities and kinematics of the body segments at landing. The configuration of body segments at the impact instant provides information on the loading conditions, which is related to the subject's ability to initiate and execute protective responses for a safe landing. The induced impact energy is then partially attenuated by the hip soft tissues and the rest is transferred to the greater trochanter. Meanwhile, the joint force is applied from the pelvis to the femoral head and affects the stress distribution in the proximal femur. This chapter first provides a general description of the two-level biomechanical model, and then justifies the need for subject-specifically developing a whole-body dynamics model and a proximal femur finite element model for assessing hip fracture risk.

3.1 Two-Level Subject-Specific Biomechanical Modeling of Sideways Falls

This study introduces a two-level biomechanical model consisting of a whole-body dynamics model and a proximal femur finite element model. The whole-body dynamics model is used to predict the impact force onto the greater trochanter in a sideways fall. The load/constraint conditions determined from the whole-body dynamics simulation are then applied to the proximal femur finite element model to calculate the stresses in the femur bone. All information required to construct the models is extracted from the subject's whole-body and hip DXA scan in order to make the models subject-specific. The DXA images used in this study are obtained from the Manitoba Bone Mineral Density Program under a human body research ethics approval issued by the University Human Research Ethics Board. The procedure of constructing the two-level biomechanical model is illustrated in Figure 3.1 and described in detail in the following sections.

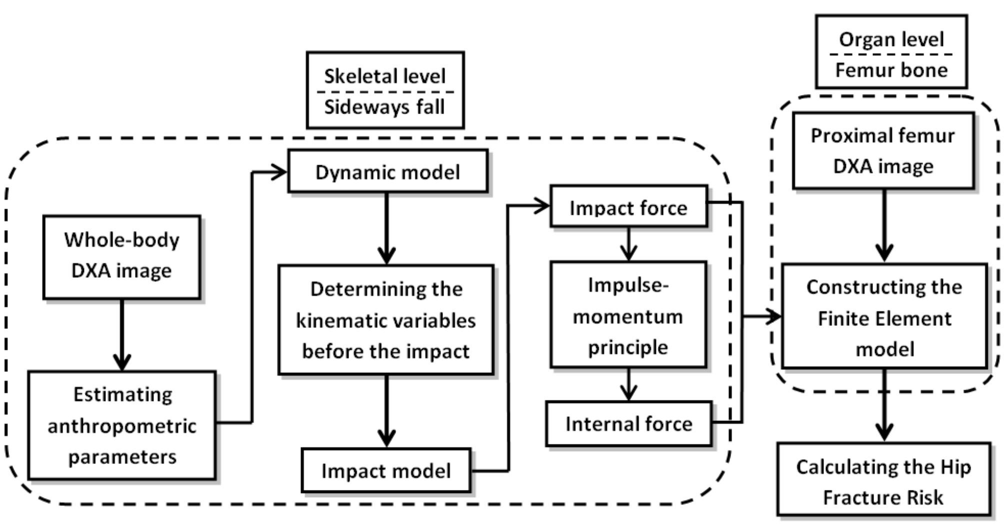

Figure 3.1. Procedure of constructing the two-level biomechanical model for assessing hip fracture risk [141]

3.1.1 The Whole-body Dynamics Model for Predicting the Impact Force Induced in Sideways Falls

There are many situations where hip fracture can be developed, but for the elderly clinical data have shown that more than 90% of hip fractures are caused by fall, mostly from standing height [25, 29-31]. Reasons may include the decreased muscular strength of the elderly as well as the impairment of cognition, perception and vision [6] that may increase the fall risk. Growing evidence suggests that body segments kinematics at the impact moment is one of the most important determinants of the fall-induced hip fracture [142]. Of primary importance is whether or not the impact occurs to the lateral aspect of the pelvis or the side of the leg [39, 143]. It has been reported that sideways falls create a 6-fold greater risk for hip fracture than forward or backward falls [33], as the hip is covered by less soft tissues and lower portion of the impact energy is thus attenuated during the impact. Statistical studies revealed that 63-69% of fall-related fractures occurred in sideways falls [8, 32]. Hence, dynamics study of the sideways fall is necessary for assessing hip fracture risk and for investigating factors contributing to the hip fracture.

Falls coupled with high impact velocity are more likely to result in the hip fracture [39], which implies that kinematic parameters play important roles in the hip fracture etiology [54]. It also indicates that hip fracture risk depends largely on fall dynamics. There are a number of challenges in studying fall dynamics, for example, the limitation in fall experimentation due to safety concerns, technical difficulties in measuring rapid impact motions, inability to generate in vivo joint kinetics and kinematics, specimen variability, etc. [144]. To resolve the mentioned issues, a practical way is to develop and validate a whole-body dynamics model, and then implement the model into computer simulation softwares. Simulation results can provide a valuable insight into the biomechanical aspects of fall-induced hip fracture. The simplest yet effective biodynamics model of falling is a single degree-of-freedom (DoF) model subjected to an initial velocity or an impulse force [134], which can be extended to multi-DoF models [133, 144-147] or more sophisticated rigid-body link models [148-153].

Although more complex dynamics models of the human body are available in the literature, with a consideration of a balance between the model complexity, the accuracy in predicting the loading conditions, the computational efficiency, and the applicability in clinics, a three-link dynamics model is developed in this study to investigate sideways falls.

3.1.2 The Proximal Femur Finite Element Model for Evaluating Hip Fracture Risk

Apart from the need for a valid dynamics model to predict the body kinematics and the impact force induced in fall, a method is required to predict the behavior of the proximal femur under the fall loading conditions. Currently available methods for in vivo hip fracture risk assessment are mainly based on statistical models. One major deficiency of a statistical approach is that it is only suitable on averaging over a group of people rather than individual analysis. Therefore, a reliable method for the assessment of hip fracture risk considering individual femur properties is needed.

A considerable amount of in vitro studies have been performed over the last two decades in an attempt to develop more accurate models to predict femoral fracture [137, 138, 154-164]. However, care must be taken to ensure that these in vitro models accurately describe the in vivo condition [165].

The limitations of current in vitro and statistical methods make image-based FE modeling attractive as one of the potential tools for assessing hip fracture risk. However, the currently available image-based FE models have a number of limitations, mainly in applying load/constraint conditions that has been discussed in Section 2.1.5. In this study, the mentioned limitations are eliminated by developing the two-level subject-specific biomechanical model.

3.2 The Need for a Two-Level Model

Hip fracture is affected by a number of parameters such as body weight, body height, body configuration at the instant of the impact, femur bone geometry, local bone density, etc. These parameters take effect at different scale levels and affect different physical outcomes. For example, body weight, body height, and body mass distribution take effect at the musculoskeletal level and affect the magnitude of the impact force induced in a sideways fall, while the femur bone geometry and local bone density take effect at the organ level (femur bone) and affect the stress distribution in the femur bone. It is very difficult to consider all these parameters within a single-level biomechanical model. The currently available models for assessing hip fracture risk are of single-level and mainly consider the parameters at the femur bone level, while the parameters at the musculoskeletal level are missed, which may considerably affect the predicted fracture risk. Therefore, the development of a two-level biomechanical model is necessary for improving assessment of hip fracture risk. Figure 3.2 conceptually shows how assessing hip fracture risk requires a two-level biomechanical model.

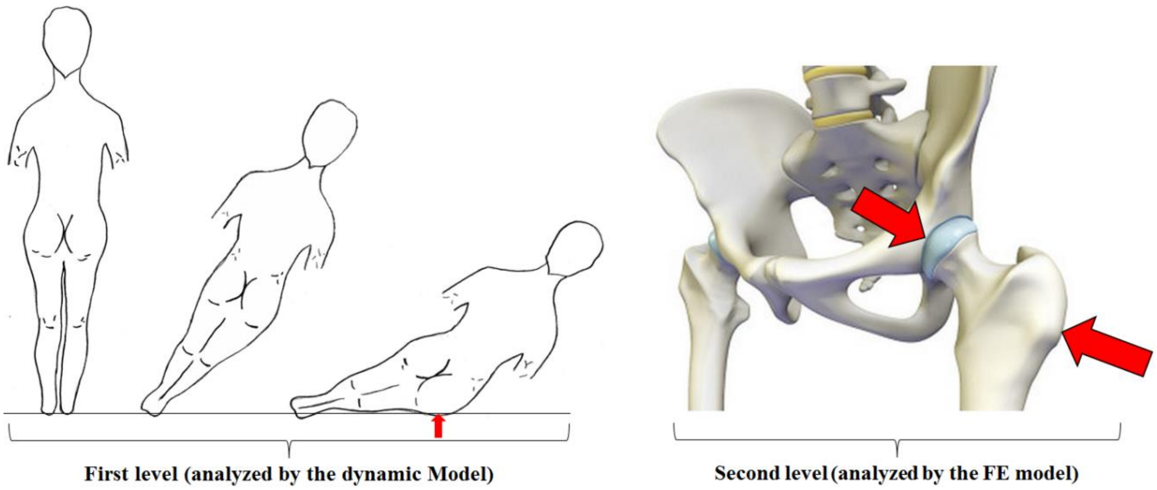

Figure 3.2. A two-level biomechanical model is necessary for accurately assessing hip fracture risk. Parameters at the musculoskeletal level (body weight, body height, body mass distribution, and joint torques) affect the magnitude of the impact force induced in a sideways fall while the femur-related factors (proximal femur anatomy, bone geometry, cortical thickness, and porosity) affect the stress distribution in the femur bone [24].

3.3 The Need for a Subject-Specific Model

Advances in techniques for subject-specific biomechanical modeling can result in patient-specific prevention and protection planning. Although the use of non-subject specific simulations is now quite widespread, there have been several empirical demonstrations of advantages of the subject-specific modeling in biomechanical studies [137, 154, 159]. Various clinical and FE studies have demonstrated that hip fracture is related to anthropometric parameters, bone quality [165], proximal femur anatomy [166-169], cortical thickness [170, 171], porosity [172, 173], hip soft tissue thickness [20, 174, 175], landing surface [70, 176], etc. All these parameters are individual-dependent as they vary with gender, race and age [177-179]. Therefore, hip fracture risk in a sideways fall differs widely from individual to individual, and for one individual from fall to fall. It is thus necessary to integrate all the subject-specific parameters to accurately assess hip fracture risk. Figure 3.3 illustrates how various parameters may change the hip fracture risk in different subjects. The main advantages of a subject-specific model over existing non-subject-specific models in assessing the hip fracture risk are as follows:

- All factors affecting the fall-induced forces to the proximal femur are considered and thus the predicted loading conditions are more realistic.
- The subject's femur anatomy and material properties are considered in the FE modeling and therefore the predicted stresses and strains in the femur are more accurate.
- As the models are constructed from the subject's medical images, the biofidelity of the models is improved.

As this study introduces a two-level biomechanical model consisted of a dynamics model and a finite element model, both should be subject-specific for more accurately assessing hip fracture risk. Anthropometric parameters, which can considerably affect the loading scenario in a sideways fall, are determined subject-specifically using the whole-body DXA image. Femur anatomy and bone material distribution are also considered in a subject-specific FE model using the proximal femur DXA image.

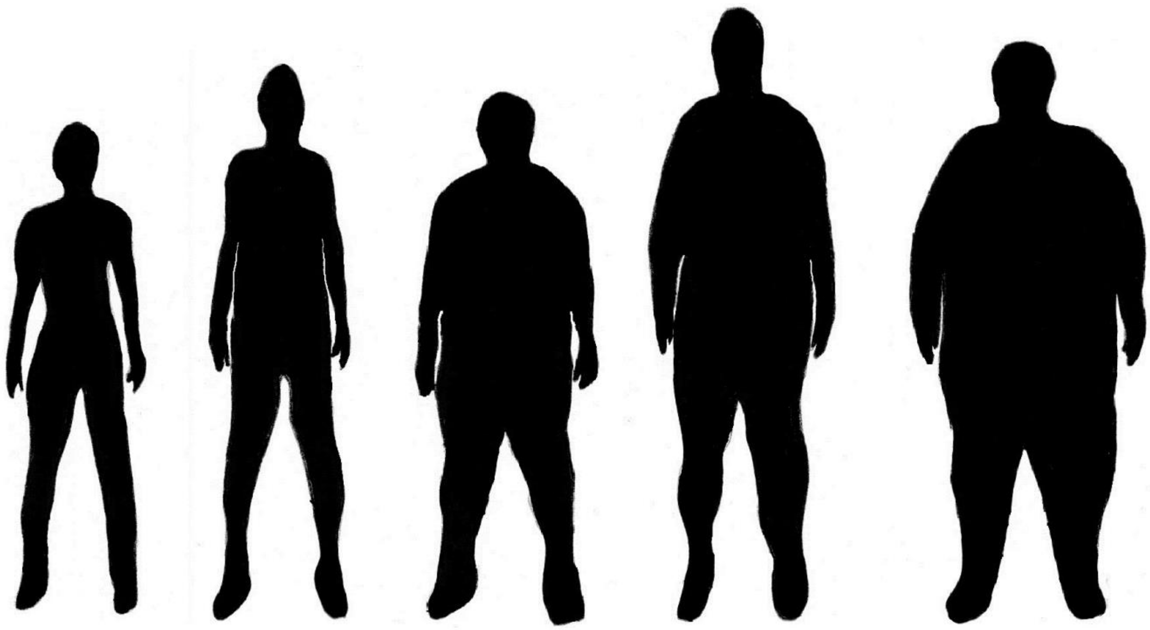

(a)

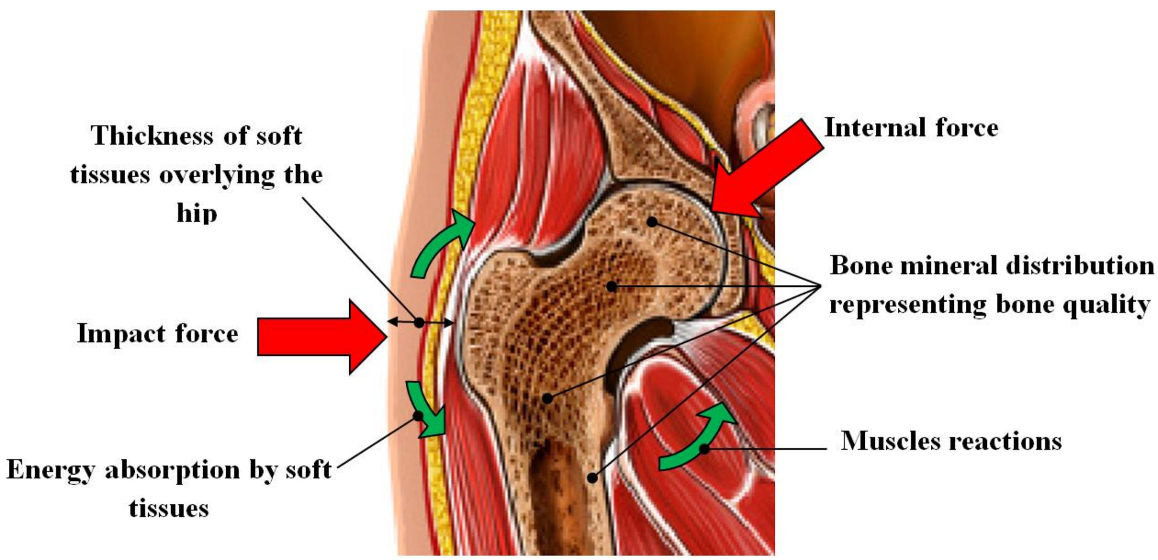

(b)

Figure 3.3. How hip fracture risk is affected by subject-specific anthropometric parameters. (a) Body weight, body height, and body mass distribution vary from individual to individual which strongly affect the kinematics of body falling and the applied impact force to the femur. (b) Trochanteric soft tissue thickness and femur-related parameters are thoroughly different in different subjects which significantly change the induced stress on the femur in a sideways fall [180].

Chapter 4

Subject-Specific Whole-Body Dynamics Model

Dynamics simulation of a sideways fall based on a multibody dynamics model is an effective and practical way for determining the impact force in a lateral fall of the elderly. However, there are a number of parameters affecting the accuracy of the predicted impact force, including the body anthropometric parameters, mass distribution, etc., which are all subject-dependent. Therefore, there must be an in vivo, non-invasive and convenient method for determining the parameters. Body tissue mass estimation based on the whole body DXA image meets all these requirements and it is thus adopted in this study. The method is described in more details in Section 4.1. The sideways fall process can be split into two stages: the fall of the body before the hip touches the ground and the impact of the hip with the ground. These two stages are governed by different mechanical principles and thus mathematical equations which are described, respectively, in Sections 4.2 and 4.3. The validity of the whole body dynamics model must be examined before it can be applied in clinical environments. The validation was done by controlled and protected fall tests using young volunteers, as described in Section 4.4.

4.1 Estimation of Body Segment Parameters Using the Whole-Body DXA Image

Most previous studies [133, 134, 144, 149, 152, 153] have used Newtonian forward dynamic simulations of falling, which require predetermined model parameters. Thus, inaccurate estimation of model parameters such as anthropometric parameters can limit the validity of the model itself and compromise the accuracy of simulation results [20]. Therefore, an accurate and convenient method is required for determining anthropometric parameters of the subject. In this study, an image-based method is used to determine the required parameters in constructing the whole-body dynamics model.

Among all medical images, DXA scanning is selected to be used in this study, which was primarily developed for diagnosis of osteoporosis. The wide demand of DXA scanners in clinics has led to the development of different competing generations of the equipment. Improvements have been achieved through advances in X-ray generation and detection technology as well as implementation of more sophisticated image analysis algorithms [181]. As a result, DXA has been extended to allow the study of the total skeleton and its regional parts, as well as soft-tissue composition measurement [181]. Since DXA scanning is cheap, non-invasive, quick, quantitative and reproducible with low dosage of radiation and acceptable accuracy compared to other imaging techniques [125, 181-198], it is used in our study for determining the parameters required in the dynamics model [199, 200]. The concept that the attenuation coefficients of X-ray are proportional to mineral contents in the tissues is used in this study to estimate the anthropometric parameters from whole-body DXA images.

A conventional method of using physical measurements of body segments, e.g., circumference, height, length and breadth, has been introduced to estimate the mass of body segments [196], but the results are not applicable for all image formats. Correlations between tissue mass density and pixel intensities in DXA images have been established and validated by experiments [201]. Bone and soft tissue masses can be estimated by considering the attenuation coefficients resulted from passing X-ray through a scanned segment [201]. In this section, a method is presented to extract the anthropometric parameters from a whole-body DXA image.

First, a DXA image (Figure 4.1) is loaded in developed in-house MATLAB codes, noise is filtered, and the pixel size is determined. It has been demonstrated that there is a linear correlation between the pixel intensity in the DXA image and the tissue mass density [201-203]. The correlation coefficient in this study has been determined as

$$CC = \frac{W}{\sum_{i=1}^{n} P_i}, \tag{4.1}$$

where W is the body weight of the subject, n is the total number of pixels enclosed in the body contour, and P_i is the pixel intensity of pixel i. With the above correlation coefficient, the mass of pixel i is obtained as follows:

$$\rho_i = CC \times P_i. \tag{4.2}$$

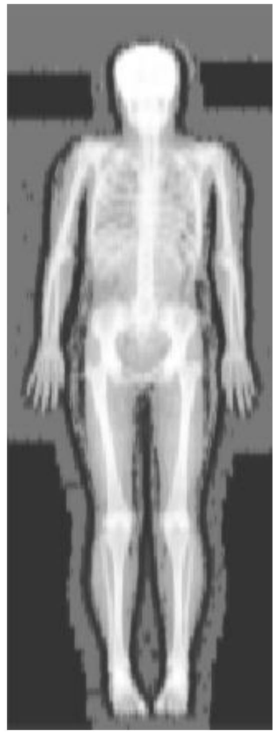

Figure 4.1. A whole-body DXA image

Then, mass, mass centre, and mass moment of inertia of the body segments are calculated as

$$m_k = \sum_{i=1}^{N_k} \rho_i\,, \qquad r_k = \frac{\sum_{i=1}^{N_k} \rho_i r_i}{m_k}, \qquad I_k = \sum_{i=1}^{N_k} \rho_i {r_i}^2\,, \tag{4.3}$$

$$(k = \text{number of body segment})$$

where N_k is the number of pixels enclosed in the contour of body segment k and r_i is the distance of pixel i from the distal end of the link. The above method has been used in this study to determine the body anthropometric parameters required in the dynamics model.

Since the mass constant is defined based on the attenuation coefficients in the image, this method is able to estimate the body mass from a wide range of DXA image formats. It increases the applicability of our biomechanical model in clinics.

4.2 Whole-body Dynamics Model

Based on the available literature [133], an improved human body dynamics model is introduced in this chapter. Design of the model starts with the selection of the number of links. In designing the multibody dynamics model, the model complexity, computational efficiency, ease of adopting in clinics, as well as the ability to represent the most effective body segments in a fall are considered and as the result, a three-link model is adopted from [133] and improved in this study. Since most of the body motions during falls are described by the positions of the ankle, the knee, and the hip joint, a three-link model that includes these joints is appropriate. The three-segment dynamic system used in the locomotion simulation is depicted in Figure 4.2. The first segment represents the lower leg between the ankle and the knee joint, the second segment represents the upper leg between the knee and the hip joint, and the third segment represents the combined mass and inertia of the rest of the body (trunk, arms, and head). The mass (m_i) and inertia (I_i) of each segment is assumed to be constant with respect to the local coordinate system. In reality, movement of the arms in fall would likely alter the inertia of the third segment, but it is assumed that this alteration would not have a large enough impact on the forces and moments at the hip joint [204] to warrant the much greater complexity that would be required in the model to account for this. A rectangular coordinate system x-y-z is set up in the Figure 4.2 for describing the motion of the links. Each segment is described by its length (l_i), and the mass center measured from the distal end (l'_i). The mass center of each segment is assumed to lie along the line connecting the joints. The links are connected by articulation joints at the hip and the knee. The model is connected to the ground by the ankle joint with the assumption that there is no slippage between the feet and the ground during the fall. This assumption is considered in order to avoid the significantly greater complexity of modeling a dynamic system that is not anchored to the ground. It is anticipated that a fall due to slipping would not significantly increase the applied force to the hip during impact [204] since the same potential energy is involved in either case and an anchored fall would likely increase the kinetic energy before the impact since a part of energy is lost due to friction in slipping. Therefore, the vertical impact velocity and subsequently the impact force is greater in the anchored fall compared to the fall with slippage [204].

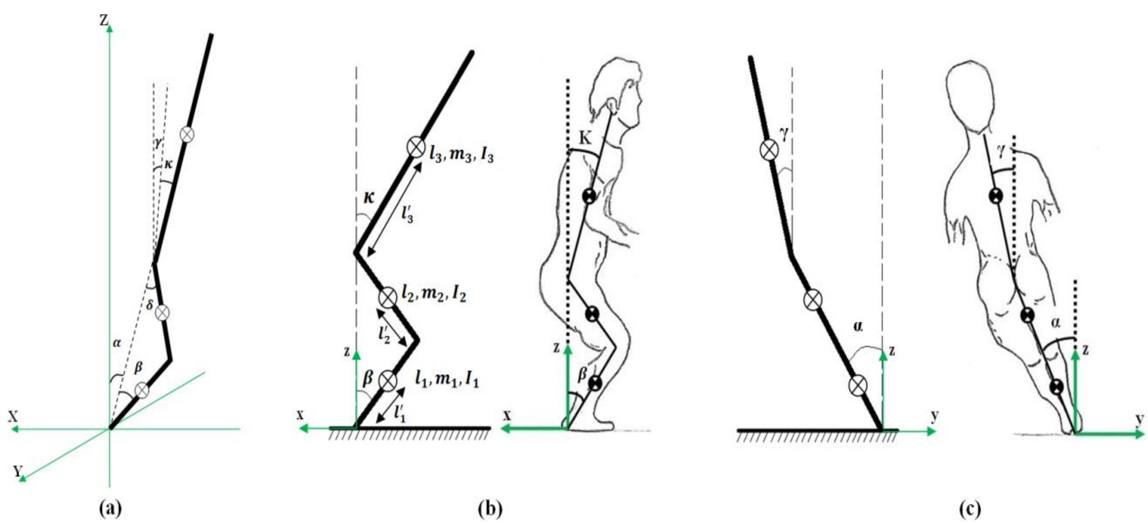

Figure 4.2. Three-link whole-body dynamics model: (a) three-dimensional view; (b) projection on sagittal plane; (c) projection on coronal plane [141]

Degrees of freedom are defined at the joints. The ankle joint has two degrees of freedom, representing flexion/extension in the sagittal (xz) plane and abduction/adduction in the coronal (yz) plane. The knee joint has a single DoF describing the flexion/extension rotation. The hip joint has a rotational DoF representing hip abduction/adduction. Therefore, three generalized coordinates, α, β and γ as shown in Figure 4.2, are required to describe the motion of the links. The physical meanings of the degrees of freedom are described as follows:

- α: the angle between the vertical and the projection of the leg segment on the yz plane
- β: the angle between the shank segment and the line connecting the hinge at the floor with the hip joint
- γ: the angle between the vertical and the projection of the trunk segment on the yz plane

Angle κ between the trunk and the line through the hinge at the floor and the hip joint is assumed to have a constant value in a fall [133]. Lateral flexion of the trunk is described by the γ angle, which usually changes in a sideways fall compared to the trunk angle in the sagittal plane [133]. However, κ may have different values in different falls depending on the initial conditions.

Motion equations of the three-link three-DoF dynamics model are established by the Lagrange Dynamics [205, 206]. As the derivation is not trivial, MAPLE codes are developed to derive the specific equations from the following general Lagrange equation. The resulting equations contain the generalized coordinates, their first and second order time derivatives.

$$\frac{\partial}{\partial t}\left(\frac{\partial T}{\partial \dot{q}_i}\right) - \frac{\partial T}{\partial q_i} + \frac{\partial V}{\partial q_i} = \tau_i \quad (i = 1, 2, 3) \tag{4.4}$$

In the above equation, $q_1 = \alpha$, $q_2 = \beta$, $q_3 = \gamma$; T and V are respectively the kinetic and potential energy in the system expressed by the three generalized coordinates and their time derivatives. Derivation of the terms in the left-hand side of the Eq. (4.4) is given in Appendix A. The generalized moments τ_i (i = 1, 2, 3) in Eq. (4.4) are the integral results of actions of muscles, tendons, and ligaments across the joints that have a complex configuration and vary in different body motions. Ligaments and tendons sustain relatively large deformations, rotations and displacements, have a highly non-linear behavior and show a time and strain rate dependency [207, 208]. In this study, a combination of the dynamics model and the experimental data is used in a reverse procedure to estimate the joint moments.

The right-hand side of the Eq. (4.4) which describes joint moments can be expressed as a function of time since the generalized coordinates are time-dependent expressions. To find the time history of α, β, and γ from the experiments, which are conducted on three participants, information of each angle is recorded from the release point to the impact moment. Then, a fourth-order polynomial is used to interpolate their variations with respect to time as

$$\begin{aligned} \alpha_t &= -363.5t^4 + 144.3t^3 - 13.39t^2 + 0.3320t + 1.175 \\ \beta_t &= -217.2t^4 + 111.3t^3 - 11.30t^2 + 0.2987t + 0.8931 \end{aligned} \tag{4.5}$$

$$\gamma_t = 174.7t^4 - 70.43t^3 + 5.015t^2 - 0.0716t + 0.6375,$$

for subject 1, and

$$\begin{aligned}
\alpha_t &= -349.1t^4 + 118.4t^3 - 9.291t^2 + 0.5201t + 1.096 \\
\beta_t &= -613.2t^4 + 223.8t^3 - 20.66t^2 + 0.7108t + 0.8379 \\
\gamma_t &= -108.9t^4 + 62.25t^3 - 5.207t^2 - 0.2187t + 0.6719,
\end{aligned} \tag{4.6}$$

for subject 2, and

$$\begin{aligned}
\alpha_t &= -103.4t^4 + 72.57t^3 - 11.66t^2 + 0.4491t + 0.6935 \\
\beta_t &= -110.2t^4 + 68.78t^3 - 6.776t^2 + 0.1765t + 0.5192 \\
\gamma_t &= 78.83t^4 - 24.77t^3 - 3.791t^2 + 0.3226t + 0.8588,
\end{aligned} \tag{4.7}$$

for subject 3. The interpolated time-dependent functions of the generalized coordinates and their derivatives, i.e., the angles, angular velocities and angular accelerations, are then substituted to the left-hand side of the Eq. (4.4) to obtain joint moments, i.e., τ_β and τ_γ. The moments are therefore obtained as functions of time. Due to complexities in the expressions, MAPLE codes are written to aid the derivation of the equations. The resulted time-dependent functions for the moments τ_β and τ_γ are then re-substituted in the system equations of motion to find the time history of the generalized coordinates.

After determination of required matrices using MAPLE, equations are coded into a MATLAB script. In the MATLAB codes, the whole body DXA image is an input and anthropometric parameters are calculated. The mass properties, connectivity, and initial conditions are then specified for the dynamics model. The codes implement the equations of motion, solve them with initial conditions, and record the resulting kinematic and kinetic variables. The simulation is carried out in the following steps:

1. setting anthropometric parameters
2. setting initial conditions
3. determining joint positions, velocities, and subsequently accelerations by solving a set of differential equations
4. decreasing time increment to achieve a higher accuracy

Two sets of initial conditions are used in this study; first, the initial conditions of the dynamics model are matched with those of performed experiments to evaluate the accuracy of the model; second, initial conditions of sideways falls from standing height are used to investigate hip fracture risk in 130 clinical cases. For the second part of this study, the initial configuration of the system is set in accordance with configurations described in other experimental studies [21]. Angle α is set at 9.78 degrees, angle β is set at 4.13°, and the hip angle (γ) is set at 12.7 degrees. The initial angular velocities ($\dot{\alpha}$, $\dot{\beta}$, and $\dot{\gamma}$) are considered to be 46.9, 23.5, and $37.2\ {}^{\circ}/\mathrm{s}$, respectively.

The improved feature of the presented dynamics model to what was proposed by Kroonenberg et al. [133] is the use of whole-body DXA image to estimate the segment masses and moments of inertia for the 3D fall model. Also, the limitations of the adopted dynamics model including the restriction for the length of shank and thigh and the location of mass centre of body segments are eliminated. In addition, the impact moment is defined subject-specifically based on the hip width of the patient and the body configuration before the impact.

4.3 Impact Model

The human body's sideways fall is simulated by the proposed dynamics model in this study. The dynamics model predicts the kinematics of the body segments from the initial position to the impact moment, i.e., before the hip touches the ground. The interaction between the body and the ground is described by an impact model. The impact model is used to predict the hip impact force based on 1) the vertical hip impact velocity, 2) the effective mass, and 3) the hip stiffness and damping properties during impact.

The impact force is applied once the ankle eversion angle exceeds ε (Figure 4.3), which is defined base on the subject's hip width and the kinematics of the body segments during the fall. The impact force is applied to the hip, assuming that other parts of the leg and body do not come into contact with the ground before the hip, as has been found to be generally true in sideways falls in kinematic studies performed by Kroonenberg et al. [21]. The configuration of the body segments at the time instant when the hip touches the ground is used in constructing the impact model.

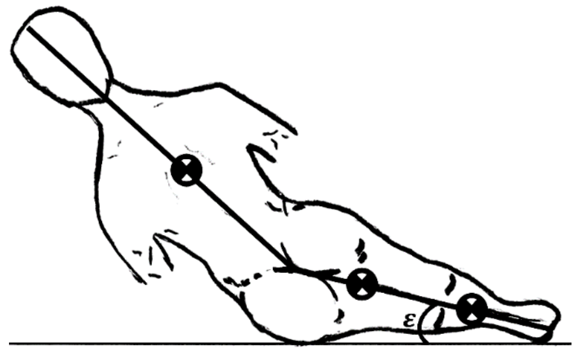

Figure 4.3. Body configuration at the impact instant

In order to estimate the impact force applied to the greater trochanter in a sideways fall, the body is modeled as a damped vibrational system (Figure 4.4) proposed by Robinovitch et a. [134]. In the vibrational system, the effective mass is moving in the vertical direction with the velocity V prior to the impact. Damping is considered in this model to simulate the attenuation of the impact energy by the trochanteric soft tissues. To make the impact model subject-specific, the required parameters are taken from the concerned subject. The effective mass is determined from the body kinematics prior to the impact as described in Section 4.2. Hip stiffness and damping properties during the impact are determined from experimental data, which is described in Section 4.3.2. The improved feature of the implemented model is that the stiffness/damping properties are determined subject-specifically.

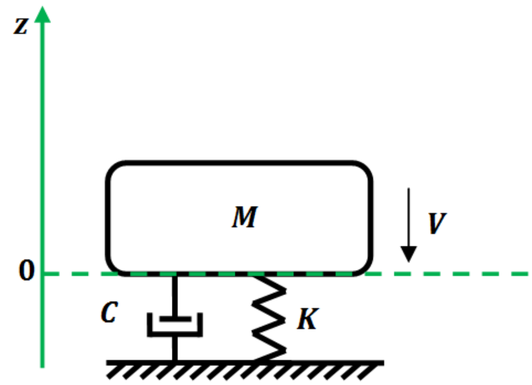

Figure 4.4. Impact model in simulating the interaction between the hip and the ground in a sideways fall

4.3.1 Effective Mass

The effective mass is that part of the body mass that moves in the vertical direction prior to impact and affects the impact force [133, 209, 210]. As shown in Figure 4.3, once the hip touches the ground at the impact instant, the body can be divided to two parts from the hip, i.e., the upper trunk and the lower extremity. The effective mass is an equivalent mass located at the hip joint and simulates the vertical movement of the body during the impact. Hence, kinematic parameters of both the upper and the lower extremities are involved in determination of the effective mass. The derivation of effective mass equations is given in Appendix B.

4.3.2 Hip Stiffness and Damping Properties during the Impact

Hip stiffness (K) and damping coefficient (C) during the impact are required to obtain the impact force. In this study, two methods are used to determine the subject-specific K/C in the impact model. In the first method, experimental data of controlled and protected fall tests, conducted by our research collaborators, are used to determine the system parameters. In the second method, experiment data from the literature are used to determine the correlations between the hip soft tissue thickness and K and C in the impact model. The first method is able to more properly simulate the response of hip soft tissues during the impact, as the parameters are determined from the subjects' testing data. However, it needs conducting an experiment, which may introduce complexities to the model and is obviously not practical for the elderly. The second method proposes a more convenient and applicable way to determine the system parameters while the accuracy does not stay in the same level, inevitably. The two methods are described in detail in the following.

In the first method, logarithmic decrement theory [211] is used to determine the stiffness/damping properties for each subject. It has been demonstrated that the body motion during the impact can be described by an underdamped vibrational system [134, 209, 212]. The logarithmic decrement method identifies the system parameters based on the rate at which the amplitude of a free-damped vibration decreases. The logarithmic decrement is defined using the vibrational amplitudes from any two successive periods [211], as follows:

$$\delta = \ln\left(\frac{z_i}{z_{i+1}}\right) = \frac{2\pi\xi}{\sqrt{1-\xi^2}}, \tag{4.8}$$

where z_i and z_{i+1} are any two successive amplitudes and ξ is the damping ratio. The time histories of the hip position and velocity, obtained from the experiment, are used to determine the damping ratio in Eq. (4.8). The frequency of the damped vibration (ω_d) can be obtained as

$$\tau_d = \frac{2\pi}{\omega_d}. \tag{4.9}$$

The natural frequency of the system is then determined by

$$\omega_n = \frac{\omega_d}{\sqrt{1-\xi^2}}, \tag{4.10}$$

from which the stiffness of the system can be obtained as follows:

$$K = M{\omega_n}^2. \tag{4.11}$$

Damping coefficient can also be determined as

$$C = 2\xi M\omega_n. \tag{4.12}$$

In the above equations, z_i, z_{i+1}, and ω_d are determined from experiments and other parameters are subsequently calculated.

After determination of system parameters, the time history of the hip impact force can be predicted by solving the damped free vibrational equation. As the tissue is compressed, the restoring force is calculated according to the following equation

$$F = Kz + C\dot{z}, \tag{4.13}$$

where z and $\dot{z}$ are respectively the hip vertical position and velocity during the impact.

As the purpose of this study is to develop a simple, accurate, and generally applicable model in clinics, and considering that performing protected fall tests is expensive, time consuming, and not feasible for the elderly, an alternative experiment-free method is proposed to estimate the system parameters. In this method, experiment data of seven females and seven males are extracted from [134], where K and C of each subject were experimentally measured. Then, nonlinear least-square fits of power functions are used to establish correlations between K/C in the impact model and body parameters including hip soft tissue thickness, body mass index, body height, and body weight as presented in Tables 4.1 and 4.2.

Table 4.1. Correlations between $\boldsymbol{K/C}$ in the impact model and body parameters in male subjects

Body parameters	Correlation between K and body parameters	R^2 (p-value)	Correlation between C and body parameters	R^2 (p-value)
Soft tissue thickness (STT)	$K = 12.51(STT)^{-0.33}$	0.3891 (0.0134)	$C = 3.99(STT)^{0.58}$	0.3968 (0.0129)
Body weight (BW)	$K = 442.28(BW)^{-0.51}$	0.1447 (0.0399)	$C = 0.0007(STT)^{1.43}$	0.2158 (0.0282)
Body height (BH)	$K = 60.78(BH)^{-0.36}$	0.0052 (0.3777)	$C = 0.03(STT)^{4.27}$	0.2349 (0.0245)
Body mass index (BMI)	$K = 3.41(BMI)^{-1.31}$	0.3403 (0.0169)	$C = 0.0084(STT)^{1.17}$	0.2936 (0.0206)

Table 4.2. Correlations between $\boldsymbol{K/C}$ in the impact model and body parameters in female subjects

Body parameters	Correlation between K and body parameters	R^2 (p-value)	Correlation between C and body parameters	R^2 (p-value)
Soft tissue thickness (STT)	$K = 1.19(STT)^{-0.91}$	0.8390 (0.0037)	$C = 0.5047(STT)^{0.13}$	0.1047 (0.0436)
Body weight (BW)	$K = 5138.50(BW)^{-1.30}$	0.3465 (0.0163)	$C = 0.0059(BW)^{0.97}$	0.0938 (0.0508)
Body height (BH)	$K = 17.91(BH)^{-0.89}$	0.0165 (0.1836)	$C = 0.0870(BH)^{2.66}$	0.08669 (0.0662)
Body mass index (BMI)	$K = 5748.00(BMI)^{-1.70}$	0.5752 (0.0086)	$C = 0.0818(BMI)^{0.43}$	0.0391 (0.1570)

In the above correlations, STT, BW, BH, BMI, K, and C are respectively in m, kg, m, kg/m^2, kN/m, and $kN.s/m$.

The strongest correlations were observed between K/C and the hip soft tissue thickness for both female and male subjects. The proposed functions provide the ability to determine subject-specific stiffness/damping properties of the impact model using the soft tissue thickness obtained from the whole-body DXA image.

4.3.3 Determination of the Internal Force

In a lateral fall, the greater trochanter is subjected to the impact force applied from the ground. Meanwhile, the femoral head is subjected to the joint (internal) force applied from the acetabulum. The impact force can be determined either experimentally or theoretically. However, the complex configuration of muscles, tendons, and ligaments that are involved in fall process ensures that the configuration of internal forces is too complicated to be measured experimentally [213-215]. Therefore, the only practical way to obtain the joint force is to use the dynamics principles. The impulse-momentum principle [216] is used in this study to determine the force applied from the acetabulum to the femoral head in a sideways fall. If the femur as a part of the lower extremity is isolated from the acetabulum, the internal force is applied to the femur head as shown in Figure 4.5.

To determine the joint force, the impulse momentum principle can be written as

$$\int F.dt = G_2 - G_1, \tag{4.14}$$

where G_2 and G_1 are respectively the linear momentums just before and after the impact and $\int F.dt$ is the linear impulse of all external forces which act on the femur including the weight, the impact and the joint forces.

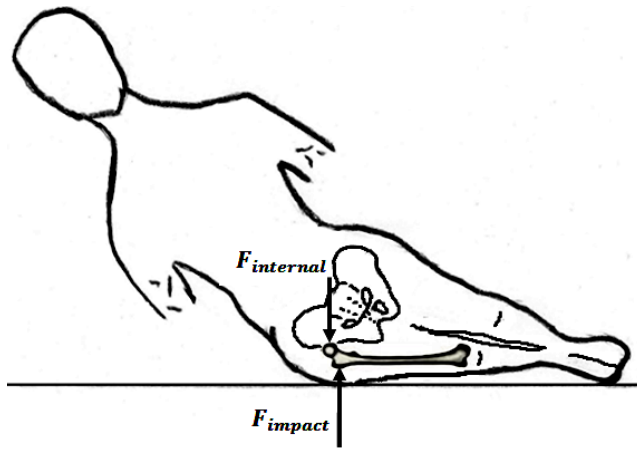

Figure 4.5. The load application on the proximal femur in the impact stage of a sideways fall

Instead of integrating on the whole period of the impact duration, the equation can be solved in a small time interval where the forces can be considered as constants, i.e.,

$$\left(F_{impact} + F_{joint} - EM_{lower\ extremity}.\, g\right).\, \Delta t = EM_{lower\ extremity}(V_2 - V_1), \qquad (4.15)$$

where EM is the effective mass of the body during the impact, V_1 and V_2 are vertical hip velocities before and after each time interval (Δt) within the impact duration. Time history of kinematic variables and the impact force are determined by the subject-specific impact model and therefore Eq. (4.15) can find the magnitude of the joint force in each time interval. Figure 4.6 shows the procedure of determining the required parameters in Eq. (4.15) to obtain the joint force. A shorter time interval results in higher accuracy in numerically solving an integral equation. Therefore, the time interval is considered to be 0.0001 second to reach adequate precision with a reasonable computational time.

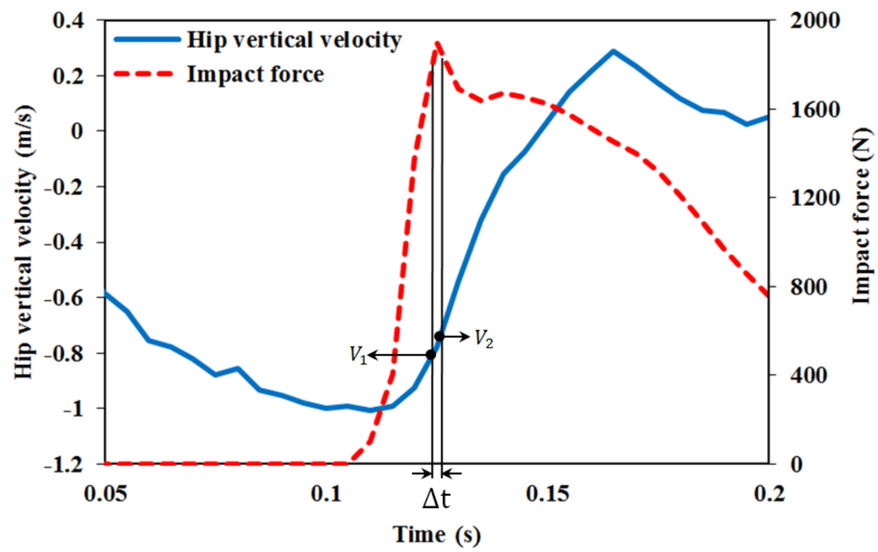

Figure 4.6. A sample of time history of the impact force and the hip vertical velocity during the impact. The selected time interval starts moving from the beginning of the impact towards the end of the impact time period to obtain the joint force time history.

Generally, the magnitude of the peak impact force determines whether a hip fracture would occur or not [120, 217-220]. To simulate the critical condition in a sideways fall, the maximum value of the impact force time history and its corresponding internal force are applied to the FE model.

4.4 Controlled and Protected Fall Tests for Model Validation

The dynamics models described in Sections 4.2 and 4.3 are validated by controlled and protected fall tests. To perform the experiments, it was asked from 150 people, mainly including graduate students and staff members in the university community. Only three graduate students were willing to participate in the fall tests. Therefore, three young male volunteers with the age of 30, 27, and 24 years were recruited in this study under a human body research ethics approval. The subjects were first scanned by a clinical DXA scanner and their whole body DXA images were obtained. Subject-specific anthropometric parameters were then calculated from their DXA images. The volunteers then participated in protected and controlled fall tests. The layout of the fall testing system is illustrated in Figure 4.7. The system mainly consisted of an electromagnetic release switch, nylon slings, a harness and six cameras that are connected to a computer-controlled motion capture system. The participants were asked not to use their arms to break the fall when they were released to mimic a realistic fall from sideways. Each participant experienced falls from different heights, i.e., $5cm$, $10cm$, $15cm$, $20cm$, $30cm$, and $40cm$. The fall height is the distance between the hip and the ground. In the falls from $5cm$, the subjects were released on the ground. For the falls from higher distance from the ground, a foam pad was placed under the hip to avoid bruising and other possible injuries. Reflective markers were put at main joints of the subject on both of the left and the right side.. After the subject was released, the motion time histories of the reflective markers were automatically recorded by the motion capture system. A data sampling rate of 200 frames per second was used in the tests. The camera placement ensured that the three-dimensional coordinates of all markers were recorded throughout the fall event. The collected motion data contained the x, y, and z coordinates of the reflective markers at different time instants during the fall process. The motion data was then used to calculate the angles (the generalized coordinates), angular velocities and angular accelerations of the links. First, the spatial coordinates of the left and the right markers were averaged to obtain the motions of the body central line. The rectangular coordinates of the central line at the head, the hip, the knee and the ankle were used to calculate the angles. Time derivatives of the angles were calculated using finite difference method [221]. In addition to the reflective markers, a force plate was placed under the impact location to record the time history of the impact force to the hip. The participants were asked to perform each experiment more than once if it was convenient for them. The first participant performed all the experiments once, however, the other participants performed most of the experiments twice. Results of the experiments are used in evaluating the dynamics model, determining the body stiffness/damping properties during the impact as described in Section 4.3.2, and calculating the joints moments in Section 4.2.

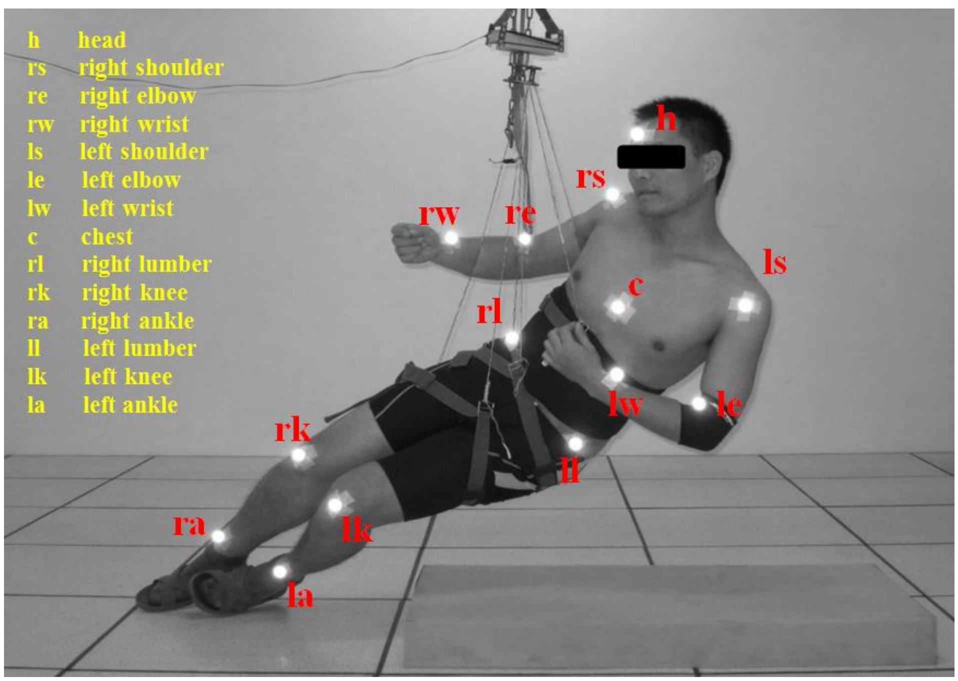

Figure 4.7. A controlled and protected fall test for validating the dynamics model in simulating a sideways fall

Chapter 5

DXA-Based Proximal Femur Finite Element Model

Finite element analysis is a powerful engineering tool to simulate the mechanical behavior of a complex structure. Prior to calculating stress/strain distributions, a set of pre-processing operations including generation of the finite element mesh, assignment of material properties, application of load/boundary conditions, and selection of failure criterion have to be performed. The recently developed DXA-based finite element model by our research group [118] is adopted and further developed in this study. As a general introduction to the model construction, in-house MATLAB codes are developed to obtain the contour of the proximal femur by extracting necessary information from the DXA image. The obtained geometry is then meshed by a two-dimensional mesh generation algorithm and the material properties are assigned using the extracted data from the DXA image. The loading and boundary conditions are applied to the constructed FE model for simulating a sideways fall. Finally, fracture risk indices are calculated at three critical cross-sections, i.e., the femoral neck, the intertrochanter and the subtrochanter. The following sections will describe in detail how to assess hip fracture risk using the DXA-based finite element modeling.

5.1 Detection of Edge and Critical Cross-Sections of the Proximal Femur

To construct a finite element model, geometric data and material property information is required which are extracted from the femur DXA image. The edge detection procedure includes femur isolation from surrounding soft tissues and the pelvis. Edge detection is performed based on the mathematical feature of the DXA image which is expressed as a matrix in MATLAB. In a DXA image after thresholding, the femur bone has positive pixel intensities whereas the background has negative ones. If the signs of neighboring pixels change from positive to negative, or vice versa, it represents the location of the boundary of the femur bone. Hence, all the boundary pixels are identified in the above way, which is shown as a red line in Figure 5.1 (b).

It is much more complicated to separate the femoral head in DXA image than in CT or MRI image because the femoral head overlaps with pelvis bone resulting in the unclearness of the edge. As the femoral head can be in general approximated by a circle, it can be fitted by three points. Instead of picking up three points manually to define the circle, two corners are identified using the so-called corner detector [222]. The third point is the apex of the femoral head that has the minimum intensity along the femoral neck axis. With the obtained femur contour, the narrowest femoral neck which has the minimum diameter can be located within a user-defined femoral neck region. Then, the femoral neck axis, which is orthogonal to the narrowest femoral neck cross-section [223], is defined and utilized to locate the apex. With the explained operations, the contour of the proximal femur has been extracted and the coordinates of the contour points have been saved. The femoral shaft axis is defined as the central line of the femoral shaft in the DXA image [224], which can be obtained by a perpendicular line at the midpoint of a shaft cross-section. However, it should be pointed out that due to the improper positioning error, the femoral shaft axis may be significantly different if only a single shaft cross-section is used. Hence, six shaft cross-sections from the distal end of the proximal femur are selected and their midpoints are utilized to define the femoral shaft axis. Finally, the intertrochanter cross-section is defined as the bisector of the neck-shaft angle [110], as shown in Figure 5.2.

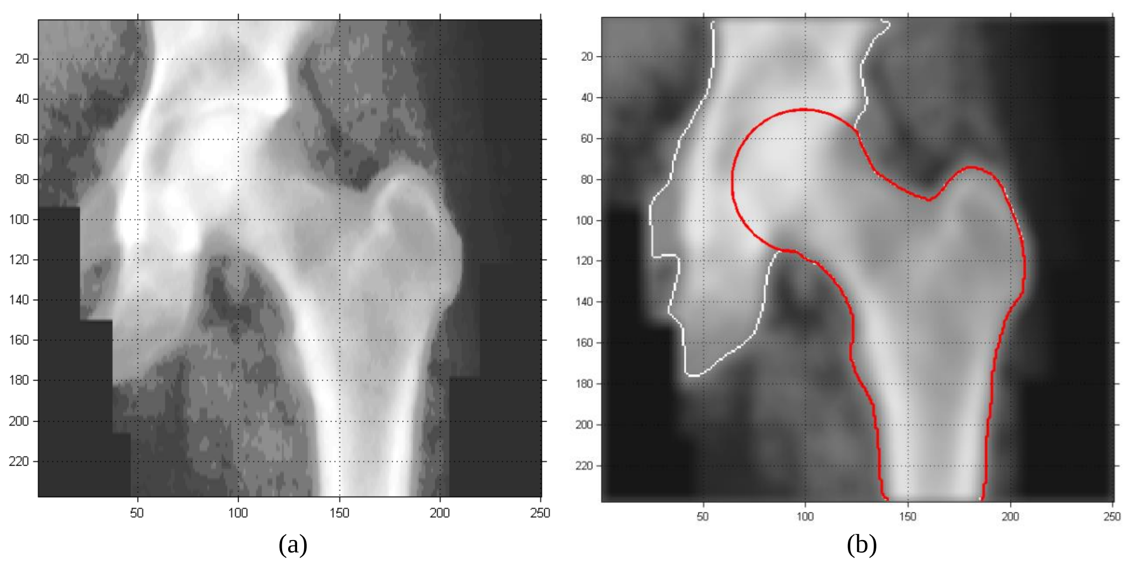

Figure 5.1. (a) Original DXA image, (b) detected contour of the proximal femur

The narrowest neck and the intertrochanter cross-section are identified using the above procedure. The femoral shaft cross-section is located at 1.5 times narrowest femoral neck, distal to intersection of the neck-shaft axes [110], as displayed in Figure 5.2.

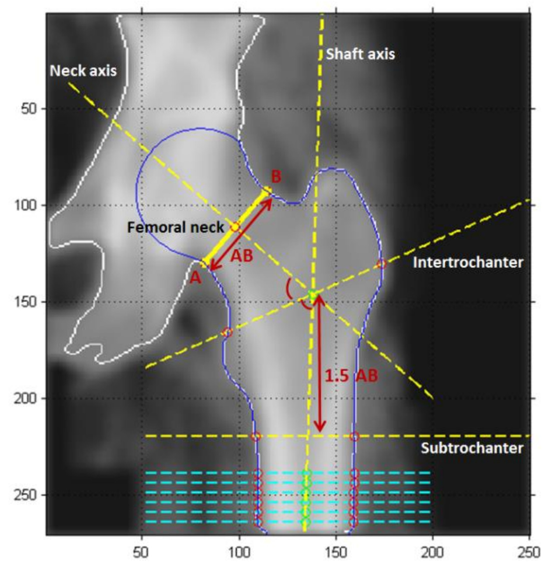

Figure 5.2. Extracted contour of the proximal femur and the three critical cross-sections

5.2 Proximal Femur Finite Element Model

The segmented proximal femur from the DXA image is used to generate the FE model. As DXA image is inherently two-dimensional, only a 2D finite element model can be constructed. The validity of using a 2D DXA-based FE model to predict the strength of a three-dimensional femur bone has been evaluated by Naylor et al. [120] and Buijs et al. [119]. By experimental validation, they demonstrated that femur stiffness and strength can be accurately calculated ($r^2 = 0.71$) by a 2D FE model constructed from a DXA scan.. Therefore, a DXA-based 2D FE model is generated in this study to analyze the proximal femur in a sideways fall. It is assumed that the 2D model has a uniform thickness and inhomogeneous material distribution.

A three-node triangular element is selected for the finite element simulation (Figure 5.3). Although the triangle element is a simple type of mesh, it is used in this study because of its ability in meshing erratic geometries. As we want to mesh the proximal femur that has sharp edges and angles, a triangular element is the best tool to reach all corners. In addition, triangular element mesh generation requires a shorter computational time that increases its applicability in biomechanical FE modeling.

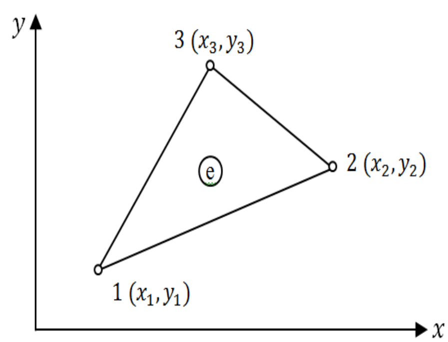

Figure 5.3. A three-node triangular element

Mesh size is a critical factor affecting the accuracy of the finite element analysis. The more refined the mesh, the more accurate the results will be. However, by considering a balance between the computational cost and the accuracy requirement, a suitable mesh size is determined based on convergence tests. Figure 5.4 shows a sample femur finite element model generated from a DXA image.

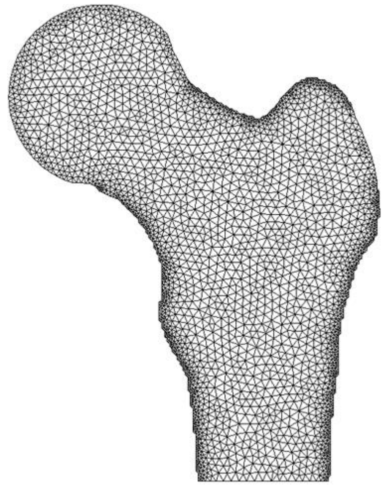

Figure 5.4. A proximal femur finite element mesh generated from a DXA image

In a 2D model, the motion of a material particle is described by two displacements in the x- and the y-direction:

$$u^{(e)} = \begin{Bmatrix} u_x^{(e)} \\ u_y^{(e)} \end{Bmatrix}. \tag{5.1}$$

The displacements are approximately expressed by shape functions ($N^{(e)}$) multiplied by the element nodal displacements ($U^{(e)}$) as

$$u^{(e)} = N^{(e)^T} \cdot U^{(e)}. \tag{5.2}$$

For a linear triangle element, $N^{(e)}$ and $U^{(e)}$ are defined as

$$\begin{gathered} N^{(e)^T} = \begin{bmatrix} N_1 & 0 & N_2 & 0 & N_3 & 0 \\ 0 & N_1 & 0 & N_2 & 0 & N_3 \end{bmatrix}, \\ U^{(e)^T} = \begin{Bmatrix} u_{x1}^{(e)} & u_{y1}^{(e)} & u_{x2}^{(e)} & u_{y2}^{(e)} & u_{x3}^{(e)} & u_{y3}^{(e)} \end{Bmatrix}. \end{gathered} \tag{5.3}$$

The shape functions are expressed by physical coordinates as follows:

$$\begin{bmatrix} N_1 \\ N_2 \\ N_3 \end{bmatrix} = \frac{1}{2A} \begin{bmatrix} (x_2y_3 - x_3y_2) & y_2 - y_3 & x_3 - x_2 \\ (x_3y_1 - x_1y_3) & y_3 - y_1 & x_1 - x_3 \\ (x_1y_2 - x_2y_1) & y_1 - y_2 & x_2 - x_1 \end{bmatrix} \begin{Bmatrix} 1 \\ x \\ y \end{Bmatrix}, \tag{5.4}$$

$$\text{where } A = \frac{1}{2}\begin{vmatrix} 1 & x_1 & y_1 \\ 1 & x_2 & y_2 \\ 1 & x_3 & y_3 \end{vmatrix}.$$

The general expression of the strain-displacement matrix (B-matrix) for a 3-node triangle element is

$$B = \begin{bmatrix} \frac{\partial N_1}{\partial x} & 0 & \frac{\partial N_2}{\partial x} & 0 & \frac{\partial N_3}{\partial x} & 0 \\ 0 & \frac{\partial N_1}{\partial y} & 0 & \frac{\partial N_2}{\partial y} & 0 & \frac{\partial N_3}{\partial y} \\ \frac{\partial N_1}{\partial y} & \frac{\partial N_1}{\partial x} & \frac{\partial N_2}{\partial y} & \frac{\partial N_2}{\partial x} & \frac{\partial N_3}{\partial y} & \frac{\partial N_3}{\partial x} \end{bmatrix}, \tag{5.5}$$

which is used to respectively determine the element strain vector and the element stiffness matrix as

$$\begin{aligned} \{\varepsilon\} &= [B]\{U^{(e)}\}, \\ [K^{(e)}] &= \int [B]^T [D][B] dV_e, \end{aligned} \tag{5.6}$$

where $[D]$ is the material property matrix.

5.3 Assignment of Material Properties

Bone essentially has anisotropic and inhomogeneous material properties due to its complex microscopic architecture and composition. However, bone anisotropy information has not been captured in DXA images. It has also been demonstrated that the assignment of isotropic or anisotropic material properties only results in small differences in the final stress/strain distributions [222]. Therefore, an isotropic inhomogeneous material model is adopted to represent the proximal femur in this study.

For a triangle element, the material matrix D has the following expression,

$$D = \frac{E}{1-\nu^2}\begin{bmatrix} 1 & \nu & 0 \\ \nu & 1 & 0 \\ 0 & 0 & \frac{1-\nu}{2} \end{bmatrix} \tag{5.7}$$

where E and ν are respectively Young's modulus and Poisson's ratio. The Poisson's ratio is taken as a constant of 0.3 [7]. To assign the material properties, the proximal femur thickness of the subject is first approximated from the width of the femoral neck. This thickness is then used to convert areal BMD to volumetric BMD ($\mathrm{vBMD} = \mathrm{BMD}/\mathrm{thickness}$) [120, 225]. Material properties are then determined from vBMD (ρ) using the empirical equation of Morgan and colleagues [226]:

$$E = 6850\rho^{1.49}, \tag{5.8}$$

where E is the Young's modulus in MPa. A sample distribution of Young's modulus is shown in Figure 5.5.

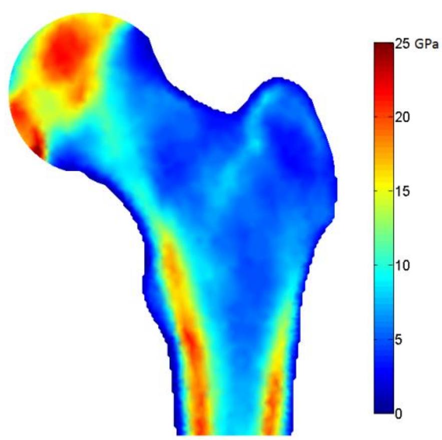

Figure 5.5. A sample distribution of Young's modulus in a proximal femur

5.4 Load and Boundary Conditions

The applied boundary and loading conditions are intended to simulate the lateral fall. In a sideways fall, the greater trochanter contacts the ground with an impact. Meanwhile, the femoral head is subjected to the joint force, i.e., the force applied from the pelvis (Figure 4.5). Two sets of load/constraint conditions are considered to perform the subject-specific and non-subject-specific simulation of a sideways fall and compare the results. In the subject-specific simulation, the impact and joint forces are respectively applied to the greater trochanter and the femoral head. The femoral shaft is fully constrained to translation. In the non-subject-specific simulation, based on the mostly used examples in literature [22, 163, 165, 219], the femoral shaft is fully constrained, the impact force is applied to the greater trochanter, and the femoral head is fixed in horizontal direction of the coronal plane. The forces are evenly distributed on the surface of the greater trochanter and the femoral head as pressure loads. Figure 5.6 shows the load/constraint conditions in subject-specific and non-subject-specific simulations.

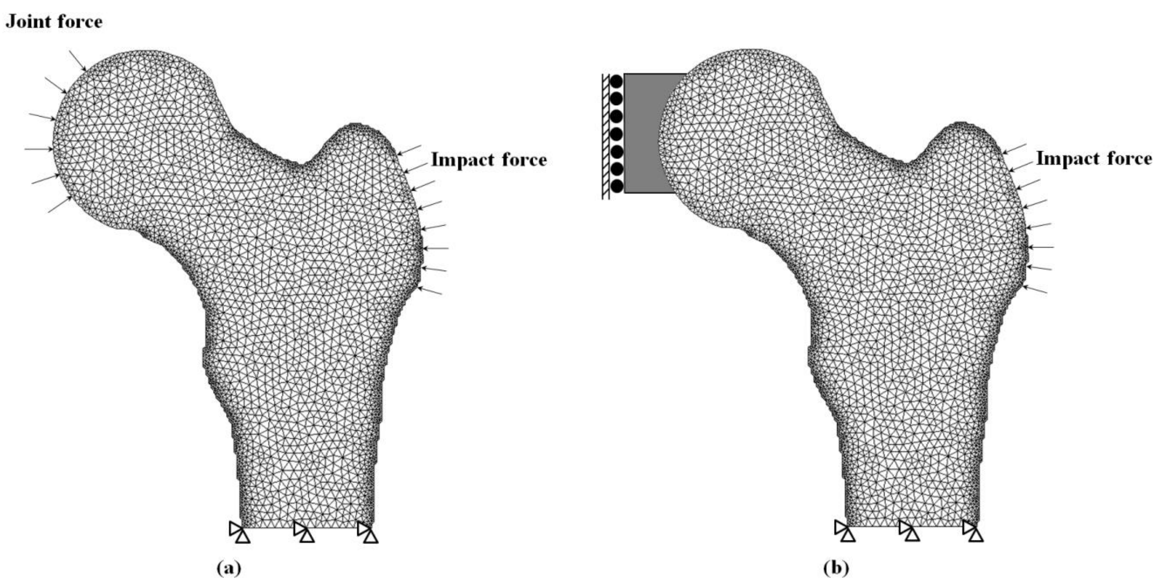

Figure 5.6. Load/constraint conditions in simulating the lateral fall. (a) The subject-specific simulation: the femoral shaft is fully constrained; the impact and the joint forces determined by the dynamics model are respectively applied to the greater trochanter and the femoral head. (b) The non-subject-specific simulation: the impact force determined by empirical functions is applied to the greater trochanter; the femoral shaft is fully constrained and the femoral head is constrained in the horizontal direction of the coronal plane [141].

5.5 Hip Fracture Risk Index at the Three Critical Cross-sections

In order to be consistent with the clinical practices, i.e., using the average BMD over a region of interest, and to enhance the short-term repeatability of the calculations, fracture risk is obtained in critical ROIs of the proximal femur [136]. In Figure 5.7, the dashed blue lines are the boundary of the ROIs which have been defined in Section 5.1.

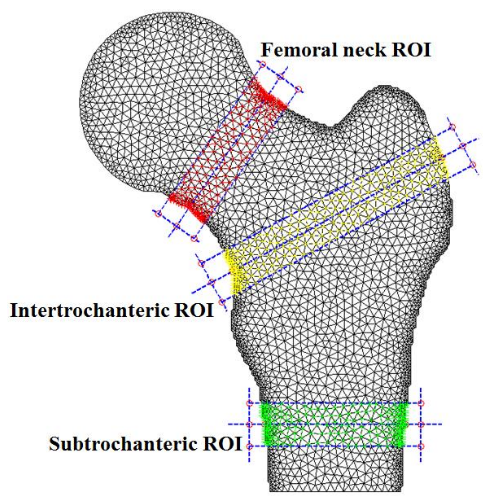

Figure 5.7. Three critical regions of the proximal femur

After defining the ROIs, a failure criterion should be selected. One commonly used criterion for determining material integrity in the domain of biomechanics is the von Mises criterion [136-138, 155]. Based on the von Mises theory, even though none of the principal stresses exceeds the yield stress of the material, yielding is still possible for the combination of stresses [227]. This criterion defines whether the stress combination at a given point will cause failure or not. For our model, the von Mises stress σ_{VM} is defined by the three stress components as [227]

$$\sigma_{von-Mises} = \frac{1}{\sqrt{2}}\sqrt{\left(\sigma_x - \sigma_y\right)^2 + \sigma_x{}^2 + \sigma_y{}^2 + 6\tau_{xy}{}^2}. \tag{5.9}$$

The yield stress (σ_Y), obtained from the empirical equation of Morgan and colleagues [228] is used to determine the bone failure. After calculating the actual and ultimate stresses by the finite element analysis, the FRI over an ROI is obtained as [136]

$$\eta_{ROI} = \frac{\sum_i^N \int \frac{\sigma_{VM}}{\sigma_Y} dA}{\sum_1^N A_i} \tag{5.10}$$

where A_i $(i = 1,2, \dots, N)$ are the areas of the finite elements encompassed in the specific ROI.

Chapter 6

Results and Discussion

All the results obtained in this study are reported in this chapter. Section 6.1 presents the results of estimating body anthropometric parameters from DXA images. Results of the dynamics model in predicting the position, velocity, and acceleration of the hip during a sideways fall are compared with the experimental data of the three participants in Section 6.2. Section 6.3 reports the results of the proposed model in determining the FRIs of 80 women and 50 men and investigates the effect of body habitus on hip fracture risk.

6.1 Estimation of Body Segment Anthropometric and Dynamics Parameters

Three volunteers participated in fall experiments to obtain the kinematics of body segments during a sideways fall and to measure the applied force to the hip during the impact. Their anthropometric parameters are determined using the proposed method in Section 4.1 as listed in Table 6.1.

Table 6.1. Subject anthropometric parameters identified from the whole body DXA images

Subject		1	2	3
Segment Length (m)	Shank	0.431008	0.427708	0.43978
	Thigh	0.446272	0.42953	0.464901
	Trunk	0.85272	0.862762	0.855319
Body Height (m)		1.73	1.72	1.74
Segment Mass (kg)	Shank	8.064401	7.440908	6.966644
	Thigh	20.13896	18.90323	18.72842
	Trunk	48.43878	44.8866	37.82738
Body Mass (kg)		77	72	64
Segment Mass Center (l')	Shank	0.244431	0.232716	0.242857
	Thigh	0.264029	0.255202	0.281402
	Trunk	0.354687	0.365823	0.352015
Segment Mass Moment of Iner-tia (kgm^2)	Shank	0.130673	0.128419	0.142413
	Thigh	0.306119	0.251342	0.300008
	Trunk	2.396565	2.194685	1.837087

One of the advantages of the proposed model in determining the anthropometric parameters is that it is applicable for all formats of clinical DXA images (e.g., MAT and JPG). A change in the range of attenuated coefficients, which is DXA machine dependent, does not affect the accuracy of the proposed method in estimating the body segments properties. The reason is that the mass constant is determined from the subject's whole body DXA image and therefore, all the factors affecting the attenuated energy in the imaging process are implicitly considered in calculations.

6.2 Validation of the Dynamics Model

First, the dynamics model is used to predict the body segments kinematics before the impact. The impact model is subsequently used to predict the impact force to the hip. Results of the dynamics and the impact model are then compared with findings of experiments to evaluate the accuracy of the proposed models in simulating a sideways fall.

As the motion of the hip has a direct effect on the impact force, the kinematics at the hip is used as a baseline for the validation. A sample of predicted and the experimentally measured time histories of the hip vertical position, velocity, acceleration, and the impact force of the three volunteers are displayed in Figures 6.1-6.3.

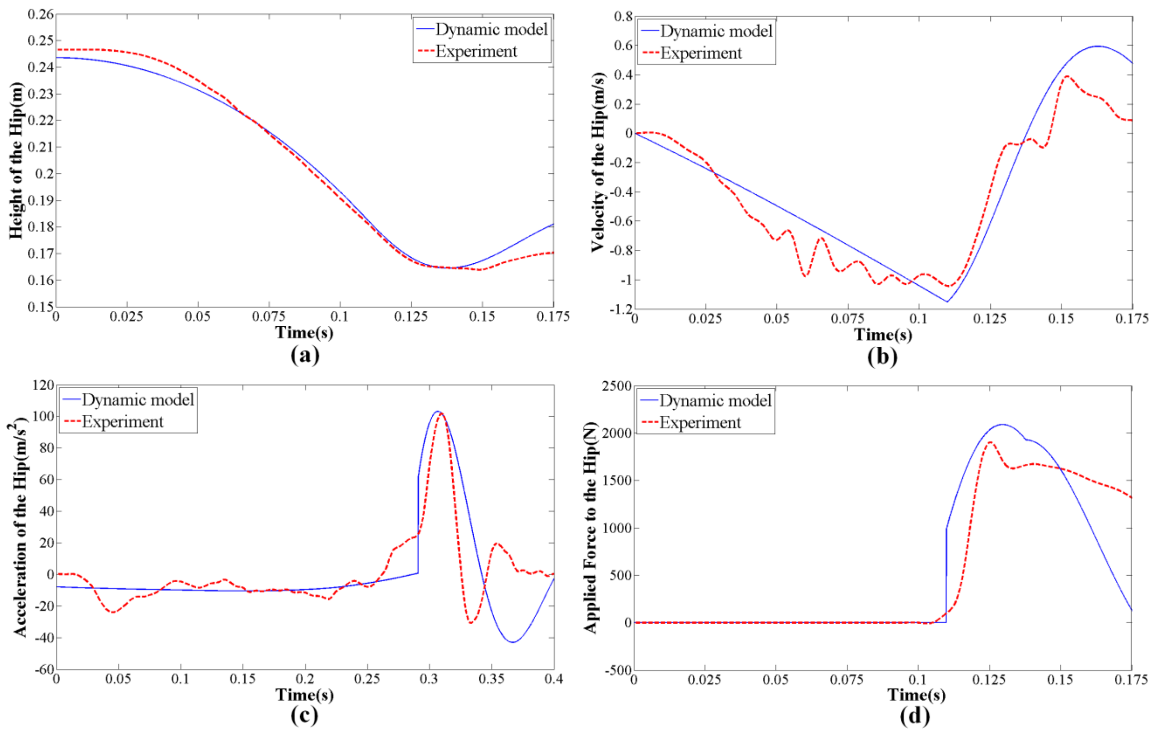

Figure 6.1. **Subject #1**. (a) Hip vertical position; (b) hip vertical velocity; (c) hip vertical acceleration; (d) impact force to the hip in the fall from 5cm without protective pad

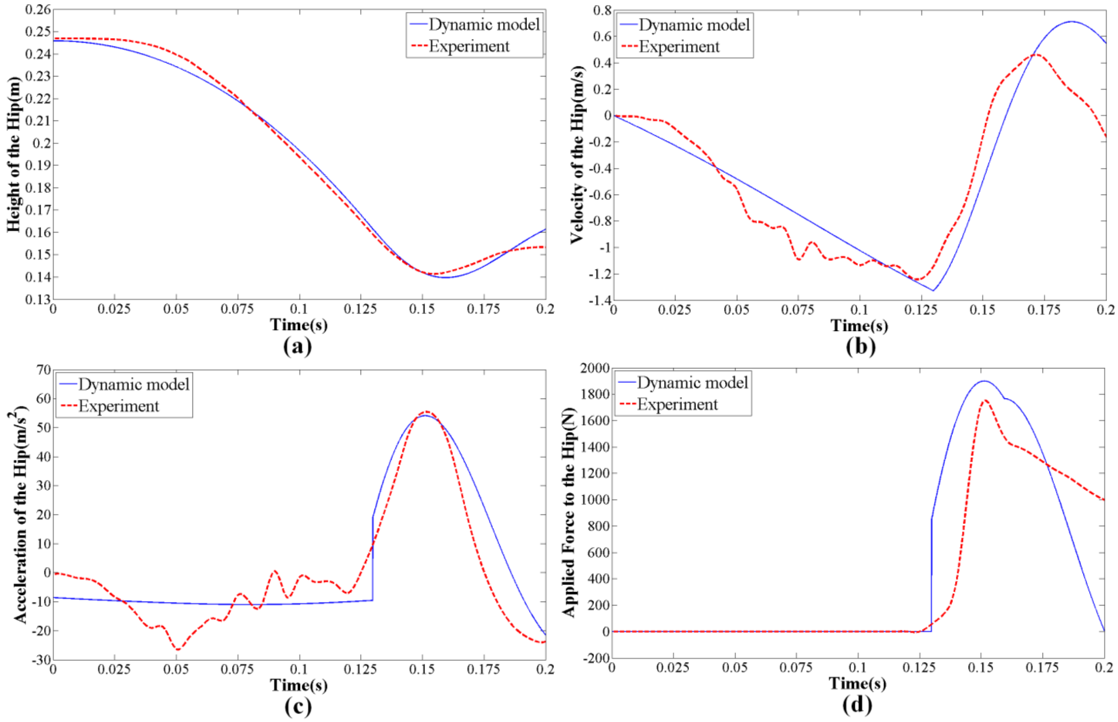

Figure 6.2. **Subject #2**. (a) Hip vertical position; (b) hip vertical velocity; (c) hip vertical acceleration; (d) impact force to the hip in the fall from 5cm without protective pad

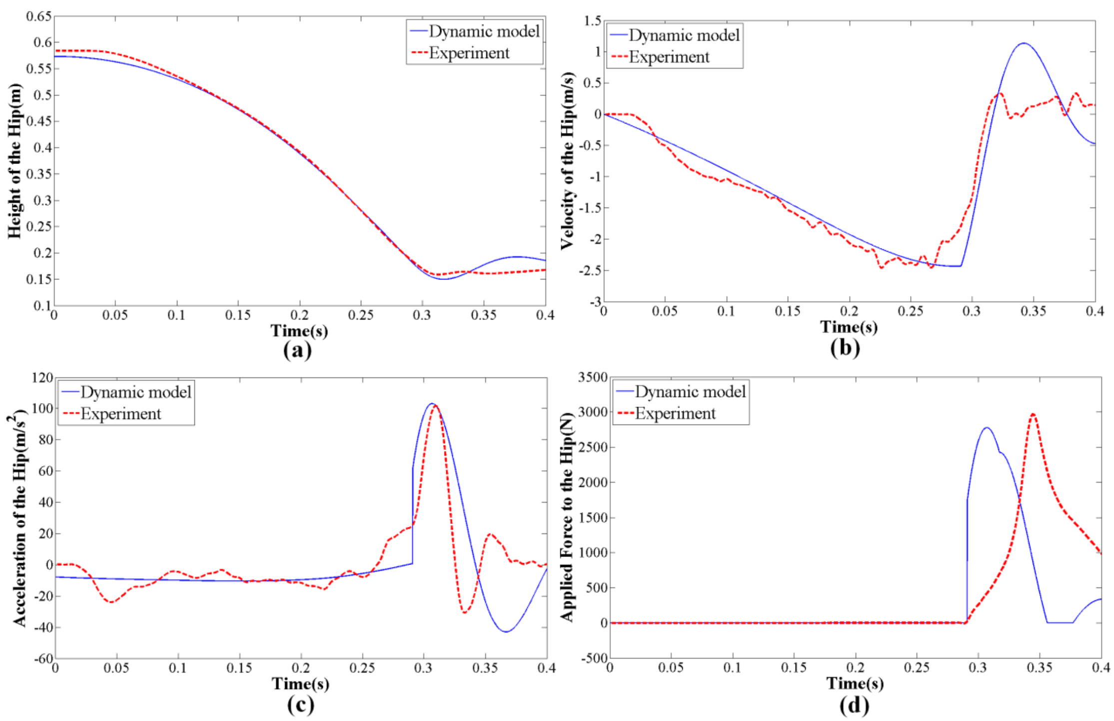

Figure 6.3. **Subject #3**. (a) Hip vertical position; (b) hip vertical velocity; (c) hip vertical acceleration; (d) impact force to the hip in the fall from 30cm with protective pad

The maximum impact force to the hip, induced in a sideways fall, is a critical factor to predict the hip fracture risk [20, 133, 134, 229]. The impact velocity is also an effective parameter which represents the severity of the fall and can widely affect the magnitude of the impact force. For the validation purposes, the predicted maximum hip vertical velocity and peak impact force for each volunteer are compared to the corresponding experimental results as shown in Table 6.2.

Table 6.2. Comparison between the dynamics model and experimental results in determining the maximum hip vertical velocity and peak impact force in sideways falls from different heights for 3 subjects. G stands for the fall on the ground and F stands for the fall on the protective pad. The number after G/F denotes the fall height in cm. The information of some of the trials is not available due to technical problems.

Subject	Trial	Max. Hip Vertical Velocity (m/s)			Peak Impact Force (N)		
		Dynamics Model	Experiment	Relative Error (%)	Dynamics Model	Experiment	Relative Error (%)
1	G5	-1.153	-1.063	8.4	2090.1	1900.8	9.9
	F5	-1.261	-1.198	5.3	2455.4	2304.1	6.5
	F10	-1.458	-1.332	9.5	2840.5	2545.5	11.5
	F15	-1.932	-1.803	7.1	3172.1	2891.8	9.7
	F20	2.163	-1.991	8.6	2641.6	2392.5	10.4
	F30	-	-	-	-	4389.0	-
	F40	-2.859	-2.679	7.5	5652.8	5213.6	8.4
2	G5	-1.328	-1.236	7.4	1899.6	1714.4	10.8
	F5	-	-	-	-	1837.9	-
	F10	-1.760	-1.653	6.5	2390.4	2215.8	7.9
		-1.775	-1.622	9.4	2512.8	2265.4	11.0
	F15	-	-	-	-	2299.8	-
	F20	-1.927	-1.824	5.6	2456.1	2268.7	8.0
		-1.957	-1.788	9.4	2662.7	2392.5	11.3
		-	-	-	-	2371.2	-
	F30	-2.493	-2.305	8.1	3020.7	2761.1	9.4
		-2.229	-2.097	6.2	3352.5	3063.0	9.5
	F40	-2.398	-2.235	7.3	4264.5	3312.6	10.5
		-	-	-	-	2946.4	-
3	G5	-	-	-	-	1654.6	-
		-	-	-	-	1420.5	-
	F5	-1.210	-1.127	7.3	1748.2	1606.2	8.8
		-	-	-	-	1441.7	-
	F10	-1.613	-1.489	8.3	1952.7	1786.0	9.3
		-1.697	-1.596	6.3	2247.9	2042.8	10.0
	F15	-2.088	-1.953	6.9	2867.7	2641.4	8.5
		-2.157	-1.953	10.4	3244.8	2893.9	12.1
	F20	-2.231	-2.186	2.1	3109.3	2934.6	5.9
		2.405	-2.261	6.4	3255.8	2971.0	9.6
	F30	-2.434	-2.493	2.3	2777.4	2961.8	6.2
		-2.458	-2.376	3.4	3218.4	2990.3	7.6
	F40	-	-	-	-	3856.3	-
		-2.631	-2.943	10.6	3014.5	3390.0	11.1

Then, results of our model are compared with findings of a currently available model in the literature [133] to investigate the effect of considering subject-specific anthropometric and dynamics parameters on simulating sideways falls. The available model in the literature predicted the maximum impact velocity and force in a sideways fall for 5th percentile (short and light) and 95th percentile (tall and heavy) females. Table 6.3 compares the accuracy of our subject-specific and the available non-subject-specific model in predicting the maximum hip vertical velocity and peak impact force.

Table 6.3. Comparison between the proposed subject-specific and the existing non-subject-specific model in predicting the hip vertical velocity and the peak impact force

Model	Average Relative Error (%)	
	Max. Hip Vertical Velocity	Peak Impact Force
Subject-specific model	7.2	9.3
Non-subject-specific model [133]	40.1	35.4

Compared with the non-subject-specific dynamics model , the prediction accuracy has been greatly improved by our subject-specific model. Table 6.3 shows that the relative errors in the predicted hip vertical velocity and peak impact force have been reduced in average from 40.1% and 35.4% to 6.1% and 8.9%, respectively. The improvements have been achieved mainly due to the use of subject-specific anthropometric parameters in predicting the kinematic and kinetic variables in a sideways fall. Also, considering the subject-specific stiffness/damping properties of the impact model has improved the accuracy of results. In addition, removing the limitations of the adopted dynamics model, including the restrictions for the length of the shank and the thigh and the location of mass center of body segments, has effect on the improvement of the model accuracy. Furthermore, considering the subject-specific impact moment based on the hip width of the patient and the body configuration before the impact may have effect on reducing the overestimated impact velocity and subsequently the overestimated impact force.

By examining the governing equations of motion and the energy expressions in Chapter 4, it can be understood that there are basically three groups of variables involved in the dynamics of a sideways fall. The first group consists of kinematic variables such as the link rotation angles and angular velocities in a sideways fall, which are determined by solving the governing equations of motions of the dynamics model. The second group is the system parameters such as the effective mass, stiffness, and damping coefficients in the impact model. The third group includes anthropometric parameters such as the segments length, mass, mass center and mass moment of inertia. These segmental anthropometric parameters are not only affected by the subject's overall physiological attributes such as body weight and body height, but also by the distribution of the body mass. Two subjects having the same weight and height but different shapes, for example, longer trunk vs. longer lower extremity, pear-shaped vs. upside-down pear-shaped, may have different segmental anthropometric parameters. The differences affect the body segments kinematics in a fall, e.g., the hip velocity, via the governing equations, and thus also affect the impact force. From the impact model shown in Figure 4.4 and the expression in Eq. (4.11-4.13), the impact force is explicitly related to the hip vertical velocity and the effective mass. The effective mass is in turn related to other kinematic variables and anthropometric parameters via the expressions in Appendix B. Therefore, a person would suffer different impact forces in different falls, if the body configurations before the impact are different. It justifies the need for a subject-specific model to predict the fall-induced impact force to the hip. In this study, the impact force is determined by considering both anthropometric parameters and kinematic variables of the body segments just before the impact.

6.3 Results of the Proposed Biomechanical Model in Predicting FRIs

The introduced DXA-based finite element model is linked to the dynamics and the impact model to investigate the hip fracture risk in 130 clinical cases. First, the optimized mesh size of the FE model is determined conducting convergence tests. Second, FRIs in critical ROIs are calculated under subject-specific and non-subject-specific loading conditions. Third, the effect of subject-specific loading condition on hip fracture risk assessment is investigated and results are compared with clinical observations.

6.3.1 Convergence test

Although finer meshes come with accuracy, however, more calculation time and large memory are needed. It is desired to find the minimum number of elements that gives a converged solution. Convergence tests are thus conducted to find out a mesh size that can meet both the accuracy and the computational cost requirement. To perform the convergence tests, the simulation begins with a mesh discretization and the result is recorded. Then, the simulation is repeated with a finer mesh, i.e., more elements, and results are compared with findings of the previous test. If the results are nearly similar, then the first mesh is good enough to solve our problem with the specific geometry, loading, and constraints. If the results differ by a large amount however, a finer mesh is tried. For the three critical cross-sections described in Section 5.1 and the whole proximal femur, the variations of calculated FRIs versus the number of nodes in the FE hip model are plotted in Figure 6.4.

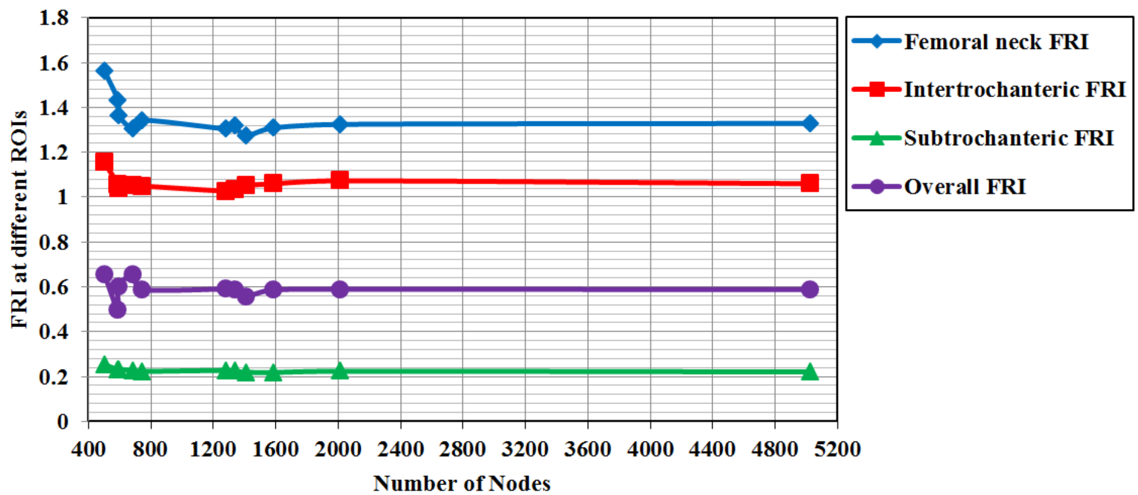

Figure 6.4. Variations of FRIs with the number of nodes at the femoral neck, intertrochanter, subtrochanter and the whole-proximal femur

6.3.2 Comparison between the Dynamics Model and Existing Empirical Functions in Predicting the Impact Force

Hip fracture depends on various anthropometric parameters such as body height, body weight, body segments mass center, and trochanteric soft tissue thickness. Therefore, patients with different body habitus are exposed to a wide range of hip fracture risk. To show the effectiveness of our model, we retrieved 130 subjects including 80 females with the mean age of 53.7 ± 19.9 $(20.1 - 87.8)$ years and 50 males with the mean age of 39.8 ± 22.1 $(16.0 - 86.0)$ years. Both whole-body and hip DXA image of all 130 subjects were available and none of the individuals had experienced a hip fracture. The subjects are of varying body habitus, in terms of body weight and body height, to investigate the effect of body parameters on impact force and hip fracture risk. To be consistent with the studies reported in the literature, the 80 female and 50 male subjects are separately categorized into four groups of BMI, i.e., underweight (BMI $<$ 18.5), normal (18.5 $<$ BMI $<$ 25), overweight (25 $<$ BMI $<$ 30) and obese (BMI $>$ 30), according to the WHO criteria [230]. Body parameters of the female and male subjects are respectively listed in Tables 6.4 and 6.5.

Table 6.4. Mean (SD) body parameters of female subjects across BMI groups

BMI groups	Number of subjects	Age (years)	BH (cm)	BW (kg)	BMI (kg/m^2)	STT (mm)	BMD (g/cm^2)	K (kN/m)	C (N.s/m)
Underweight	5	51.2 (21.1)	156.8 (8.4)	40.8 (5.1)	16.6 (1.2)	24.3 (10.2)	0.739 (0.123)	41.5 (18.8)	303.9 (19.4)
Normal	34	50.4 (23.1)	157.9 (10.2)	56.2 (8.0)	22.5 (1.9)	44.7 (16.6)	0.769 (0.126)	22.7 (9.1)	330.8 (15.7)
Overweight	17	63.7 (16.0)	156.6 (7.5)	66.3 (8.3)	26.9 (1.5)	55.5 (11.9)	0.847 (0.181)	17.4 (3.6)	341.9 (9.9)
Obese	24	51.8 (15.6)	158.3 (4.7)	90.7 (20.1)	35.9 (5.7)	73.4 (25.3)	0.935 (0.194)	14.2 (4.5)	353.6 (16.1)
Total	80	53.7 (19.9)	157.7 (10.1)	67.7 (20.6)	27.1 (7.2)	54.3 (23.3)	0.834 (0.175)	20.2 (10.2)	338.4 (19.8)

Table 6.5. Mean (SD) body parameters of male subjects across BMI groups

BMI groups	Number of subjects	Age (years)	BH (cm)	BW (kg)	BMI (kg/m^2)	STT (mm)	BMD (g/cm^2)	K (kN/m)	C (N.s/m)
Underweight	6	23.9 (8.8)	172.6 (8.6)	52.5 (5.5)	17.6 (0.4)	20.3 (5.3)	0.837 (0.146)	46.2 (3.8)	399.6 (60.6)
Normal	18	30.1 (19.4)	169.3 (11.0)	60.7 (7.2)	21.0 (1.8)	36.3 (18.6)	0.990 (0.212)	39.3 (5.4)	552.7 (157.8)
Overweight	20	50.3 (21.9)	169.2 (10.2)	78.5 (12.2)	27.3 (1.6)	64.5 (13.2)	0.874 (0.180)	31.4 (2.1)	791.4 (95.3)
Obese	6	49.6 (20.1)	168.5 (8.8)	88.3 (6.3)	31.4 (1.1)	71.8 (14.9)	0.952 (0.192)	30.3 (2.0)	843.3 (102.9)
Total	50	39.8 (22.1)	169.7 (9.9)	70.2 (14.9)	24.4 (4.6)	49.9 (23.1)	0.921 (0.195)	35.9 (6.6)	664.7 (193.1)

Although this study proposes the first subject-specific model to predict the fall-induced impact and joint forces, there are also empirical functions in the literature to predict the impact force in a sideways fall. As body anthropometric parameters, effect of hip soft tissues in absorbing the impact energy, and kinematic/kinetic variables in fall are not considered in the empirical functions, they are called non-subject-specific methods. To compare our model with currently available methods, the most common non-subject-specific methods in the literature are used to predict the impact force for the clinical cases as follows:

1) The equation proposed by Kroonenberg et al. [133] as

$$F_{peak} = 9.81 \times EM \times (n \sin \omega - \cos \omega + 1), \tag{6.1}$$

where $n = V \frac{\sqrt{(\frac{71000}{EM})}}{9.81}$, $V = 2.72\sqrt{h}$, and $\omega = \pi - tan^{-1} n$. EM is the effective mass which is 0.35 of body weight, V is the impact velocity, and h is the body height.

2) The empirical equation proposed by Robinovitch et al. [134] and extrapolated by Yoshikawa et al [132] as

$$F_{peak} = 8.25 \times W \times \sqrt{\left(\frac{h}{170}\right)}, \tag{6.2}$$

$$h\ (body\ height) in\ cm\ and\ W\ (body\ weight)\ in\ Newton.$$

It should be pointed out that these empirical functions are being adopted to predict the fracture risk for our study population in a way that was not intended by the original authors. Results of the above mentioned methods are respectively called non-subject-specific 1 (Kroonenberg) and 2 (Yoshikawa).

Figure 6.5 shows the comparison between predicted impact force by our model and non-subject-specific methods for each BMI group of men and women.

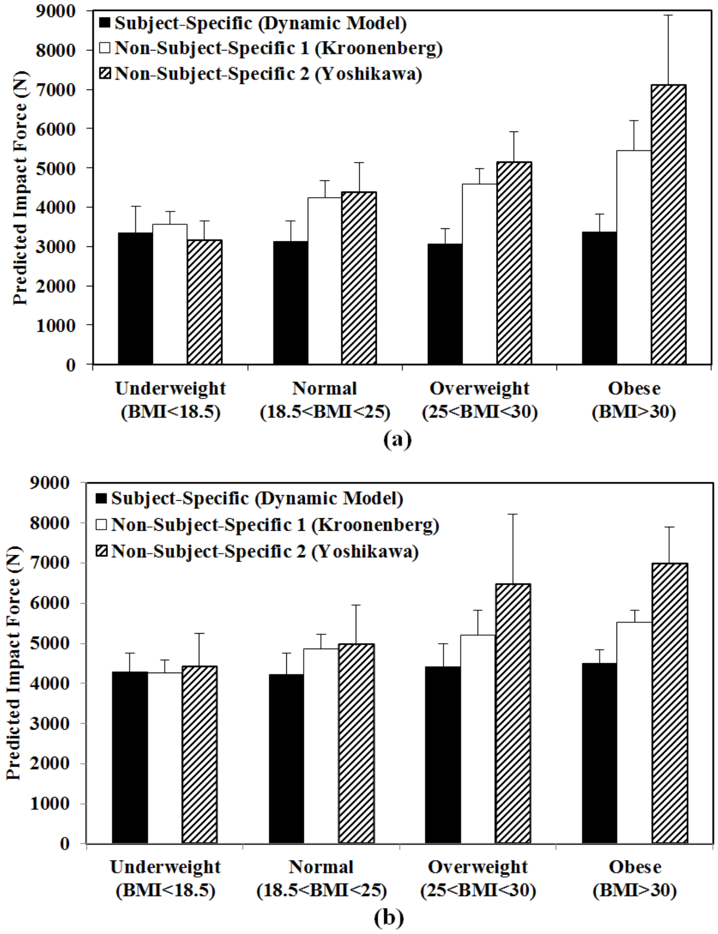

Figure 6.5. Mean value of predicted impact force for underweight, normal, overweight and obese subjects by the subject-specific and the non-subject-specific methods for (a) female and (b) male subjects

As shown in Figure 6.5, predicted impact forces by the subject-specific model and the non-subject-specific methods are in a similar range for underweight subjects in both genders. For high BMI subjects, however, a big difference is observed.

In the second empirical equations, the only considered parameters are total body weight and height while all other segmental anthropometric parameters, such as segments length, masse, mass center and mass moment of inertia are taken into account in the subject-specific dynamics model. Also, in our subject-specific model, the effect of STT is considered in determining the stiffness and the damping properties of the impact model; while the non-subject-specific methods neglect the effect of STT in attenuating the impact energy. Robinovitch and colleagues [229] proposed another approach to take the effect of STT into account in calculating the impact force. They suggested that for each 1 mm increase in tissue thickness, the peak force decreases by approximately 71 N. However, this estimation is valid only for subjects with 8-45 mm trochanteric soft tissue thickness and is not recommended for outside 8-45 mm measurement range. There were several subjects among our study population with STT greater than 45 mm and therefore, the effect of STT should be considered in calculating the stiffness/damping properties of the impact model. However, subject-specific segmental anthropometric parameters and energy absorbing capacity of the hip soft tissues are not considered in the empirical functions. In obese subjects, shapes of body segments and soft tissue thickness are considerably different from normal subjects which significantly affect the predicted loading conditions. That is a possible reason why results of the subject-specific dynamics model and the non-subject-specific empirical functions are substantially different for high BMI subjects. It should be pointed out that among non-subject-specific methods, the results of Kroonenberg’s method are generally closer to the findings of the subject-specific model.

Correlation coefficients between the impact force and individual factors including body weight, body height, BMI, STT, and effective mass are listed in Table 6.6. Positive correlations between body weight, body height, and the impact force in both subject-specific and non-subject-specific models demonstrate the direct effect of these factors on the applied force to the hip in a lateral fall. Greater body weight increases the available potential energy during the fall which is converted to the kinetic energy during the impact and increases the impact severity. Heavier body weight may also increase the effective mass during the impact which considerably affects the applied force to the femur. Body height has also a direct effect on the impact velocity [133] and therefore taller subjects are more likely to experience a severer impact in a fall.

The correlation between the impact force and STT is positive in both non-subject-specific methods while it is negative in our subject-specific model. The reason is that STT does not interfere the calculations in the non-subject-specific empirical equations. Our results are in agreement with findings of previously reported researches. Majmder et al. [175] reported that the decrease in soft tissue thickness has a direct effect on increased impact force. Robinovitch et al. [229] also demonstrated that STT has a remarkable effect on absorbing the impact energy. In addition, Etheridge et al. [220] showed that trochanteric STT significantly influences the absorbed energy and load distribution during a sideways fall.

Table 6.6. Correlation coefficient r (p value) between the impact force and individual factors in women and men

		BW	BH	BMI	STT	Effective mass
Women	Subject-specific impact force	0.32 (<0.005)	0.43 (<0.001)	0.15 (>0.05)	-0.27 (<0.05)	0.35 (<0.05)
	Non-subject-specific impact force 1	0.98 (<0.001)	0.59 (<0.001)	0.81 (<0.001)	0.74 (<0.001)	0.98 (<0.001)
	Non-subject-specific impact force 2	0.99 (<0.001)	0.52 (<0.001)	0.85 (<0.001)	0.76 (<0.001)	0.95 (<0.001)
Men	Subject-specific impact force	0.63 (<0.001)	0.76 (<0.001)	0.25 (>0.05)	-0.17 (>0.05)	0.69 (<0.001)
	Non-subject-specific impact force 1	0.98 (<0.001)	0.61 (<0.001)	0.71 (<0.001)	0.41 (<0.01)	0.97 (<0.001)
	Non-subject-specific impact force 2	0.94 (<0.001)	0.71 (<0.001)	0.60 (<0.001)	0.39 (<0.01)	0.93 (<0.001)

Results of non-subject-specific methods show that the fall-induced impact force is proportional to the BMI which indicates that higher BMI subjects experience much greater impact force in a sideways fall. However, such a strong association between the BMI and the subject-specific impact force is not observed, although this association is still positive ($r = 0.15$, $p > 0.05$ in women, $r = 0.25$, $p > 0.05$ in men). Increases in BMI are typically associated with increased total body and effective mass, which results in elevated impact loads [231]. However, body mass index is positively associated with thickness of the soft tissue overlying the greater trochanter which increases the impact energy absorption [232]. Relatively high STT in high BMI subjects may underlie the positive but weak association between the BMI and the subject-specific impact force.

Table 6.6 shows that the body weight is the most dominant factor in determining the impact force in the empirical functions for both men and women; while a complex combination of factors affects the results of our model. Correlations between the body parameters and the impact force predicted by the two empirical functions are quite similar for both genders. However, differences are observed between the results of our model for men and women. In male subjects, the correlation between body weight and impact force is stronger than that in female subjects. Potential reasons are two-fold. First, there is a stronger association between body weight and STT in women ($r = 0.77$) than in men ($r = 0.58$). It demonstrates that women with higher BW have thick hip soft tissues which absorb a great amount of energy during the impact and compensate the effect of BW on increased impact force; while heavy men do not have such trochanteric soft tissue thickness. Therefore, the thickness of trochanteric soft tissues in heavy men is not sufficient to overcome the effect of BW on increased impact force. A similar scenario exists for BH.

The second probable reason is differences in correlations between hip stiffness/damping properties and STT in men and women. Men with higher BW and BH not only have thinner trochanteric soft tissues than women, their hip soft tissues are stiffer. In the other words, if a man and a woman with the same trochanteric soft tissue thickness and the same effective mass experience a sideways fall with the same impact velocity, the applied impact force to the woman's femur is lower than that in the male subject [231]. Therefore, the absorbed energy by hip soft tissues in heavy and tall men is not as much as that in women and thus BW and BH in men have a stronger effect on the impact force.

Figure 6.6 compares the impact force predicted by our subject-specific model for male and female subjects in each BMI category. The average value of the predicted impact force by our subjects-specific model is higher for men (4332.8$\pm$522.6 N) compared to that of women (3200.6$\pm$517.3 N). It may be attributed to the thicker hip soft tissues of women (54.3$\pm$23.3 mm) compared to that of men (49.8$\pm$23.1 mm) and also greater body height and body weight of male subjects than those of female subjects (body height: 169.6 ± 9.9 cm vs. 157.7 ± 10.1 cm; body weight: 70.17 ± 14.9 kg vs. 67.7 ± 20.6 kg).

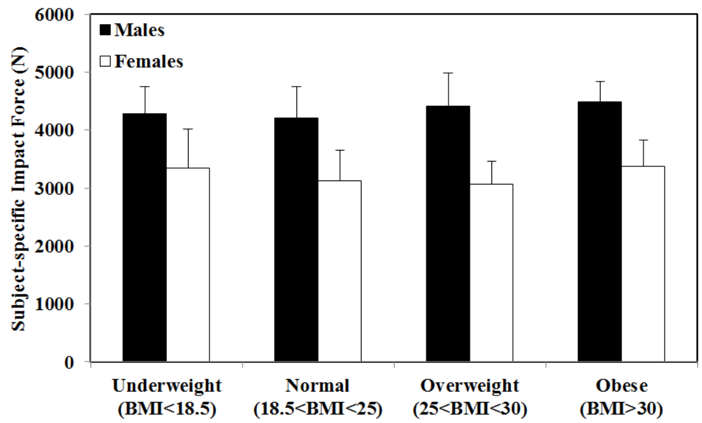

Figure 6.6. Mean value of the sideways fall-induced peak impact force for male and female subjects across BMI groups

6.3.3 Effect of Subject-Specific Loading on Assessing Hip Fracture Risk

To investigate the effect of loading conditions on hip fracture risk assessment, the determined impact forces by the subject-specific dynamics model and the empirical functions are applied to the presented DXA-based proximal femur FE model. As it is mentioned in Section 5.4, two load/constraint conditions are considered to simulate the lateral fall. In the subject-specific simulation, the impact and joint forces are respectively applied to the greater trochanter and the femoral head. In the non-subject-specific simulation, the impact force is applied to the greater trochanter and the femoral head is fixed in horizontal direction of the coronal plane. The distal end of the proximal femur is completely fixed in both simulations. FRIs in critical locations of the proximal femur are obtained for the 80 women and the 50 men under the both load/constraint conditions. Figure 6.7 shows the mean value of the FRIs in all critical ROIs using the subject-specific and non-subject-specific methods.

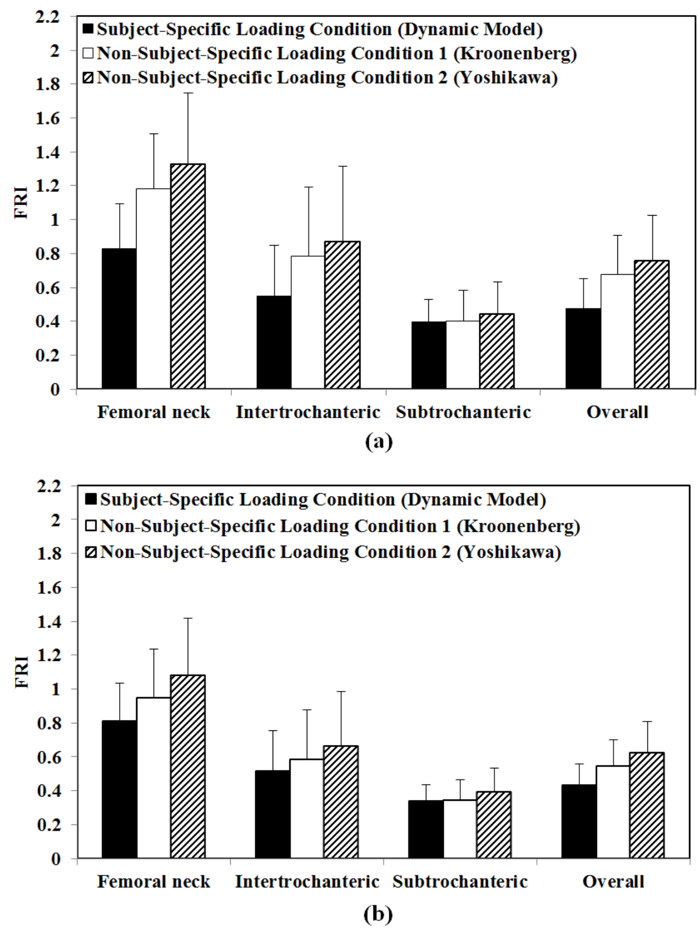

Figure 6.7. Mean value of predicted FRIs in critical ROIs and the whole proximal femur under subject-specific and non-subject-specific loading conditions for (a) 80 women and (b) 50 men

As shown in Figure 6.7, femoral neck FRI is greater than fracture risk at other locations. It demonstrates that the femoral neck is the most critical region of the proximal femur. To investigate the effect of loading conditions on hip fracture risk, FRIs at critical ROIs for all BMI groups of women and men are calculated and the results are shown in Figures 6.8 and 6.9.

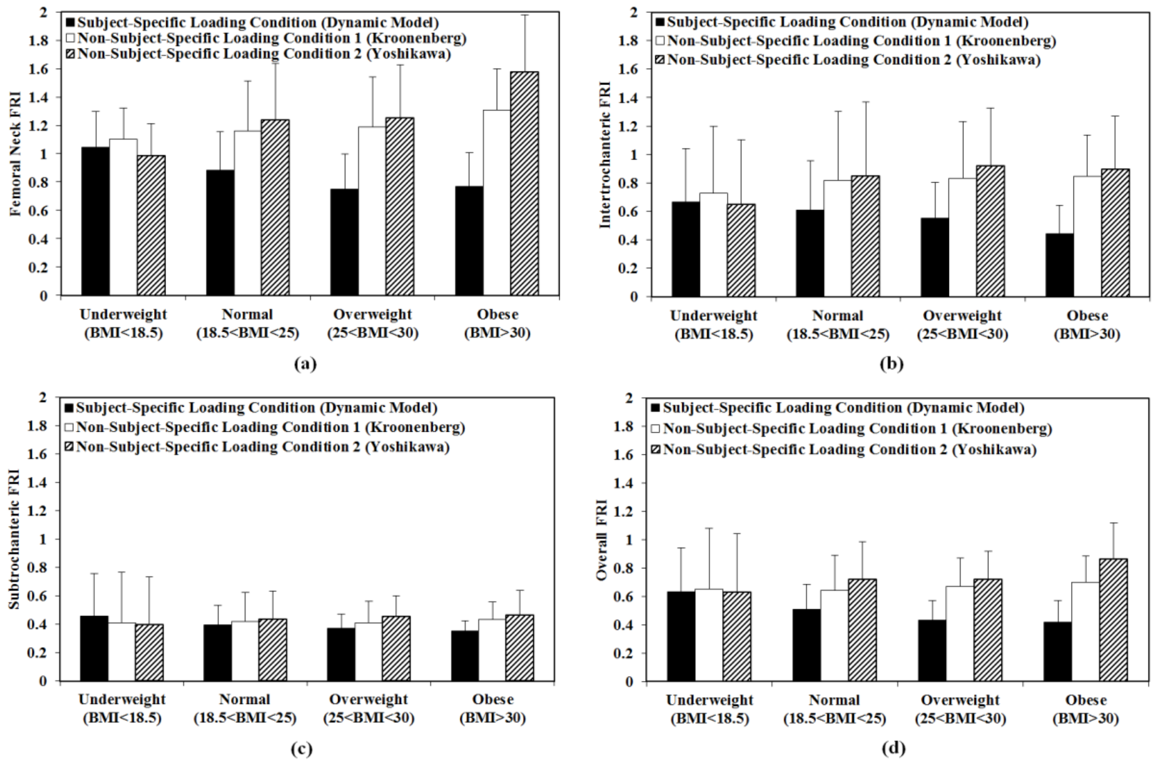

Figure 6.8. Mean value of FRIs at (a) the femoral neck, (b) the intertrochanter, (c) the subtrochanter, and (d) the whole proximal femur for the four BMI groups of female subjects, predicted by the subject-specific and non-subject-specific (1 and 2) methods [141]

The predicted FRIs in all critical ROIs by the subject-specific model and the non-subject-specific methods are in a similar range for underweight women. For higher BMI women, however, a big difference is observed. Figure 6.8 shows that FRIs calculated by the non-subject-specific methods have an increasing trend in all ROIs for female subjects while BMI is increasing. Conversely, this trend is decreasing for results of subject-specific FRIs. In non-subject-specific methods, the highest FRI is predicted for obese women. In contrast, our subject-specific model suggests that low BMI women are in the highest risk of hip fracture.

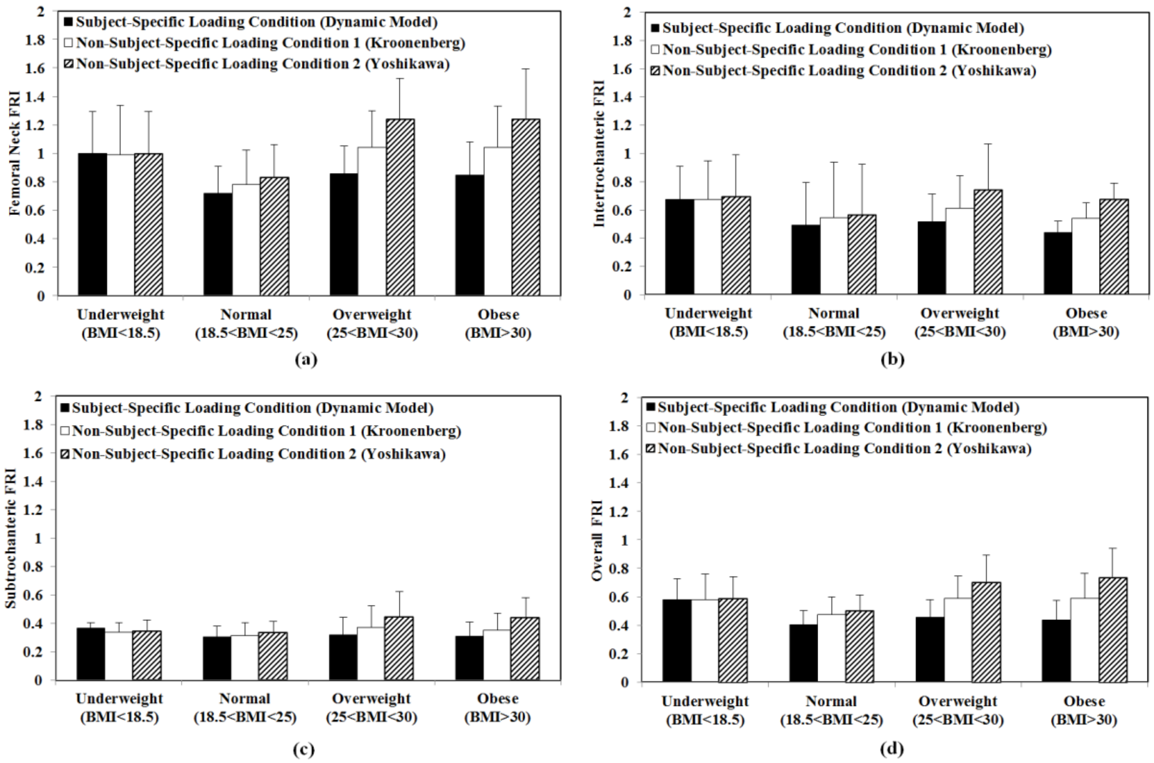

Figure 6.9. Mean value of FRIs at (a) the femoral neck, (b) the intertrochanter, (c) the subtrochanter, and (d) the whole proximal femur for the four BMI groups of male subjects, predicted by the subject-specific and non-subject-specific (1 and 2) methods

Similar to the results of female subjects, non-subject-specific methods suggest that men with higher BMI are more likely to experience hip fracture; while our subject-specific model predicts the highest FRI for underweight men. From Figures 6.5, 6.8, and 6.9, it is observed that the trends in predicted impact forces by different methods are quite similar to those of hip fracture risk. For example, similar to the predicted impact forces, the higher FRI is estimated for higher BMI subjects using non-subject-specific methods. It demonstrates the significant effect of the impact force on hip fracture risk assessment.

Figure 6.10 shows the trend of FRI at the femoral neck, as the most critical ROI, with respect to the BMI for the three implemented methods. Generally, in both genders, FRIs calculated by non-subjects-specific methods have a positive association with BMI. This association is strongly negative for women in the results of our model. Our findings that reduced BMI in women increases the risk for hip fracture are in a very good agreement with clinical observations. As a result of meta-analyses, Johansson et al. [233] and Laet et al. [234] observed that low BMI is associated with a greater hip fracture risk in women. The reason is that the trochanteric soft tissues influence the hip fracture risk by reducing the applied impact force to the femur [20, 229]. Bhan and colleagues also performed lateral pelvis release experiments on twenty participants and observed that energy absorption is a common mechanism underlying the reduced risk of hip fracture for persons with high BMI [232]. Furthermore, Bouxsein et al. [235] found that women with high BMI are less likely to experience hip fracture as they have thicker hip soft tissues through a strong association between trochanteric soft tissue thickness and BMI ($r = 0.72, p < 0.001$ among our female subjects). Also, results of our model show that obese and overweight men have lower fracture risk than underweights, however, the association between BMI and FRI in men ($p > 0.05$) is not as strong as it is in women ($p < 0.001$). Our result is consistent with findings of prospective studies [236, 237] that the association between BMI and FRI is not significant among men. It is due to the thinner trochanteric soft tissues in high BMI men compared to that in women. As a result, in contrast to women, BMI cannot be considered as a protective factor against hip fracture in men. Nevertheless, low BMI males are still in the highest risk of hip fracture. This study presents the first subject-specific biomechanical model to assess the fall-related hip fracture risk. Previous fracture risk indicators have only used the femur-related parameters for hip fracture risk assessment and the loading condition has been roughly estimated. However, all involved parameters in simulating the sideways fall, calculating the impact/joint force, and determining the stress distribution in the proximal femur are subject-specifically taken into account in the proposed model.

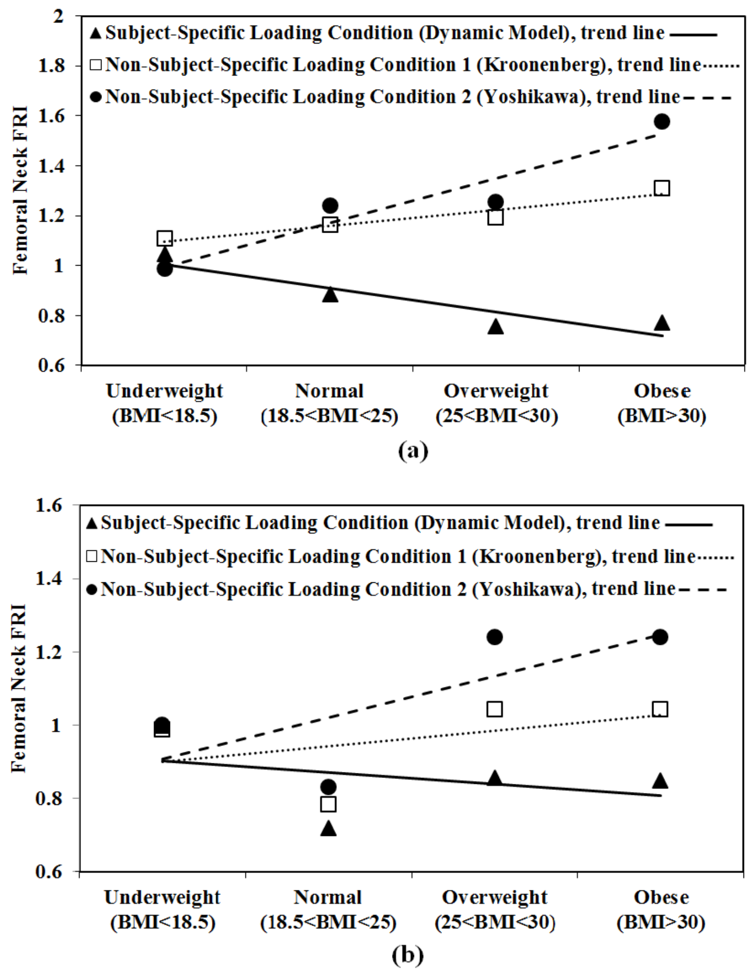

Figure 6.10. Variation of FRI at femoral neck with BMI in subject-specific model and non-subject-specific methods for (a) women and (b) men

6.3.4 Comparison between the effects of body parameters on hip fracture risk in men and women

Correlation coefficients between the subject-specific hip fracture risk and individual factors including body weight, body height, STT, BMD, and impact force are listed in Table

6.7 for women and men. As shown in Table 6.7, the hip fracture risk is influenced by a number of parameters and it cannot be accurately assessed by single factor predictors, such as aBMD, as they only partially surrogate effective parameters on hip fracture risk.

Table 6.7. Association, r (p value), between FRIs and individual factors in women and men

	FRI at	Body Weight	Body Height	STT	BMD	Impact Force
Women	Femoral neck	-.24 (<0.05)	0.04 (>0.05)	-0.50 (<0.001)	-0.68 (<0.001)	0.42 (<0.001)
	Intertrochanter	-.27 (<0.05)	-0.06 (>0.05)	-0.38 (<0.001)	-0.58 (<0.001)	0.14 (>0.05)
	Subtrochanter	-0.33 (<0.01)	-0.10 (>0.05)	-0.36 (<0.01)	-0.56 (<0.001)	0.05 (>0.05)
	Overall	-0.27 (<0.05)	-0.10 (>0.05)	-0.43 (<0.001)	-0.71 (<0.001)	0.24 (<0.05)
Men	Femoral neck	-0.08 (>0.05)	-0.36 (<0.01)	0.39 (<0.01)	-0.83 (<0.001)	-0.31 (<0.05)
	Intertrochanter	-0.16 (>0.05)	-0.19 (>0.05)	0.21 (>0.05)	-0.72 (<0.001)	-0.26 (>0.05)
	Subtrochanter	-0.18 (>0.05)	-0.32 (<0.05)	0.15 (>0.05)	-0.63 (<0.001)	-0.25 (>0.05)
	Overall	-0.17 (>0.05)	-0.33 (<0.05)	0.22 (>0.05)	-0.82 (<0.001)	-0.26 (>0.05)

In both genders, BMD has the strongest negative correlation with FRIs. Similarly, Dufour et al. [238] observed in a study on 5,209 men and women that femoral strength seems to be the strongest determinant of hip fracture in both genders. However, our results showed that this correlation is stronger in men ($r = -0.83, p < 0.001$) compared to that in women ($r = -0.68, p < 0.001$). It may indicate that BMD plays a more protective role against hip fracture in men than in women. Our findings are in a very good consistency with clinical statistics. As a result of a prospective study on 5,384 men and 7,871 women during 4.4 years follow-up, Cummings et al. [81] observed that hip BMD is very strongly associated with hip fracture in men (3.2-fold increased risk per sex-specific SD decrease in BMD; 95% CI, 2.4–4.1), stronger than that in women. Therefore, they suggested that hip BMD is an excellent test for predicting the fracture risk in men. It is also suggested by Keyak et al. [239] that femoral strength is a more powerful discriminatory tool for assessing hip fracture risk in men than in women. In addition, results of a prospective multicenter study of 3,549 men [240] shows that femoral strength is highly predictive of incident hip fractures in men. The difference in the association between bone quality and hip fracture risk in men and women is the reason why many researchers suggested using a gender-specific T-score, rather than female-normalized, for discriminating hip fracture [241-243]. Our results also demonstrate that the bone quality is the most dominant parameter against hip fracture in men and it can be used as a proper predictor of hip fracture. Although not as strong as in men, BMD among all body parameters nevertheless has the strongest negative correlation with hip fracture risk in women. However, BMD-based determination of hip fracture risk for females is not accurate without considering the effect of other parameters, especially STT and impact force.

In female subjects, strong negative correlations are observed between STT and FRIs in all critical locations of the proximal femur. After BMD, STT plays the most important protective role against the hip fracture in women. It has been demonstrated in experimental side impacts [220] and statistical studies [235] that thicker trochanteric soft tissues can significantly reduce the risk of femur fracture in women as hip soft tissues remarkably absorb the impact energy. However, significant associations are not observed between STT and FRIs in most ROIs among male subjects. Our findings indicate that trochanteric soft tissue thickness does not have a notable effect on protecting against hip fracture in men. Completely consistent to our results, Nielson et al. [237] found in a follow-up study on 5,995 men that although increased tissue thickness reduces the fall force, tissue thickness is not significantly associated with the risk of hip fracture. Dufour and colleagues also found in a large, longitudinal population-based study [238] that decreased soft tissue thickness is associated with increased hip fracture risk in women, but there is no association in men. Reasons for this phenomenon are three-fold. First, in contrast to women, the thickness of trochanteric soft tissue in men may not be great enough [237] to effectively reduce the forces applied to the hip during a fall. Second, the relative proportion of fat and lean tissue over the trochanter differs in men and women [237] and as a result the attenuation of force is affected. Third, among our study population, the correlation between STT and BMD is positively stronger in women ($r = 0.58, p < 0.001$) than that in men ($r = -0.37, p < 0.01$). It indicates that women with higher STT have stronger bones while this trend is not observed in men. Therefore, trochanteric soft tissue thickness can be considered as a significant factor in reducing the risk of hip fracture in women, but not in men.

6.4 Clinical Validation

Clinical validation of a model requires a study population with hip fracture patients and non-fracture controls. Then, the model has to be used to discriminate the hip fracture patients and the comparison should be performed between the model accuracy and the gold standard. As the whole-body DXA is usually not scanned in clinics, we could not access to a study population with hip fracture patients who have whole-body DXA images. Therefore, the predicted impact forces for 130 subjects are used to derive a correlation between the impact force and body parameters. As the effect of body parameters on the impact force can be different in men and women, the functions are derived gender-specifically. Half of the subjects are randomly selected to interpolate the function and half others are used to test the interpolated function in predicting the impact force. In the interpolated functions, the body parameters that can be determined without the necessity for the whole-body DXA image are considered. Eq. (6.3) and (6.4) describe the correlation between the impact force, BW, BH, and STT for women and men, respectively;

$$F = 0.811 \times \frac{BH^{0.261} \times BW^{0.769}}{STT^{0.504}} \tag{6.3}$$

$$F = 0.517 \times \frac{BH^{0.349} \times BW^{0.628}}{STT^{0.192}} \tag{6.4}$$

where BH, BW, STT, and F are respectively in m, kg, mm, and kN. Figure 6.11 shows the accuracy of the derived functions in predicting the impact force for the test subjects.

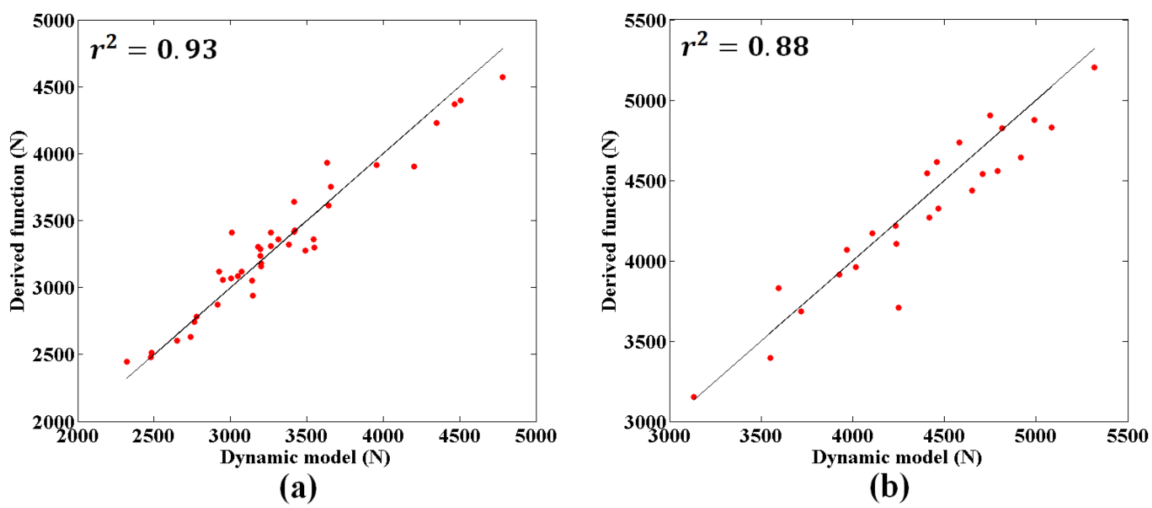

Figure 6.11. Accuracy of the derived functions in predicting the impact force for test study population of (a) women and (b) men

As the r-square is reasonably well for both women and men, the proposed functions can be used to predict the impact force without the necessity of the whole-body DXA image.

Then, 294 women (mean age= 75.4 ± 6.9 years) are extracted from the Manitoba Bone Mineral Density Database, including 99 hip fractures and 195 matched controls with similar age, weight, height, and STT. The proposed function for women is used to predict the impact force and then the hip DXA image is used to construct the proximal femur finite element model and determine the fracture risk. The validation is conducted in a blind way, i.e., the fracture risk is calculated without any cognition of the hip fracture patients. Gold standard is also used to assess the hip fracture risk for 295 clinical cases. In addition, the most frequently used empirical function for predicting the impact force in the literature, i.e., Yoshikawa's formula (Eq. 6.2), is used to predict the impact force and the FE model is then used to calculate the fracture risk. Table 6.8 shows the accuracy of different methods in discriminating the hip fracture patients.

Table 6.8. AUC and odds ratio in discriminating the hip fracture patients for different methods

Method of hip fracture risk assessment	AUC	OR, (95% CI)
DXA-based BMD (gold standard)	0.710, $p < 0.001$	2.56, (1.89 – 3.46) , $p < 0.001$
Yoshikawa's formula for impact force + FE model for calculating FRI	0.718, $p < 0.001$	2.85, (2.10 – 3.84) , $p < 0.001$
The proposed formula for impact force + FE model for calculating FRI	0.772, $p < 0.001$	3.95, (2.41 – 6.45) , $p < 0.001$

As shown in Table 6.9, the AUC (area under the ROC curve) has been improved from 0.710 to 0.718 using the available empirical function in the literature to predict the impact force and the FE model to calculate the FRI. Using the finite element model of the proximal femur can definitely have effect on the improved accuracy of determining the FRI as the bone geometry is considered in modeling, in addition to the bone quality.

However, the AUC for the proposed model in this study (0.772) is significantly greater than the gold standard. Also, the odds ratio of the two-level subject-specific model is greater than other methods (3.95 vs. 2.85 and 2.56) that shows the proposed model in this study is a more powerful discriminatory tool for assessing hip fracture risk. It demonstrates the advantages of the proposed two-level subject-specific model in assessing the risk of hip fracture compared to the available conventional methods.

6.5 Effect of Boundary Conditions on Fall-Induced Fracture Risk of the Proximal Femur

As shown in Section 5.4, two boundary conditions are implemented to simulate the sideways fall to the femur. In one simulation, the femoral head is subjected to the joint force and in the other simulation, the femoral head is fixed. Differences in boundary conditions lead to changes in fracture risk assessment. To investigate the explicit effect of the joint force on the predicted FRIs, two simulations are repeated for each subject with the same impact force. First, the femoral head is subjected to the joint force, and then, the femoral head is fixed in the horizontal direction of the coronal plane. Figure 6.12 shows how boundary conditions affect the FRIs in different critical ROIs.

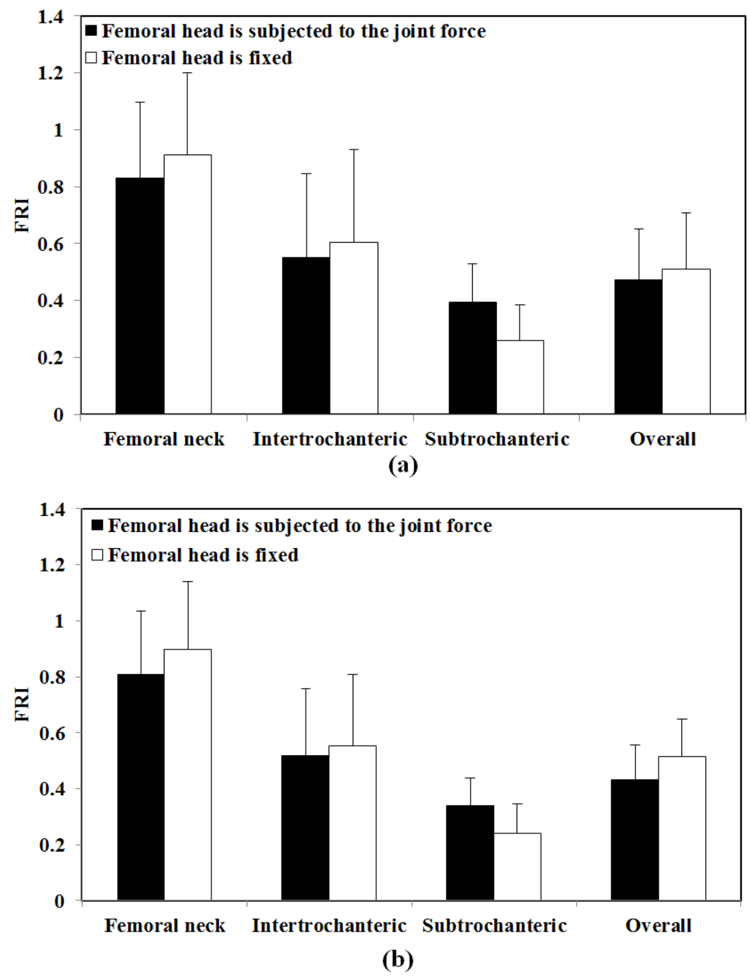

Figure 6.12. Effect of boundary conditions on the calculated FRIs in critical ROIs of the proximal femur in (a) women and (b) men

As shown in Figure 6.12, FRIs at the femoral neck, the intertrochanter, and the whole proximal femur are relatively higher while the femoral head is fixed. However, the sub-trochanteric FRI is greater when the joint force is applied to the femoral head. In subject-specific boundary conditions, the impact force overcomes the joint force as its magnitude is generally higher, and thus it tends to bend the proximal femur about the constrained section at the distal end. Therefore, much stress is concentrated around the femoral shaft. In non-subject-specific boundary conditions, as the femoral head is fixed, the impact force tends to compress the upper level of the proximal femur and thus higher stress concentration appears around the femoral neck and the intertrochanter. That is the reason why femoral neck FRI and intertrochanteric FRI are higher in non-subject-specific boundary conditions. However, both boundary conditions predict that the femoral neck and the subtrochanter are respectively the most and the least critical locations of the proximal femur. Comparing Figure 6.12 with Figures 6.9 and 6.8, it can be concluded that the effect of impact force on hip fracture risk assessment is much higher than the effect of joint force. Figures 6.8 and 6.9 show that changes in the impact force (subject-specific versus non-subject-specific) may lead to a remarkable change in the predicted FRIs. Figure 6.12 also shows that considering the joint force affects the resulted FRIs; however, its effect is not as strong as the effect of the impact force.

6.6 Limitations of the Study

Although the advantages of the proposed model can be regarded as a strength of this study, it includes a number of assumptions and simplifications and therefore can also be considered as limitations.

- The dynamics model is developed based on a number of assumptions. For example, it is assumed that other parts of the leg and body do not come into contact with the ground before the hip. Although this assumption is proven to be generally true in sideways falls in kinematic studies performed by Kroonenberg et al. [21], it is possible that a subject initiates the impact with other parts of the body. Obviously, if the arm or hand impacts the ground before the hip, a portion of the available potential energy is attenuated and a smaller impact force is applied to the hip and thus the hip fracture risk is decreased. However, there is no guarantee that the subject (especially elderly) impacts the ground with hands or other parts of the body. Therefore, the proposed biomechanical model has to predict the worst-case scenario, which is impacting with hip, and so that it can be used in production of subject-specific hip protective systems. The other assumption in developing the dynamics model is that no slippage is considered between the feet and the ground during the fall. An anchored fall causes a greater vertical impact velocity, and subsequently a greater impact force, compared to a slipping fall since a part of available potential energy is lost due to friction in slipping. Again, the anchored fall is the worst-case scenario and should be considered in development of the biomechanical modeling.

- A single degree of freedom vibrational system based on the body configuration at the impact instant is developed to simulate the impact in a lateral fall. Therefore, the linear impulse-momentum is used to determine the joint force time-history. But human body has a complex configuration during the impact and it may change after the impact instant. However, the time from the impact instant to the peak force is very short (20-50 msec) [210, 229] and the body configuration cannot be changed largely in this time period, especially for the elderly. Therefore, it can be assumed that the effective mass properly represents the vertical movement of the human body in this short period of time.

- The stiffness and damping of the body during impact to the hip depends not only on the thickness of the trochanteric soft tissues, but also on the fat/muscle mass on the hip region and the age of the individual. However, in this study, trochanteric soft tissue thickness was used to determine the stiffness/damping properties of the body during impact to the hip due to the lack of information about the effect of other parameters on K/C in the impact model.

- In determining the subject-specific stiffness/damping properties of the impact model, the association between C and STT is not as strong as that between K and STT. Similarly, Robinovitch et al. [244] demonstrated that impact dynamics during sideways falls are more dependent on elastic than viscous properties and that is the reason why Kroonenberg et al. [133] and Laing et al. [210] proposed a mass spring model without damper as an impact model. However, damping is considered in this study using the proposed correlation between C and STT as this is the strongest correlation between C and any of other body parameters such as body height, body weight, and BMI. Our results are also in a good consistency with the findings of Majumder et al. [20] who identified that trochanteric soft tissue thickness is likely to be the most dominant criteria for attenuating the applied force to the femur in a fall.

- The proposed model only predicts the hip fracture risk in the event that the fall occurs, i.e., it does not take the individual's fall risk into account. The fall risk may play an important role in hip fracture risk. Therefore, if the model is used to assess the hip fracture risk for an individual who usually experiences falls, results should be considered more seriously.

- The proposed model does not consider the pre-impact movement strategies for determining the impact force. Breaking the fall using arms [34], stepping and impacting with knees [245], and forward/backward rotation during descent [212] can reduce the applied impact force to the hip. Including the possible common pre-impact movement strategies in the modeling may improve the accuracy in simulating the real-life body falling.

- There are differences in results of the proposed two methods for estimating the stiffness/damping properties of the impact model. Although estimating the properties of hip soft tissues from experimental data, using logarithmic decrement method, is more accurate, it requires performing the controlled and protected fall tests which is not practical for the elderly. Therefore, using soft tissue thickness to determine the K and the C in the impact model provides an experiment-free method, although the accuracy does not stand in the same level.

- The model only assesses the subject-specific hip fracture risk in sideways falls, and may not be applied for falls with different mechanics, i.e., impact to the anterior-lateral or posterior-lateral aspect of the hip, and knee or hand impact before pelvis impact.

- Due to the limitations in the number of our fall experiments and the number of subjects, we could not explore how the mechanics of the fall, e.g., landing surface, pelvis and femoral configuration at impact, affect fracture risk.

- The FE model ignores muscle forces (abductors), which can have effect on stresses in the proximal femur, and assumes bone isotropy.

- The limitations of DXA images are involved in our model. Subject positioning in DXA scanning may introduce differences into the constructed FE model and influence the precision of results. However, DXA scanners are more widely available to clinicians compared to CT scanners [120]. Therefore, using the DXA image increases the applicability of our model in clinics.

It also should be pointed out that a subject can show various unexpected reactions during a fall that may change the fall characteristics and subsequently hip fracture risk. However, a fall with critical conditions is considered in developing the models.

Chapter 7

Conclusions and Recommendations

Hip fracture is a serious global health issue, which has imposed significant burden on community healthcare systems. Therefore, it is commonly desired to develop an improved predictor to estimate the individual's hip fracture risk for timely prevention and protection measurements in order to reduce consequences such as morbidity, mortality, disability, and therapy cost. The objective of this research was to develop a two-level subject-specific biomechanical model for improving assessment of hip fracture risk. The reported study has been conducted in three phases: (1) the first phase was to develop a subject-specific dynamics model of the human body to simulate sideways falls and determine the applied forces to the hip during the impact; (2) the second phase was to present a FE model of the proximal femur to calculate the hip fracture risk in critical locations; and (3) the last phase was to apply the proposed two-level model on 130 clinical cases and evaluate the advantages of the presented model over existing methods.

7.1 Concluding Remarks

In the proposed model, all effective parameters are considered including anthropometric parameters, loading condition, effect of hip soft tissues on absorbing the impact energy, bone quality and bone geometry. This study introduces a model that eliminates the existing limitations and provides a subject-specific procedure to precisely assess the hip fracture risk.

The major findings of the research can be summarized as follows:

1. There exists an association between pixel intensity value in a DXA image and the body density. As the DXA imaging requires low dosage of radiation compared to 3D imaging techniques, it is the best method for the estimation of anthropometric parameters. Compared to other methods proposed for estimation of anthropometric parameters such as underwater weighting and air displacement plethysmography, using DXA image is cost effective with higher precision.
2. Loading condition is one of the most effective parameters in hip fracture risk assessment and should be determined precisely. A subject-specific dynamics model can reduce the error in predicting the applied forces to the femur in lateral falls and therefore it is a prerequisite for assessing hip fracture risk.
3. Joint torques affect the kinematics of body segments in a lateral fall and subsequently the applied impact force to the femur. To better simulate sideways falls, joint torques should be considered in the dynamics model.

4. Trochanteric soft tissues can significantly absorb the impact energy in a sideways fall and thus neglecting this parameter in calculating the impact force will considerably affect the accuracy of results.
5. Hip fracture is affected by a complex combination of parameters and thus it is not predictable by single risk factors. Neglecting any of the effective factors will affect the accuracy of hip fracture risk assessment.
6. Obesity is a protective factor against hip fracture in women as obese females usually have thicker hip soft tissues to attenuate the impact energy. Although falls of obese subjects are severer than those of low BMI subjects, the transferred energy to the femur is lower since a big amount of energy is absorbed by hip soft tissues.
7. Low BMI men and women are in the highest risk of hip fracture in lateral falls due to their thin layer of hip soft tissues and lower BMD. Thin layer of hip soft tissues transfers a significant amount of impact energy to the femur. As the BMD is generally low in low BMI subjects, the femur is not strong enough to sustain under the high impact force and the hip fracture risk increases.
8. Although biomechanical determinants of hip fracture are gender-specific, body parameters which generally increase the risk of hip fracture are low body mass index, thin layer of trochanteric soft tissues, and low bone mineral density.
9. As the trends observed clinically in women and men between hip fracture risk and both BMI and BMD were described more accurately by subject-specific than non-subject-specific models, the current observations support the value of future studies to examine the accuracy of our model in predicting fracture risk.

The main contributions of the current study are stated as follows:

1. An algorithm for estimating anthropometric parameters from whole-body DXA images has been introduced. The proposed method is able to determine physical properties of the human body segments, such as centre of mass and mass moment of inertia, which are highly required in biomechanical simulations.
2. A subject-specific dynamics model is developed to simulate the kinematics of body segments in lateral falls from any arbitrary initial conditions. Compared to an existing non-subject-specific dynamics model, our model reduced the relative errors in the predicted hip vertical velocity and peak impact force from 40.1% and 35.4% to 6.1% and 8.9%, respectively.
3. A novel method is proposed to determine joint torques during the fall. The actions of hip and knee joints change the kinematics of body segments during the fall and therefore affect the applied forces to the femur in the impact stage. Complex integral results of actions of muscles, tendons, ligaments, and articular surfaces across the joints are determined as the joint moments using a reverse dynamic procedure.
4. An algorithm is proposed to predict the response of the body in the impact stage of a lateral fall using a subject-specific spring-damper combination. The spring-damper system is modeled by determining the association between hip soft tissue thickness and amount of absorbed energy. This algorithm eliminates the limitation of previous hip fracture predictors in considering the attenuation of impact energy by hip soft tissues.
5. Two distinct models are developed and linked together to have a comprehensive subject-specific biomechanical model for more accurately assessing hip fracture

risk. Bone material properties, bone geometry, and individual parameters such as body mass distribution are considered in modeling.

6. Sensitivity of the proximal femur FE model to the location of critical cross-sections and the boundary of the femur is eliminated using a semi-automatic method for femur contour detection, and a fully-automatic procedure for detection of critical locations of the proximal femur.

7.2 Recommendations for Future Research

In the next decade, significant efforts are anticipated to be devoted to experiments and computational simulations, which make further progress in the improvement of hip fracture risk assessment. In the following list, some recommendations for future works that may be possible by exploiting the interplay between computational simulations and experiments are suggested.

1. One of the limitations of the current study is that the model encounters difficulties to fulfill a successful experiment-free simulation of joint actions in sideways falls. The proposed model uses a reverse dynamic procedure to estimate the actions of joints and their effects on the kinematics of body segments in lateral falls, which requires experimental data. Therefore, establishing a general method needs performing a large number of experiments in order to fully investigate how joints act during a fall from different initial conditions. However, it is still challenging to perform fall experiments from great heights as it may cause inconveniences and

bruising. Proposing a method to accurately simulate the joint actions in sideways falls may significantly improve the precision of predicted impact force.

2. Subject-specific determination of the stiffness and the damping properties of hip soft tissues can be further improved. A number of factors may affect the behaviour of trochanteric soft tissues in the impact stage of the fall including the thickness of trochanteric soft tissues, width of the hip, age of the subject, etc. K and C in the impact model may be changed even for one person in falls from different heights. Improving determination of hip stiffness and damping properties can greatly improve the accuracy of hip fracture risk assessment.
3. Considering the effect of pre-impact movement strategies in the dynamics model, including the use of the hands and stepping in breaking the falls or rotating forward or backward during descent, may increase the reliability of the model in simulating the sideways falls.
4. One of the purposes of this study was to improve assessment of hip fracture risk in order to start the timely prevention and protection measurements. According to the undefined threshold of FRI for starting the treatment, future potential studies on hip fracture prediction should involve scaling the FRI for determining the level of fracture risk. In calculating the FRI, the effective stress is compared with the yield stress which declares a high risk of fracture for patients with FRI > 1. However, the prevention activities should be started much earlier than facing a high risk of fracture. Defining this threshold requires a systematic study on patients who experienced hip fracture by investigating their pre-fracture history.

Bibliography

[1] Shao CJ, Hsieh YH, Tsai CH, Lai KA. A nationwide seven-year trend of hip fractures in the elderly population of Taiwan. Bone 2009;44: 125-129.

[2] Green C, Molony D, Fitzpatrick C, ORourke K. Age-specific incidence of hip fracture in the elderly: A healthy decline. The Surgeon 2010;8: 310-313.

[3] Gronskag AB, Forsmo S, Romundstad P, Langhammer A, Schei B. Incidence and seasonal variation in hip fracture incidence among elderly women in Norway. The HUNT Study. Bone 2010;46: 1294-1298.

[4] Alvarez-Nebreda ML, Jimenez AB, Rodriguez P, Serra JA. Epidemiology of hip fracture in the elderly in Spain. Bone 2008;42: 278-285.

[5] Wilson RT, Chase GA, Chrischilles EA, Wallace RB. Hip Fracture Risk Among Community-Dwelling Elderly People in the United States: A Prospective Study of Physical, Cognitive, and Socioeconomic Indicators. American Journal of Public Health 2006;96: 1210-1218.

[6] Marks R, Allegrante JP, Ronald MacKenzie C, Lane JM. Hip fractures among the elderly: causes, consequences and control. Ageing Research Reviews 2003;2: 57-93.

[7] Testi D, Viceconti M, Baruffaldi F, Cappello A. Risk of fracture in elderly patients: a new predictive index based on bone mineral density and finite element analysis. Computer Methods and Programs in Biomedicine 1999;60: 23-33.

[8] Greenspan SL, Myers ER, Kiel DP, Parker RA, Hayes WC, Resnick NM. Fall Direction, Bone Mineral Density, and Function: Risk Factors for Hip Fracture in Frail Nursing Home Elderly. The American Journal of Medicine 1998;104: 539-545.

[9] Cooper C, Campion G, LJ MI. Hip fractures in the elderly: a world-wide projection. Osteoporos International 1992;2: 285–259.

[10] Kanis JA, Oden A, McCloskey EV, Johansson H, Wahl DA, Cooper C. A systematic review of hip fracture incidence and probability of fracture worldwide. Osteoporosis International 2012;23: 2239-2256.

[11] WHO. Assessment of fracture risk and its application to screening for osteoporosis. WHO technical report series 843 1994;Geneva.

[12] Sernbo I, Johnell O. Consequences of a hip fracture: A prospective study over 1 year. Osteoporosis International 1993;3: 148-153.

[13] Chrischilles E, Butler C, Davis C, Wallace R. A model of lifetime osteoporosis impact. Arch Intern Med 1991;151: 2026-2032.

[14] Gullberg B, Johnell O, Kanis JA. World-wide projections for hip fracture. Osteoporosis International 1997;7: 407-413.
[15] Roche JJW, Wenn RT, Sahota O, Moran CG. Effect of comorbidities and postoperative complications on mortality after hip fracture in elderly people: prospective observational cohort study; 2005.
[16] Boonen S, Autier P, Barette M, Vanderschueren D, Lips P, Haentjens P. Functional outcome and quality of life following hip fracture in elderly women: a prospective controlled study. Osteoporosis International 2004;15: 87-94.
[17] Lieberman D, Friger M, Fried V, Grinshpun Y, Mytlis N, Tylis R, Galinsky D. Characterization of elderly patients in rehabilitation: stroke versus hip fracture; 1999.
[18] Phy MP, Vanness DJ, Melton L, Iii, et al. Effects of a hospitalist model on elderly patients with hip fracture. Archives of Internal Medicine 2005;165: 796-801.
[19] Huddleston JM, Whitford KJ. Medical Care of Elderly Patients With Hip Fractures. Mayo Clinic Proceedings 2001;76: 295-298.
[20] Majumder S, Roychowdhury A, Pal S. Hip fracture and anthropometric variations: Dominance among trochanteric soft tissue thickness, body height and body weight during sideways fall. Clinical Biomechanics 2013;28: 1034-1040.
[21] Van den Kroonenberg AJ, Hayes WC, McMahon TA. Hip impact velocities and body configurations for voluntary falls from standing height. Journal of Biomechanics 1996;29: 807-811.
[22] Roberts BJ, Thrall E, Muller JA, Bouxsein ML. Comparison of hip fracture risk prediction by femoral aBMD to experimentally measured factor of risk. Bone 2010;46: 742-746.
[23] Marieb EN, Mallatt J. Human Anatomy and Physiology: Pearson plc; 2002.
[24] Hirshorn K. http://stpetehipandknee.com/anatomy-hip-joint/. In; 2014.
[25] Cumming R, Klineberg R. Fall frequency and characteristics and the risk of hip fractures. Journal of the American Geriatrics Society 1994;42: 774-778.
[26] Ford CM, Keaveny TM, Hayes WC. The effect of impact direction on the structural capacity of the proximal femur during falls. Journal of Bone and Mineral Research 1996;11: 377-383.
[27] Parker MJ. Fractures of the Hip. Surgery (Oxford) 2003;21: 221-224.
[28] Zioupos P, Wang XT, Currey JD. Experimental and theoretical quantification of the development of damage in fatigue tests of bone and antler. Journal of Biomechanics 1996;29: 989-1002.
[29] Youm T, Koval KJ, Kummer FJ, Zuckerman JD. Do all hip fractures result from a fall? American Journal of Orthopedics 1999;28: 190-194.
[30] Teppo LNJ, Harri S, Karim MK, Ari H, Pekka K. Shifting the focus in fracture prevention from osteoporosis to falls. BMJ 2008;336: 124-126.
[31] Cummings SR, Melton LJ. Epidemiology and outcomes of osteoporotic fractures. The Lancet 2002;359: 1761-1767.
[32] Kannus P, Leiponen P, Parkkari J, Palvanen M, Jarvinen M. A sideways fall and hip fracture. Bone 2006;39: 383-384.
[33] Greenspan SL, Myers ER, Maitland LA, Resnick NM, Hayes WC. FAll severity and bone mineral density as risk factors for hip fracture in ambulatory elderly. JAMA 1994;271: 128-133.

[34] Sabick MB, Hay JG, Goel VK, Banks SA. Active responses decrease impact forces at the hip and shoulder in falls to the side. Journal of Biomechanics 1999;32: 993-998.
[35] Kanis JA. Diagnosis of osteoporosis and assessment of fracture risk. The Lancet 2002;359: 1929-1936.
[36] Carpintero P, Caeiro JR, Carpintero R, Morales A, Silva S, Mesa M. Complications of hip fractures: A review. World Journal of Orthopedics 2014;5: 402-411.
[37] Rizzoli R, Bruyere O, Cannata-Andia JB, Devogelaer JP, Lyritis G, Ringe JD, Vellas B, Reginster JY. Management of osteoporosis in the elderly. Current Medical Research and Opinion 2009;25: 2373-2387.
[38] Jee W. Integrated Bone Tissue Physiology: Anatomy and Physiology. New York, Informa Healthcare: In Cowin Bone Mechanics Handbook; 2001.
[39] Cummings SR, Nevitt MC, Browner WS, Stone K, Fox KM, Ensrud KE, Cauley J, Black D, Vogt TM. Risk Factors for Hip Fracture in White Women. New England Journal of Medicine 1995;332: 767-774.
[40] Fisher AA, O'Brien ED, Davis MW. Trends in hip fracture epidemiology in Australia: Possible impact of bisphosphonates and hormone replacement therapy. Bone 2009;45: 246-253.
[41] Johnell O, Kanis JA. An estimate of the worldwide prevalence and disability associated with osteoporotic fractures. Osteoporosis International 2006;17: 1726-1733.
[42] Brauer CA, Coca-Perraillon M, Cutler DM, Rosen AB. Incidence and Mortality of Hip Fractures in the United States. The Journal of the American Medical Association 2009;302: 1573-1579.
[43] Leibson CL, Tosteson ANA, Gabriel SE, Ransom JE, Melton LJ. Mortality, Disability, and Nursing Home Use for Persons with and without Hip Fracture: A Population-Based Study. Journal of the American Geriatrics Society 2002;50: 1644-1650.
[44] Haentjens P, Magaziner J, Colon-Emeric CS, Vanderschueren D, Milisen K, Velkeniers B, Boonen S. Meta-analysis: Excess Mortality After Hip Fracture among Older Women and Men. Annals of Internal Medicine 2010;152: 380-390.
[45] Greendale G, Barrett-Connor E. Outcomes of osteoporotic fractures. 2 ed. San Diego: Academic Press; 2001.
[46] Ross PD. Clinical consequences of vertebral fractures. The American Journal of Medicine 1997;103: S30-S43.
[47] Gold D, Lyles K, Shipp K, Drezner M. Osteoporosis and its nonskeletal consequences: Their impact on treatment decisions. 2 ed. San Diego: Academic Press; 2001.
[48] Gallup. Osteoporosis Prevalence Figures; State-by-State Report. Washington, D.C.: National Osteoporosis Foundation; 1997.
[49] Tosteson ANA, Gabriel SE, Grove MR, Moncur MM, Kneeland TS, Melton Iii LJ. Impact of Hip and Vertebral Fractures on Quality-Adjusted Life Years. Osteoporosis International 2001;12: 1042-1049.
[50] Phillips S, Fox N, Jacobs J, Wright WE. The direct medical costs of osteoporosis for American women aged 45 and older. Bone 1988;9: 271-279.

[51] Lonnroos E, Kautiainen H, Karppi P, Huusko T, Hartikainen S, Kiviranta I, Sulkava R. Increased incidence of hip fractures. A population based-study in Finland. Bone 2006;39: 623-627.
[52] Wiktorowicz ME, Goeree R, Papaioannou A, Adachi JD, Papadimitropoulos E. Economic Implications of Hip Fracture: Health Service Use, Institutional Care and Cost in Canada. Osteoporosis International 2001;12: 271-278.
[53] Dy CJ, McCollister KE, Lubarsky DA, Lane JM. An Economic Evaluation of a Systems-Based Strategy to Expedite Surgical Treatment of Hip Fractures. The Journal of Bone & Joint Surgery 2011;93: 1326-1334.
[54] Hayes WC, Myers ER, Robinovitch SN, Van Den Kroonenberg A, Courtney AC, McMahon TA. Etiology and prevention of age-related hip fractures. Bone 1996;18: S77-S86.
[55] Kannus P, Parkkari J, SievÃ¤nen H, Heinonen A, Vuori I, JÃ¤rvinen M. Epidemiology of hip fractures. Bone 1996;18: S57-S63.
[56] An YH, Draughn RA. Mechanical testing of bone and the bone-implant interface. CRC Press, Florida 2000: 407-438.
[57] Butler M, Forte M, Kane R. Treatment of Common Hip Fractures. Evidence Reports, Technology Assessments 2009;184.
[58] Peters M. http://advancedortho.net/info/hipfractureinfo.php. In; 2000.
[59] Dhanwal D, Dennison E, Harvey N, Cooper C. Epidemiology of hip fracture: Worldwide geographic variation. Indian Journal of Orthopaedics 2011;45: 15-22.
[60] Melton LJ. Hip fractures: A worldwide problem today and tomorrow. Bone 1993;14: 1-8.
[61] Jacobsen SJ, Goldberg J, Miles TP. Hip fracture among the old and very old: a population-based study of 745 435 cases. Am J Public Health 1990;80: 871-873.
[62] Cummings SR, Black DM, Rubin SM. Lifetime risks of hip, colles, or vertebral fracture and coronary heart disease among white postmenopausal women. Archives of Internal Medicine 1989;149: 2445-2448.
[63] Melton JL. Perspectives: How many women have osteoporosis now? Journal of Bone and Mineral Research 1995;10: 175-177.
[64] Winner SJ, Morgan CA, Evans JG. Perimenopausal risk of falling and incidence of distal forearm fracture. BMJ 1989;298: 1486-1488.
[65] Iwamoto J, Takeda T, Sato Y. Effect of muscle strengthening exercises on the muscle strength in patients with osteoarthritis of the knee. The Knee 2007;14: 224-230.
[66] Wijlhuizen GJ, de Jong R, Hopman-Rock M. Older persons afraid of falling reduce physical activity to prevent outdoor falls. Preventive Medicine 2007;44: 260-264.
[67] Chang WW, Friedman S. Hip Fracture Management. Hospital Medicine Clinics 2013;2: e399-e421.
[68] Kubota M, Uchida K, Kokubo Y, Shimada S, Matsuo H, Yayama T, Miyazaki T, Sugita D, Watanabe S, Baba H. Postoperative gait analysis and hip muscle strength in patients with pelvic ring fracture. Gait & Posture 2013;38: 385-390.
[69] Groen BE, Weerdesteyn V, Duysens J. Martial arts fall techniques decrease the impact forces at the hip during sideways falling. Journal of Biomechanics 2007;40: 458-462.

[70] Van der Zijden AM, Groen BE, Tanck E, Nienhuis B, Verdonschot N, Weerdesteyn V. Can martial arts techniques reduce fall severity? An in vivo study of femoral loading configurations in sideways falls. Journal of Biomechanics 2012;45: 1650-1655.
[71] Derler S, Spierings AB, Schmitt KU. Anatomical hip model for the mechanical testing of hip protectors. Medical Engineering & Physics 2005;27: 475-485.
[72] Holzer G, Holzer L. Hip protectors and prevention of hip fractures in older persons. Geriatrics 2007;62: 15-22.
[73] Holzer LA, von Skrbensky G, Holzer G. Mechanical testing of different hip protectors according to a European Standard. Injury 2009;40: 1172-1175.
[74] Laing AC, Robinovitch SN. The Force Attenuation Provided by Hip Protectors Depends on Impact Velocity, Pelvic Size, and Soft Tissue Stiffness. Journal of Biomechanical Engineering 2008;130.
[75] Li N, Tsushima E, Tsushima H. Comparison of impact force attenuation by various combinations of hip protector and flooring material using a simplified fall-impact simulation device. Journal of Biomechanics 2013;46: 1140-1146.
[76] Robinovitch SN, Evans SL, Minns J, Laing AC, Kannus P, Cripton PA, Derler S, Birge SJ, Plant D, Cameron ID, Kiel DP, Howland J, Khan K, Lauritzen JB. Hip protectors: recommendations for biomechanical testing-an international consensus statement (part I). Osteoporosis International 2009;20: 1977-1988.
[77] Lilliu H, Pamphile R, Chapuy M-C, Schulten J, Arlot M, Meunier PJ. Calcium-vitamin D3 supplementation is cost-effective in hip fractures prevention. Maturitas 2003;44: 299-305.
[78] Ascherio A, Munger KL, Simon KC. Vitamin D and multiple sclerosis. The Lancet Neurology 2010;9: 599-612.
[79] Arjmand Boroujeni E. Inflatable Hip Protectors. PhD. Thesis 2012;Simon Fraser University.
[80] Johnell O, Kanis JA, Oden A, Johansson H, De Laet C, Delmas P, Eisman JA, Fujiwara S, Kroger H, Mellstrom D, Meunier PJ, Melton LJ, O'Neill T, Pols H, Reeve J, Silman A, Tenenhouse A. Predictive Value of BMD for Hip and Other Fractures. Journal of Bone and Mineral Research 2005;20: 1185-1194.
[81] Cummings SR, Cawthon PM, Ensrud KE, Cauley JA, Fink HA, Orwoll ES. BMD and Risk of Hip and Nonvertebral Fractures in Older Men:A Prospective Study and Comparison With Older Women. Journal of Bone and Mineral Research 2006;21: 1550-1556.
[82] Binkovitz L, Henwood M. Pediatric DXA: technique and interpretation. Pediatric Radiology 2007;37: 21-31.
[83] Deborah M, Olof J, Hans W. Meta-analysis of how well measures of bone mineral density predict occurrence of osteoporotic fractures. BMJ 1996;312: 1254-1259.
[84] Blake GM, Fogelman I. Technical principles of dual energy X-ray absorptiometry. Seminars in nuclear medicine 1997;27: 210-228.
[85] Bainbridge NJ, Davie MWJ, Haddaway MJ. Bone loss after stroke over 52 weeks at os calcis: influence of sex, mobility and relation to bone density at other sites. Age and Ageing 2006;35: 127-132.

[86] Watts N. Fundamentals and pitfalls of bone densitometry using dual-energy X-ray absorptiometry (DXA). Osteoporosis International 2004;15: 847-854.
[87] Kanis JA, Melton LJ, Christiansen C, Johnston CC, Khaltaev N. The diagnosis of osteoporosis. Journal of Bone and Mineral Research 1994;9: 1137-1141.
[88] Kanis JA. Assessment of fracture risk and its application to screening for postmenopausal osteoporosis: Synopsis of a WHO report. Osteoporosis International 1994;4: 368-381.
[89] Blake GM, Fogelman I. Interpretation of bone densitometry studies. Seminars in nuclear medicine 1997;27: 248-260.
[90] Blake GM, Noon E, Spector TD, Fogelman I. Intervertebral T-Score Differences in Younger and Older Women. Journal of Clinical Densitometry 2013;16: 329-335.
[91] Njeh CF, Fuerst T, Hans D, Blake GM, Genant HK. Radiation exposure in bone mineral density assessment. Applied Radiation and Isotopes 1999;50: 215-236.
[92] Damilakis J, Adams J, Guglielmi G, Link T. Radiation exposure in X-ray-based imaging techniques used in osteoporosis. European Radiology 2010;20: 2707-2714.
[93] Beck T. Extending DXA beyond bone mineral density: Understanding hip structure analysis. Current Osteoporosis Reports 2007;5: 49-55.
[94] Carey JJ, Delaney MF, Love TE, Cromer BA, Miller PD, Richmond BJ, Manilla-McIntosh M, Lewis SA, Thomas CL, Licata AA. Dual-Energy X-ray Absorptiometry Diagnostic Discordance Between Z-Scores and T-Scores in Young Adults. Journal of Clinical Densitometry 2009;12: 11-16.
[95] Kanis JA, McCloskey EV, Johansson H, Oden A, Melton Iii LJ, Khaltaev N. A reference standard for the description of osteoporosis. Bone 2008;42: 467-475.
[96] Baim S, Binkley N, Bilezikian JP, Kendler DL, Hans DB, Lewiecki EM, Silverman S. Official Positions of the International Society for Clinical Densitometry and Executive Summary of the 2007 ISCD Position Development Conference. Journal of Clinical Densitometry 2008;11: 75-91.
[97] Pulkkinen P, Partanen J, Jalovaara P, Jamsa T. BMD T-score discriminates trochanteric fractures from unfractured controls, whereas geometry discriminates cervical fracture cases from unfractured controls of similar BMD. Osteoporosis International 2010;21: 1269-1276.
[98] Lang TF, Keyak JH, Heitz MW, Augat P, Lu Y, Mathur A, Genant HK. Volumetric quantitative computed tomography of the proximal femur: Precision and relation to bone strength. Bone 1997;21: 101-108.
[99] Cummings SR, Browner W, Black DM, Nevitt MC, Genant HK, Cauley J, Ensrud K, Scott J, Vogt TM. Bone density at various sites for prediction of hip fractures. The Lancet 1993;341: 72-75.
[100] Schott AM, Cormier C, Hans D, Favier F, Hausherr E, Dargent-Molina P, Delmas PD, Ribot C, Sebert JL, Breart G, Meunier PJ. How Hip and Whole-Body Bone Mineral Density Predict Hip Fracture in Elderly Women: The EPIDOS Prospective Study. Osteoporosis International 1998;8: 247-254.
[101] Cummings SR, Cauley JA, Palermo L, Ross PD, Wasnich RD, Black D, Faulkner KG. Racial differences in hip axis lengths might explain racial differences in rates of hip fracture. Osteoporosis International 1994;4: 226-229.

[102] Marshall LM, Lang TF, Lambert LC, Zmuda JM, Ensrud KE, Orwoll ES. Dimensions and Volumetric BMD of the Proximal Femur and Their Relation to Age Among Older U.S. Men. Journal of Bone and Mineral Research 2006;21: 1197-1206.
[103] Beck TJ, Ruff CB, Warden KE, Scott WW, Jr., Rao GU. Predicting Femoral Neck Strength From Bone Mineral Data: A Structural Approach. Investigative Radiology 1990;25: 6-18.
[104] Briot K, Benhamou CL, Roux C. Hip Cortical Thickness Assessment in Postmenopausal Women With Osteoporosis and Strontium Ranelate Effect on Hip Geometry. Journal of Clinical Densitometry 2012;15: 176-185.
[105] Takada J, Katahira G, Iba K, Yoshizaki T, Yamashita T. Hip structure analysis of bisphosphonate-treated Japanese postmenopausal women with osteoporosis. Journal of Bone and Mineral Metabolism 2011;29: 458-465.
[106] Takada J, Beck TJ, Iba K, Yamashita T. Structural trends in the aging proximal femur in Japanese postmenopausal women. Bone 2007;41: 97-102.
[107] Uusi-Rasi K, Beck T, Semanick L, Daphtary M, Crans G, Desaiah D, Harper K. Structural effects of raloxifene on the proximal femur: results from the multiple outcomes of raloxifene evaluation trial. Osteoporosis International 2006;17: 575-586.
[108] Kaptoge S, Beck TJ, Reeve J, Stone KL, Hillier TA, Cauley JA, Cummings SR. Prediction of Incident Hip Fracture Risk by Femur Geometry Variables Measured by Hip Structural Analysis in the Study of Osteoporotic Fractures. Journal of Bone and Mineral Research 2008;23: 1892-1904.
[109] Crabtree NJ, Kroger H, Martin A, Pols HAP, Lorenc R, Nijs J, Stepan JJ, Falch JA, Miazgowski T, Grazio S, Raptou P, Adams J, Collings A, Khaw KT, Rushton N, Lunt M, Dixon AK, Reeve J. Improving Risk Assessment: Hip Geometry, Bone Mineral Distribution and Bone Strength in Hip Fracture Cases and Controls. The EPOS Study. Osteoporosis International 2002;13: 48-54.
[110] Khoo BCC, Beck TJ, Qiao Q-H, Parakh P, Semanick L, Prince RL, Singer KP, Price RI. In vivo short-term precision of hip structure analysis variables in comparison with bone mineral density using paired dual-energy X-ray absorptiometry scans from multi-center clinical trials. Bone 2005;37: 112-121.
[111] Kanis J, Johnell O, Oden A, Dawson A, De Laet C, Jonsson B. Ten year probabilities of osteoporotic fractures according to BMD and diagnostic thresholds. Osteoporos Int. 2001;12: 989-995.
[112] Leslie WD, Lix LM, Johansson H, Oden A, McCloskey E, Kanis JA. Independent clinical validation of a Canadian FRAX tool: Fracture prediction and model calibration. Journal of Bone and Mineral Research 2010;25: 2350-2358.
[113] Wright N, Saag K. From Fracture Risk Prediction to Evaluating Fracture Patterns: Recent Advances in the Epidemiology of Osteoporosis. Current Rheumatology Reports 2012;14: 205-211.
[114] McClung MR. To FRAX or not to FRAX. Journal of Bone and Mineral Research 2012;27: 1240-1242.
[115] Kaptoge S, Benevolenskaya LI, Bhalla AK, Cannata JB, Boonen S, Falch JA, Felsenberg D, Finn JD, Nuti R, Hoszowski K, Lorenc R, Miazgowski T, Jajic I, Lyritis G, Masaryk P, Naves-Diaz M, Poor G, Reid DM, Scheidt-Nave C, Stepan JJ, Todd CJ, Weber K, Woolf AD, Roy DK, Lunt M, Pye SR, O'Neill TW, Silman AJ, Reeve J. Low

BMD is less predictive than reported falls for future limb fractures in women across Europe: results from the European Prospective Osteoporosis Study. Bone 2005;36: 387-398.
[116] Brekelmans WAM, Poorth HW, Slooff TJJH. A new method to analyse the mechanical behaviour of skeletal parts. Acta orthop. Scandinav. 1972;43: 301-317.
[117] Huiskes R, Chao EYS. A survey of finite element analysis in orthopedic biomechanics: The first decade. Journal of Biomechanics 1983;16: 385-409.
[118] Luo Y, Ferdous Z, Leslie WD. A preliminary dual-energy X-ray absorptiometry-based finite element model for assessing osteoporotic hip fracture risk. J. Engineering in Medicine 2011;225: 1188-1195.
[119] Op Den Buijs J, Dragomir-Daescu D. Validated finite element models of the proximal femur using two-dimensional projected geometry and bone density. Computer Methods and Programs in Biomedicine 2011;104: 168-174.
[120] Naylor KE, McCloskey EV, Eastell R, Yang L. Use of DXA-based finite element analysis of the proximal femur in a longitudinal study of hip fracture. Journal of Bone and Mineral Research 2013;28: 1014-1021.
[121] Ahmad O, Ramamurthi K, Wilson KE, Engelke K, Prince RL, Taylor RH. Volumetric DXA (VXA): A new method to extract 3D information from multiple in vivo DXA images. Journal of Bone and Mineral Research 2010;25: 2744-2751.
[122] Dragomir-Daescu D, Op Den Buijs J, McEligot S, Dai Y, Entwistle R, Salas C, Melton LJ, III, Bennet K, Khosla S, Amin S. Robust QCT/FEA Models of Proximal Femur Stiffness and Fracture Load During a Sideways Fall on the Hip. Annals of Biomedical Engineering 2011;39: 742-755.
[123] Mastmeyer A, Engelke K, Fuchs C, Kalender WA. A hierarchical 3D segmentation method and the definition of vertebral body coordinate systems for QCT of the lumbar spine. Medical Image Analysis 2006;10: 560-577.
[124] Ohnaru K, Sone T, Tanaka K, Akagi K, Ju Y-I, Choi H-J, Tomomitsu T, Fukunaga M. Hip structural analysis: a comparison of DXA with CT in postmenopausal Japanese women. SpringerPlus 2013;2: 331.
[125] Prevrhal S, Shepherd JA, Faulkner KG, Gaither KW, Black DM, Lang TF. Comparison of DXA Hip Structural Analysis with Volumetric QCT. Journal of Clinical Densitometry 2008;11: 232-236.
[126] Roberts BJ, Kopperdahl D, Thrall E, Muller JA, Keaveny TM, Bouxsein ML. Prediction of femoral strength in a sideways fall configuration using QCT-based finite element analysis. Bone 2009;44, Supplement 1: S72.
[127] Liu XS, Zhang XH, Sekhon KK, Adams MF, McMahon DJ, Bilezikian JP, Shane E, Guo XE. High-resolution peripheral quantitative computed tomography can assess microstructural and mechanical properties of human distal tibial bone. Journal of Bone and Mineral Research 2009;25: 746-756.
[128] Burghardt AJ, Issever AS, Schwartz AV, Davis KA, Masharani U, Majumdar S, Link TM. High-Resolution Peripheral Quantitative Computed Tomographic Imaging of Cortical and Trabecular Bone Microarchitecture in Patients with Type 2 Diabetes Mellitus. The Journal of Clinical Endocrinology & Metabolism 2013;95: 5045-5055.
[129] Cheung A, Adachi J, Hanley D, Kendler D, Davison KS, Josse R, Brown J, Ste-Marie L-G, Kremer R, Erlandson M, Dian L, Burghardt A, Boyd S. High-Resolution

Peripheral Quantitative Computed Tomography for the Assessment of Bone Strength and Structure: A Review by the Canadian Bone Strength Working Group. Current Osteoporosis Reports 2013;11: 136-146.
[130] Yuh I, Yamamoto I, Shigei M, Ohnaka Y, Takada M, Morita R. Vertebral bone mineral measurement: A comparative study between quantitative computed tomography and dual X-ray absorptiometry. Journal of Bone and Mineral Metabolism 1994;12: 27-31.
[131] Brenner DJ, Hall EJ. Computed Tomography, An Increasing Source of Radiation Exposure. New England Journal of Medicine 2007;357: 2277-2284.
[132] Yoshikawa T, Turner CH, Peacock M, Slemenda CW, Weaver CM, Teegarden D, Markwardt P, Burr DB. Geometric structure of the femoral neck measured using dual-energy X-ray absorptiometry. Journal of Bone and Mineral Research 1994;9: 1053-1064.
[133] Van den Kroonenberg AJ, Hayes WC, McMahon TA. Dynamic Models for Sideways Falls From Standing Height. Journal of Biomechanical Engineering 1995;117: 309-318.
[134] Robinovitch SN, Hayes WC, McMahon TA. Prediction of Femoral Impact Forces in Falls on the Hip. ASME Journal of Biomechanical Engineering 1991;113: 366-374.
[135] Keyak JH, Rossi SA, Jones KA, Skinner HB. Prediction of femoral fracture load using automated finite element modeling. Journal of Biomechanics 1998;31: 125-133.
[136] Luo Y, Ferdous Z, Leslie WD. Precision study of DXA-based patient-specific finite element modeling for assessing hip fracture risk. International Journal for Numerical Methods in Biomedical Engineering 2013;29: 615-629.
[137] Schileo E, Taddei F, Cristofolini L, Viceconti M. Subject-specific finite element models implementing a maximum principal strain criterion are able to estimate failure risk and fracture location on human femurs tested in vitro. Journal of Biomechanics 2008;41: 356-367.
[138] Lotz JC, Cheal EJ, Hayes WC. Fracture Prediction for the Proximal Femur Using Finite Element Models: Part I-Linear Analysis. Journal of Biomechanical Engineering 1991;113: 353-360.
[139] Lotz JC, Cheal EJ, Hayes WC. Fracture Prediction for the Proximal Femur Using Finite Element Models: Part II-Nonlinear Analysis. Journal of Biomechanical Engineering 1991;113: 361-365.
[140] Keyak JH, Rossi SA. Prediction of femoral fracture load using finite element models: an examination of stress- and strain-based failure theories. Journal of Biomechanics 2000;33: 209-214.
[141] Nasiri Sarvi M, Luo Y. A two-level subject-specific biomechanical model for improving prediction of hip fracture risk. Clinical Biomechanics 2015;30: 881–887.
[142] Cummings SR, Nevitt MC. A HYPOTHESIS: The Causes of Hip Fractures. Journal of Gerontology 1989;44: M107-M111.
[143] Schwartz AV, Kelsey JL, Sidney S, Grisso JA. Characteristics of Falls and Risk of Hip Fracture in Elderly Men. Osteoporosis International 1998;8: 240-246.
[144] Kim KJ, Ashton Miller JA. Segmental dynamics of forward fall arrests: A system identification approach. Clinical Biomechanics 2009;24: 348-354.
[145] Gruber K, Ruder H, Denoth J, Schneider K. A comparative study of impact dynamics: wobbling mass model versus rigid body models. Journal of Biomechanics 1998;31: 439-444.

[146] Chiu J, Robinovitch SN. Prediction of upper extremity impact forces during falls on the outstretched hand. Journal of Biomechanics 1998;31: 1169-1176.
[147] DeGoede KM, Ashton-Miller JA. Fall arrest strategy affects peak hand impact force in a forward fall. Journal of Biomechanics 2002;35: 843-848.
[148] DeGoede KM, Ashton-Miller JA. Biomechanical simulations of forward fall arrests: effects of upper extremity arrest strategy, gender and aging-related declines in muscle strength. Journal of Biomechanics 2003;36: 413-420.
[149] DeGoede KM, Ashton-Miller JA, Schultz AB. Fall-related upper body injuries in the older adult: a review of the biomechanical issues. Journal of Biomechanics 2003;36: 1043-1053.
[150] Lo J, Ashton-Miller JA. Effect of pre-impact movement strategies on the impact forces resulting from a lateral fall. Journal of Biomechanics 2008;41: 1969-1977.
[151] Lo J, Ashton-Miller JA. Effect of upper and lower extremity control strategies on predicted injury risk during simulated forward falls: a study in healthy young adults. Journal of Biomechanical Engineering 2008;130: 410-415.
[152] Schiehlen W. Computational dynamics: theory and applications of multibody systems. European Journal of Mechanics - A/Solids 2006;25: 566-594.
[153] Schiehlen W, Guse N, Seifried R. Multibody dynamics in computational mechanics and engineering applications. Computer Methods in Applied Mechanics and Engineering 2006;195: 5509-5522.
[154] Schileo E, Taddei F, Malandrino A, Cristofolini L, Viceconti M. Subject-specific finite element models can accurately predict strain levels in long bones. Journal of Biomechanics 2007;40: 2982-2989.
[155] Keyak JH, Rossi SA, Jones KA, Skinner HB. Prediction of femoral fracture load using automated finite element modeling. Journal of Biomechanics 1997;31: 125-133.
[156] Keyak JH, Skinner HB, Fleming JA. Effect of force direction on femoral fracture load for two types of loading conditions. Journal of Orthopaedic Research 2001;19: 539-544.
[157] Keyak JH, Falkinstein Y. Comparison of in situ and in vitro CT scan-based finite element model predictions of proximal femoral fracture load. Medical Engineering & Physics 2003;25: 781-787.
[158] Cody DD, Gross GJ, J. Hou F, Spencer HJ, Goldstein SA, P. Fyhrie D. Femoral strength is better predicted by finite element models than QCT and DXA. Journal of Biomechanics 1999;32: 1013-1020.
[159] Schileo E, Dall'Ara E, Taddei F, Malandrino A, Schotkamp T, Baleani M, Viceconti M. An accurate estimation of bone density improves the accuracy of subject-specific finite element models. Journal of Biomechanics 2008;41: 2483-2491.
[160] Langton CM, Pisharody S, Keyak JH. Comparison of 3D finite element analysis derived stiffness and BMD to determine the failure load of the excised proximal femur. Medical Engineering & Physics 2009;31: 668-672.
[161] Grassi L, Schileo E, Taddei F, Zani L, Juszczyk M, Cristofolini L, Viceconti M. Accuracy of finite element predictions in sideways load configurations for the proximal human femur. Journal of Biomechanics 2012;45: 394-399.

[162] Koivumaki JEM, Thevenot J, Pulkkinen P, Kuhn V, Link TM, Eckstein F, Jamsa T. Cortical bone finite element models in the estimation of experimentally measured failure loads in the proximal femur. Bone 2012.
[163] Koivumaki JEM, Thevenot J, Pulkkinen P, Kuhn V, Link TM, Eckstein F, Jamsa T. Ct-based finite element models can be used to estimate experimentally measured failure loads in the proximal femur. Bone 2012;50: 824-829.
[164] Hambli R, Allaoui S. A Robust 3D Finite Element Simulation of Human Proximal Femur Progressive Fracture Under Stance Load with Experimental Validation. Annals of Biomedical Engineering 2013;41: 2515-2527.
[165] Haider IT, Speirs AD, Frei H. Effect of boundary conditions, impact loading and hydraulic stiffening on femoral fracture strength. Journal of Biomechanics 2013;46: 2115-2121.
[166] Park BK, Bae JH, Koo BY, Kim JJ. Function-based morphing methodology for parameterizing patient-specific models of human proximal femurs. Computer-Aided Design 2014;51: 31-38.
[167] Carballido-Gamio J, Harnish R, Saeed I, Streeper T, Sigurdsson S, Amin S, Atkinson EJ, Therneau TM, Siggeirsdottir K, Cheng X, Melton Iii LJ, Keyak JH, Gudnason V, Khosla S, Harris TB, Lang TF. Structural patterns of the proximal femur in relation to age and hip fracture risk in women. Bone 2013;57: 290-299.
[168] Gregory JS, Aspden RM. Femoral geometry as a risk factor for osteoporotic hip fracture in men and women. Medical Engineering & Physics 2008;30: 1275-1286.
[169] Ito M, Wakao N, Hida T, Matsui Y, Abe Y, Aoyagi K, Uetani M, Harada A. Analysis of hip geometry by clinical CT for the assessment of hip fracture risk in elderly Japanese women. Bone 2010;46: 453-457.
[170] Loveridge N, Power J, Kroger H, Parker M, Rushton N, Reeve J. Femoral neck cortical thickness and intracapsular hip fracture: A re-appraisal. Bone 2010;47, Supplement 1: S182.
[171] Long Y, Leslie WD, Luo Y. Study of DXA-derived lateral-medial cortical bone thickness in assessing hip fracture risk. Bone Reports 2015;2: 44-51.
[172] Bell KL, Loveridge N, Power J, Garrahan N, Meggitt BF, Reeve J. Regional differences in cortical porosity in the fractured femoral neck. Bone 1999;24: 57-64.
[173] Bell KL, Loveridge N, Jordan GR, Power J, Constant CR, Reeve J. A novel mechanism for induction of increased cortical porosity in cases of intracapsular hip fracture. Bone 2000;27: 297-304.
[174] Majumder S, Roychowdhury A, Pal S. Simulation of hip fracture in sideways fall using a 3D finite element model of pelvis-femur-soft tissue complex with simplified representation of whole body. Medical Engineering & Physics 2007;29: 1167-1178.
[175] Majumder S, Roychowdhury A, Pal S. Effects of trochanteric soft tissue thickness and hip impact velocity on hip fracture in sideways fall through 3D finite element simulations. Journal of Biomechanics 2008;41: 2834-2842.
[176] Baddoura R, Hoteit M, El-Hajj Fuleihan G. Osteoporotic Fractures, DXA, and Fracture Risk Assessment: Meeting Future Challenges in the Eastern Mediterranean Region. Journal of Clinical Densitometry 2011;14: 384-394.

[177] Zhuang Z, Landsittel D, Benson S, Roberge R, Shaffer R. Facial Anthropometric Differences among Gender, Ethnicity, and Age Groups. Annals of Occupational Hygiene 2010;54: 391-402.
[178] Wang J, Thornton JC, Russell M, Burastero S, Heymsfield S, Pierson RN. Asians have lower body mass index (BMI) but higher percent body fat than do whites: comparisons of anthropometric measurements. American journal of clinical nutrition 1994;60: 23-28.
[179] Peacock M, Buckwalter KA, Persohn S, Hangartner TN, Econs MJ, Hui S. Race and sex differences in bone mineral density and geometry at the femur. Bone 2009;45: 218-225.
[180] Franser S. http://www.gettyimages.ca/detail/photo/failed-hip-replacement-ct-scan-high-res-stock-photography/547999751. In; 2010.
[181] Albanese CV, Diessel E, Genant HK. Clinical Applications of Body Composition Measurements Using DXA. Journal of Clinical Densitometry 2003;6: 75-85.
[182] Nuti R, Martini G. Measurements of bone mineral density by DXA total body absorptiometry in different skeletal sites in postmenopausal osteoporosis. Bone 1992;13: 173-178.
[183] Kalender WA, Felsenberg D, Genant HK, Fischer M, Dequeker J, Reeve J. The European Spine Phantom- a tool for standardization and quality control in spinal bone mineral measurements by DXA and QCT. European Journal of Radiology 1995;20: 83-92.
[184] Cordero-MacIntyre ZR, Peters W, Libanati CR, Espa├±a RC, Abila SO, Howell WH, Lohman TG. Reproducibility of DXA in Obese Women. Journal of Clinical Densitometry 2002;5: 35-44.
[185] Newman ED, Olenginski TP, Perruquet JL, Hummel J, Indeck C, Wood GC. Using Mobile DXA to Improve Access to Osteoporosis Care: Unit Design, Program Development, Implementation, and Outcomes. Journal of Clinical Densitometry 2004;7: 71-75.
[186] Picard D, Brown JP, Rosenthall L, Couturier M, Levesque J, Dumont M, Ste-Marie LG, Tenenhouse A, Dodin S. Ability of Peripheral DXA Measurement to Diagnose Osteoporosis As Assessed By Central DXA Measurement. Journal of Clinical Densitometry 2004;7: 111-118.
[187] Stephen AB, Pye D, Lyons AR, Oni JA, Davis TRC. Dual energy X-ray absorptiometry (DXA): can it detect acute scaphoid fractures? The Journal of Hand Surgery (British & European Volume) 2005;30: 83-84.
[188] Khan AA, Hanley DA, Bilezikian JP, Binkley N, Brown JP, Hodsman AB, Josse RG, Kendler DL, Lewiecki EM, Miller PD, Olszynski WP, Petak SM, Syed ZA, Theriault D, Watts NB. Standards for Performing DXA in Individuals With Secondary Causes of Osteoporosis. Journal of Clinical Densitometry 2006;9: 47-57.
[189] Bolotin HH. DXA in vivo BMD methodology: An erroneous and misleading research and clinical gauge of bone mineral status, bone fragility, and bone remodelling. Bone 2007;41: 138-154.
[190] Lou Bonnick S. HSA: Beyond BMD with DXA. Bone 2007;41: 9-12.
[191] Ozdemir A, Ucar M. Standardization of spine and hip BMD measurements in different DXA devices. European Journal of Radiology 2007;62: 423-426.

[192] Boehm HF, Horng A, Notohamiprodjo M, Eckstein F, Burklein D, Panteleon A, Lutz J, Reiser M. Prediction of the fracture load of whole proximal femur specimens by topological analysis of the mineral distribution in DXA-scan images. Bone 2008;43: 826-831.
[193] Mittra E, Rubin C, Gruber B, Qin Y-X. Evaluation of trabecular mechanical and microstructural properties in human calcaneal bone of advanced age using mechanical testing, CT and DXA. Journal of Biomechanics 2008;41: 368-375.
[194] Sievanen H, Weynand LS, Wacker WK, Simonelli C, Burke PK, Ragi S, Del Rio L. A Novel DXA-Based Hip Failure Index Captures Hip Fragility Independent of BMD. Journal of Clinical Densitometry 2008;11: 367-372.
[195] Albanese CV, Cepollaro C, de Terlizzi F, Brandi ML, Passariello R. Performance of Five Phalangeal QUS Parameters in the Evaluation of Gonadal-Status, Age and Vertebral Fracture Risk Compared with DXA. Ultrasound in Medicine & Biology 2009;35: 537-544.
[196] Arthurs KL, Andrews DM. Upper extremity soft and rigid tissue mass prediction using segment anthropometric measures and DXA. Journal of Biomechanics 2009;42: 389-394.
[197] Blake GM, Griffith JF, Yeung DKW, Leung PC, Fogelman I. Effect of increasing vertebral marrow fat content on BMD measurement, T-Score status and fracture risk prediction by DXA. Bone 2009;44: 495-501.
[198] Burkhart TA, Arthurs KL, Andrews DM. Manual segmentation of DXA scan images results in reliable upper and lower extremity soft and rigid tissue mass estimates. Journal of Biomechanics 2009;42: 1138-1142.
[199] Nasiri Sarvi M, Luo Y. Estimation of body segment masses using whole-body DXA image. 24th CANCAM Conference, Saskatoon, Saskatchewan, Canada, June 2-6 2013.
[200] Luo Y, Nasiri Sarvi M, Sun P, Ouyang J. A Subject specific dynamics model for predicting impact force in elderly lateral fall. Applied Mechanics and Materials 2014;446-447: 339-343.
[201] Durkin JL, Dowling JJ, Andrews DM. The measurement of body segment inertial parameters using dual energy X-ray absorptiometry. Journal of Biomechanics 2002;35: 1575-1580.
[202] Ganley KJ, Powers CM. Anthropometric parameters in children: a comparison of values obtained from dual energy x-ray absorptiometry and cadaver-based estimates. Gait & Posture 2004;19: 133-140.
[203] Wicke J, Dumas GvA, Costigan PA. Trunk density profile estimates from dual X-ray absorptiometry. Journal of Biomechanics 2008;41: 861-867.
[204] Schaffner G. Assessment of hip fracture risk in astronauts exposed to long-term weightlessness. In: Health Science and Technology. Cambridge: Harvard University, Massachusetts Institute of Technology; 1999.
[205] Kibble TWB, Berkshire FH. Classical Mechanics: Imperial College Press; 2004.
[206] Meriam JL, Kraige LG. Engineering Mechanics: Dynamics: Wiley; 2012.
[207] Pena E, Calvo B, Martinez MA, Doblare M. An anisotropic visco-hyperelastic model for ligaments at finite strains. Formulation and computational aspects. International Journal of Solids and Structures 2007;44: 760-778.

[208] Ibrahim i E, Neviman O. Articular human joint modelling. Robotica 2010;28: 321-339.
[209] Robinovitch SN, Hayes WC, McMahon TA. Distribution of contact force during impact to the hip. Ann. Biomed. Eng. 1997;25: 499–508.
[210] Laing AC, Robinovitch SN. Characterizing the effective stiffness of the pelvis during sideways falls on the hip. Journal of Biomechanics 2010;43: 1898-1904.
[211] Rao SS. Mechanical Vibrations: Pearson Education; 2004.
[212] Robinovitch SN, Inkster L, Maurer J, Warnick B. Strategies for Avoiding Hip Impact During Sideways Falls. Journal of Bone and Mineral Research 2003;18: 1267-1273.
[213] Karamanidis K, Arampatzis A. Effects of running and age-related degeneration in leg extensor muscles on recovery behaviour after a fall. Journal of Biomechanics 2006;39, Supplement 1: S90.
[214] DeGoede KM, Ashton-Miller JA, Schultz AB, Alexander NB. Biomechanical Factors Affecting the Peak Hand Reaction Force During the Bimanual Arrest of a Moving Mass. Journal of Biomechanical Engineering 2001;124: 107-112.
[215] Taylor ME, Tanner KE, Freeman MAR, Yettram AL. Stress and strain distribution within the intact femur: compression or bending? Medical Engineering & Physics 1996;18: 122-131.
[216] Meriam JL, Kraige LG. Engineering Mechanics: Dynamics: Wiley; 2006.
[217] Mirzaei M, Keshavarzian M, Naeini V. Analysis of strength and failure pattern of human proximal femur using quantitative computed tomography (QCT)-based finite element method. Bone 2014;64: 108-114.
[218] Koivumaki JEM, Thevenot J, Pulkkinen P, Kuhn V, Link TM, Eckstein F, Jamsa T. Cortical bone finite element models in the estimation of experimentally measured failure loads in the proximal femur. Bone 2012;51: 737-740.
[219] Nishiyama KK, Gilchrist S, Guy P, Cripton P, Boyd SK. Proximal femur bone strength estimated by a computationally fast finite element analysis in a sideways fall configuration. Journal of Biomechanics 2013;46: 1231-1236.
[220] Etheridge B, Beason D, Lopez R, Alonso J, McGwin G, Eberhardt A. Effects of Trochanteric Soft Tissues and Bone Density on Fracture of the Female Pelvis in Experimental Side Impacts. Annals of Biomedical Engineering 2005;33: 248-254.
[221] Chapra SC, Canale RP. Numerical Methods for Engineers: McGraw-Hill Higher Education; 2006.
[222] Peng L, Bai J, Zeng X, Zhou Y. Comparison of isotropic and orthotropic material property assignments on femoral finite element models under two loading conditions. Medical Engineering & Physics 2006;28: 227-233.
[223] Gnudi S, Ripamonti C, Gualtieri G, Malavolta N. Geometry of proximal femur in the prediction of hip fracture in osteoporotic women. The British Journal of Radiology 1999;72: 729-733.
[224] WHO. Physical status: the use and interpretation of anthropometry. Report of a WHO Expert Committee. WHO Technical Report Series 854. Geneva: World Health Organization; 1995.
[225] Yang L, Palermo L, Black DM, Eastell R. Prediction of Incident Hip Fracture with the Estimated Femoral Strength by Finite Element Analysis of DXA Scans in the

Study of Osteoporotic Fractures. Journal of Bone and Mineral Research 2014;29: 2594-2600.
[226] Morgan EF, Bayraktar HH, Keaveny TM. Trabecular bone modulus-density relationships depend on anatomic site. Journal of Biomechanics 2003;36: 897-904.
[227] Dewolf J. Mechanics Of Materials (In Si Units): McGraw-Hill Education (India) Pvt Limited; 2004.
[228] Morgan EF, Keaveny TM. Dependence of yield strain of human trabecular bone on anatomic site. Journal of Biomechanics 2001;34: 569-577.
[229] Robinovitch SN, McMahon TA, Hayes WC. Force attenuation in trochanteric soft tissues during impact from a fall. Journal of Orthopaedic Research 1995;13: 956-962.
[230] WHO. Obesity: preventing and managing the global epidemic. WHO Technical Report Series 894. Geneva, Switzerland: World Health Organization. 2000.
[231] Levine IC, Bhan S, Laing AC. The effects of body mass index and sex on impact force and effective pelvic stiffness during simulated lateral falls. Clinical Biomechanics 2013;28: 1026-1033.
[232] Bhan S, Levine IC, Laing AC. Energy absorption during impact on the proximal femur is affected by body mass index and flooring surface. Journal of Biomechanics 2014;47: 2391-2397.
[233] Johansson H, Kanis JA, Odén A, McCloskey E, Chapurlat RD, Christiansen C, Cummings SR, Diez-Perez A, Eisman JA, Fujiwara S, Glüer C-C, Goltzman D, Hans D, Khaw K-T, Krieg M-A, Kröger H, LaCroix AZ, Lau E, Leslie WD, Mellström D, Melton LJ, O'Neill TW, Pasco JA, Prior JC, Reid DM, Rivadeneira F, van Staa T, Yoshimura N, Zillikens MC. A Meta-Analysis of the Association of Fracture Risk and Body Mass Index in Women. Journal of Bone and Mineral Research 2013;29: 223-233.
[234] Laet C, Kanis JA, OdÃ©n A, Johanson H, Johnell O, Delmas P, Eisman JA, Kroger H, Fujiwara S, Garnero P, McCloskey EV, Mellstrom D, Melton LJ, 3rd, Meunier PJ, Pols HAP, Reeve J, Silman A, Tenenhouse A. Body mass index as a predictor of fracture risk: A meta-analysis. Osteoporosis International 2005;16: 1330-1338.
[235] Bouxsein ML, Szulc P, Munoz F, Thrall E, Sornay-Rendu E, Delmas PD. Contribution of Trochanteric Soft Tissues to Fall Force Estimates, the Factor of Risk, and Prediction of Hip Fracture Risk*. Journal of Bone and Mineral Research 2007;22: 825-831.
[236] Melton LJ, Atkinson EJ, O'Connor MK, O'Fallon WM, Riggs BL. Bone Density and Fracture Risk in Men. Journal of Bone and Mineral Research 1998;13: 1915-1923.
[237] Nielson C, Bouxsein M, Freitas S, Ensrud K, Orwoll E. Trochanteric Soft Tissue Thickness and Hip Fracture in Older Men. The Journal of Clinical Endocrinology & Metabolism 2009;94: 491-496.
[238] Orwoll E. Assessing Bone Density in Men. Journal of Bone and Mineral Research 2000;15: 1867-1870.
[239] Magaziner J, Hawkes W, Hebel JR, Zimmerman SI, Fox KM, Dolan M, Felsenthal G, Kenzora J. Recovery From Hip Fracture in Eight Areas of Function. The Journals of Gerontology Series A: Biological Sciences and Medical Sciences 2000;55: M498-M507.
[240] Orwoll ES, Marshall LM, Nielson CM, Cummings SR, Lapidus J, Cauley JA, Ensrud K, Lane N, Hoffmann PR, Kopperdahl DL, Keaveny TM. Finite Element

Analysis of the Proximal Femur and Hip Fracture Risk in Older Men. Journal of Bone and Mineral Research 2009;24: 475-483.
[241] Melton Iii LJ, Orwoll ES, Wasnich RD. Does Bone Density Predict Fractures Comparably in Men and Women? Osteoporosis International 2001;12: 707-709.
[242] Nguyen ND, Pongchaiyakul C, Center JR, Eisman JA, Nguyen TV. Identification of High-Risk Individuals for Hip Fracture: A 14-Year Prospective Study. Journal of Bone and Mineral Research 2005;20: 1921-1928.
[243] Farahmand BY, Michaëlsson K, Baron JA, Persson P-G, Ljunghall S, Group ftSHFS. Body Size and Hip Fracture Risk. Epidemiology 2000;11: 214-219.
[244] Robinovitch SN, Hayes WC, McMahon TA. Predicting the Impact Response of a Nonlinear Single-Degree-of-Freedom Shock-Absorbing System From the Measured Step Response. Journal of Biomechanical Engineering 1997;119: 221-227.
[245] Feldman F, Robinovitch SN. Reducing hip fracture risk during sideways falls: Evidence in young adults of the protective effects of impact to the hands and stepping. Journal of Biomechanics 2007;40: 2612-2618.

Appendix A

Equations of Motion of the Dynamics Model

This appendix represents the derivation of motion equations of the dynamics model. To build the Eq. (4.4), the kinetic and the potential energy expressions are required, which are directly related to the generalized coordinates and their first time derivatives. The velocity at the mass center of each segment is obtained and decomposed into x, y, and z-directions and used in calculating the kinetic energy (Figure A.1).

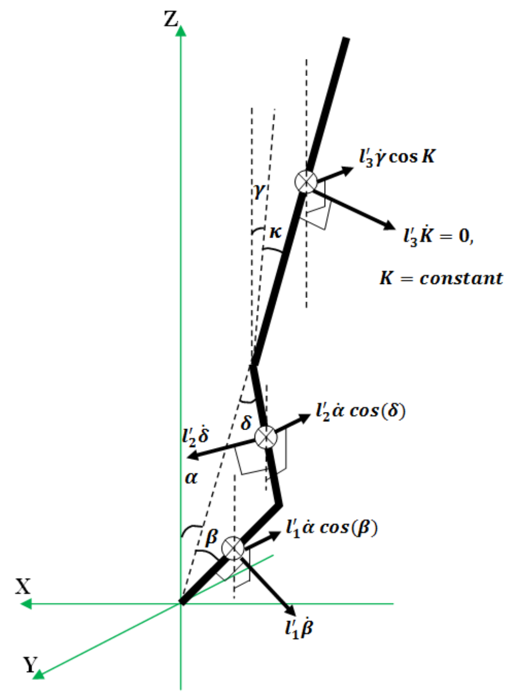

Figure A.1. Decomposed components of velocities of body segments in a sideways fall

Velocity at the shank mass center is determined by the first two generalized coordinates and the location of the shank mass center.

$$\begin{aligned} v_{cg-shank} &= \left[-l_1'\dot{\beta}\cos\beta\right]\hat{\imath} + \left[l_1'\dot{\beta}\sin\beta\sin\alpha - l_1'\dot{\alpha}\cos\beta\cos\alpha\right]\hat{\jmath} \\ &\quad + \left[-l_1'\dot{\beta}\sin\beta\cos\alpha - l_1'\dot{\alpha}\cos\beta\sin\alpha\right]\hat{k} \\ &= \left[-Pl_1\dot{\beta}\cos\beta\right]\hat{\imath} + \left[Pl_1\dot{\beta}\sin\beta\sin\alpha - Pl_1\dot{\alpha}\cos\beta\cos\alpha\right]\hat{\jmath} \\ &\quad + \left[-Pl_1\dot{\beta}\sin\beta\cos\alpha - Pl_1\dot{\alpha}\cos\beta\sin\alpha\right]\hat{k}, \qquad \mathrm{P} = \frac{\mathrm{l}_1'}{\mathrm{l}_1} \end{aligned} \tag{A.1}$$

The velocity of the knee is then obtained as

$$\begin{aligned} v_{knee} &= \left[-l_1\dot{\beta}\cos\beta\right]\hat{\imath} + \left[l_1\dot{\beta}\sin\beta\sin\alpha - l_1\dot{\alpha}\cos\beta\cos\alpha\right]\hat{\jmath} \\ &\quad + \left[-l_1\dot{\beta}\sin\beta\cos\alpha - l_1\dot{\alpha}\cos\beta\sin\alpha\right]\hat{k}. \end{aligned} \tag{A.2}$$

Therefore, the velocity at the thigh mass center can be calculated by the following equation,

$$v_{cg-thigh} = v_{knee} + v_{cg-thigh/knee}$$

$$\begin{aligned} &= \left[(Q-1)l_1\dot{\beta}\cos\beta\right]\hat{\imath} \\ &+ \left[-\dot{\alpha}\cos\alpha\,(l_1\cos\beta + Ql_2\cos\delta) + \sin\alpha\left(l_1\dot{\beta}\sin\beta + Ql_2\dot{\delta}\sin\delta\right)\right]\hat{\jmath} \\ &+ \left[-\dot{\alpha}\sin\alpha\,(l_1\cos\beta + Ql_2\cos\delta) + \cos\alpha\left(-l_1\dot{\beta}\sin\beta - Ql_2\dot{\delta}\sin\delta\right)\right]\hat{k}, \\ &\mathrm{Q} = \frac{\mathrm{l}_2'}{\mathrm{l}_2}. \end{aligned} \tag{A.3}$$

where δ represents the angle between the vertical and the projection of the thigh segment on the y-z plane. δ is not an independent DoF and can be calculated as

$$\delta = \sin^{-1}\left(\frac{l_1}{l_2}\sin\beta\right). \tag{A.4}$$

Subsequently, the velocity at the hip joint is obtained as

$$\begin{aligned} v_{hip} = &\left[-\dot{\alpha}\,cos\,\alpha\,(l_1\,cos\,\beta + l_2\,cos\,\delta) + sin\,\alpha\left(+l_1\dot{\beta}\,sin\,\beta + l_2\dot{\delta}\,sin\,\delta\right)\right]\hat{\jmath} \\ &+ \left[-\dot{\alpha}\,sin\,\alpha\,(l_1\,cos\,\beta + l_2\,cos\,\delta)\right. \\ &\left.+ cos\,\alpha\left(-l_1\dot{\beta}\,sin\,\beta - l_2\dot{\delta}\,sin\,\delta\right)\right]\hat{k} \end{aligned} \tag{A.5}$$

Trunk mass center velocity with respect to the hip is calculated by Eq. (A.6).

$$
\begin{aligned}
v_{cg-trunk} = v_{hip} + v_{cg-trunk/hip} \\
&= \left[-\dot{\alpha}\cos\alpha\,(l_1\cos\beta + l_2\cos\delta)\right. \\
&\left. + \sin\alpha\left(l_1\dot{\beta}\sin\beta + l_2\dot{\delta}\sin\delta\right) - Rl_3\dot{\gamma}\cos\kappa\cos\gamma\right]\hat{j} \\
&+ \left[-\dot{\alpha}\sin\alpha\,(l_1\cos\beta + l_2\cos\delta)\right. \\
&\left. + \cos\alpha\left(-l_1\dot{\beta}\sin\beta - l_2\dot{\delta}\sin\delta\right) - Rl_3\dot{\gamma}\cos\kappa\sin\gamma\right]\hat{k},
\end{aligned}
\tag{A.6}
$$

$$
\mathrm{R} = \frac{\mathrm{l}_3'}{\mathrm{l}_3}
$$

With the above expressions of velocities at segmental mass centers, the segmental kinetic and potential energies can be obtained as follows:

1- for the shank,

$$
\begin{aligned}
T_{shank-transfer} &= \frac{1}{2}m_1 v_{cg-shank}^2 \\
&= \frac{1}{2}m_1\left(\left[-Pl_1\dot{\beta}\cos\beta\right]^2\right. \\
&+ \left[Pl_1\dot{\beta}\sin\beta\sin\alpha - Pl_1\dot{\alpha}\cos\beta\cos\alpha\right]^2 \\
&\left.+ \left[-Pl_1\dot{\beta}\sin\beta\cos\alpha - Pl_1\dot{\alpha}\cos\beta\sin\alpha\right]^2\right) \\
&= \frac{1}{2}m_1(Pl_1)^2\left(\dot{\beta}^2 + \dot{\alpha}^2(\cos\beta)^2\right)
\end{aligned}
\tag{A.7}
$$

$$
T_{shank-rotation} = \tfrac{1}{2}I_1\left(\dot{\beta}^2 + \dot{\alpha}^2(\cos\beta)^2\right),
$$

$$
V_{shank} = m_1 g(Pl_1)\cos\beta\cos\alpha,
$$

2- for the thigh,

$$T_{thigh-transfer} = \frac{1}{2} m_2 v_{cg-thigh}^2$$

$$\begin{aligned}
&= \frac{1}{2} m_2 \Big\{ \big[(Q-1) l_1 \dot{\beta} \cos\beta\big]^2 \\
&+ \big[-\dot{\alpha} \cos\alpha \,(l_1 \cos\beta + Q l_2 \cos\delta) \\
&+ \sin\alpha \big(l_1 \dot{\beta} \sin\beta + Q l_2 \dot{\delta} \sin\delta\big)\big]^2 \\
&+ \big[-\dot{\alpha} \sin\alpha \,(l_1 \cos\beta + Q l_2 \cos\delta) \\
&+ \cos\alpha \big(-l_1 \dot{\beta} \sin\beta - Q l_2 \dot{\delta} \sin\delta\big)\big]^2 \Big\}
\end{aligned} \tag{A.8}$$

$$T_{thigh-rotation} = \tfrac{1}{2} I_2 \big(\dot{\delta}^2 + \dot{\alpha}^2 (\cos\delta)^2\big),$$

$$V_{thigh} = m_2 g (l_1 \cos\alpha \cos\beta + Q l_2 \cos\alpha \cos\delta),$$

3- for the trunk,

$$T_{trunk-transfer} = \frac{1}{2} m_3 v_{cg-thigh}^2$$

$$\begin{aligned}
&= \frac{1}{2} m_3 \Big\{ \big[-\dot{\alpha} \cos\alpha \,(l_1 \cos\beta + l_2 \cos\delta) \\
&+ \sin\alpha \big(l_1 \dot{\beta} \sin\beta + l_2 \dot{\delta} \sin\delta\big) - R l_3 \dot{\gamma} \cos\kappa \cos\gamma\big]^2 \\
&+ \big[-\dot{\alpha} \sin\alpha \,(l_1 \cos\beta + l_2 \cos\delta) \\
&+ \cos\alpha \big(-l_1 \dot{\beta} \sin\beta - l_2 \dot{\delta} \sin\delta\big) - R l_3 \dot{\gamma} \cos\kappa \sin\gamma\big]^2 \Big\}
\end{aligned} \tag{A.9}$$

$$T_{trunk-rotation} = \tfrac{1}{2} I_3 (\dot{\gamma}^2 (\cos\kappa)^2),$$

$$V_{trunk} = m_3 g (l_1 \cos\alpha \cos\beta + l_2 \cos\alpha \cos\delta + R l_3 \cos\kappa \cos\gamma).$$

The total kinetic and potential energies of the system are then calculated as bellow:

$$T = \sum_{i=1}^{3} T_{i-transfer} + \sum_{i=1}^{3} T_{i-rotation}, V = \sum_{i=1}^{3} V_i, i = 1, 2, 3 \tag{A.10}$$

$$\begin{aligned} T = {} & \frac{1}{2} m_1 (Pl_1)^2 \left(\dot{\beta}^2 + \dot{\alpha}^2 (\cos\beta)^2\right) + \frac{1}{2} I_1 \left(\dot{\beta}^2 + \dot{\alpha}^2 (\cos\beta)^2\right) \\ & + \frac{1}{2} m_2 \Big\{ \left[(Q-1) l_1 \dot{\beta} \cos\beta\right]^2 \\ & + \big[-\dot{\alpha} \cos\alpha \left(l_1 \cos\beta + Q l_2 \cos\delta\right) \\ & + \sin\alpha \left(l_1 \dot{\beta} \sin\beta + Q l_2 \dot{\delta} \sin\delta\right)\big]^2 \\ & + \big[-\dot{\alpha} \sin\alpha \left(l_1 \cos\beta + Q l_2 \cos\delta\right) \\ & + \cos\alpha \left(-l_1 \dot{\beta} \sin\beta - Q l_2 \dot{\delta} \sin\delta\right)\big]^2 \Big\} + \frac{1}{2} I_2 \left(\dot{\delta}^2 + \dot{\alpha}^2 (\cos\delta)^2\right) \\ & + \frac{1}{2} m_3 \Big\{ \big[-\dot{\alpha} \cos\alpha \left(l_1 \cos\beta + l_2 \cos\delta\right) \\ & + \sin\alpha \left(l_1 \dot{\beta} \sin\beta + l_2 \dot{\delta} \sin\delta\right) - R l_3 \dot{\gamma} \cos\kappa \cos\gamma\big]^2 \\ & + \big[-\dot{\alpha} \sin\alpha \left(l_1 \cos\beta + l_2 \cos\delta\right) + \cos\alpha \left(-l_1 \dot{\beta} \sin\beta - l_2 \dot{\delta} \sin\delta\right) \\ & - R l_3 \dot{\gamma} \cos\kappa \sin\gamma\big]^2 \Big\} + \frac{1}{2} I_3 \left(\dot{\gamma}^2 (\cos\kappa)^2\right) \end{aligned} \tag{A.11}$$

$$\begin{aligned} V = {} & m_1 g (Pl_1) \cos\beta \cos\alpha + m_2 g (l_1 \cos\alpha \cos\beta + Q l_2 \cos\alpha \cos\delta) + \\ & m_3 g (l_1 \cos\alpha \cos\beta + l_2 \cos\alpha \cos\delta + R l_3 \cos\kappa \cos\gamma). \end{aligned} \tag{A.12}$$

Motion equations of the dynamics model are obtained by substituting Eqs. (A.11) and (A.12) into the Eq. (4.4). The governing equation for this formulation, which has been simplified from its most general form by the use of generalized coordinates, is

$$\boldsymbol{H}(\boldsymbol{q})\ddot{\boldsymbol{q}} + \boldsymbol{C}(\boldsymbol{q}, \dot{\boldsymbol{q}}) + \boldsymbol{G}(\boldsymbol{q}) = \boldsymbol{T}, \tag{A.13}$$

where bold letters are used to represent vectors and matrices. The first term on the left-hand side of the above equation represents the inertial coupling between segments. It consists of the system inertia tensor ($\boldsymbol{H}$) multiplied by the joint angular acceleration vector:

$$\ddot{q} = \begin{bmatrix} \ddot{q}_1 \\ \ddot{q}_2 \\ \ddot{q}_3 \end{bmatrix}. \tag{A.14}$$

The second term ($\boldsymbol{C}$) which would generally account for torques arising due to centrifugal and Coriolis effects, in this case represents only centrifugal effects, since Coriolis terms are eliminated by the choice of generalized coordinates. The third term ($\boldsymbol{G}$) represents torques on the system due to gravity. Finally, the term on the right side ($\boldsymbol{T}$) corresponds to the external torques placed on the system such as the torques applied on the joints as joint actions.

Appendix B

Derivation of the Effective Mass Equation

This appendix represents the derivation of the effective mass equation in the impact model. The effective mass is calculated by expressing the vertical impact force applied at the hip, in terms of the vertical acceleration of the hip during impact ($\ddot{z}_{hip}$), divided by ($\ddot{z}_{hip} + g$), where g is the acceleration of gravity.

$$\mathrm{M_{effective}} = \frac{\mathrm{F_{vertical}}}{\ddot{\mathrm{z}}_{\mathrm{hip}} + g} \tag{B.1}$$

Considering the upper trunk configuration at the impact moment (Figure B.1) and the applied forces to the hip, the Newton's second law can be written as

$$\mathrm{F_{hip}d} = \mathrm{I_3}\ddot{\varphi},$$
$$-\mathrm{m_3}g + \mathrm{F_{hip}} = \mathrm{m_3}\ddot{\mathrm{z}}_{\mathrm{cg}}, \tag{B.2}$$

where $\ddot{z}_{cg}$ is the vertical acceleration of the trunk mass center and index 3 indicates the upper trunk properties. Hence, $\ddot{z}_{cg}$ can be calculated as

$$\ddot{\mathrm{z}}_{\mathrm{cg}} = \frac{\mathrm{I_3}\ddot{\varphi}}{\mathrm{d.m_3}} - g. \tag{B.3}$$

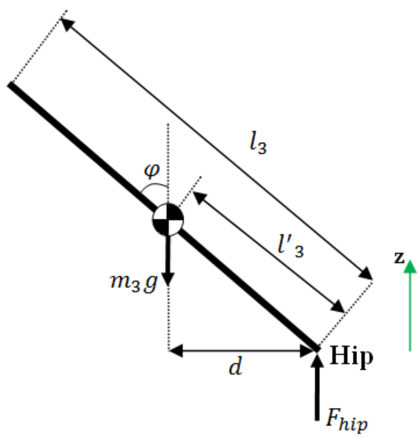

Figure B.1. Free body diagram of the upper trunk at the impact instant in the plane passing through the upper trunk and z-axis

The relation between z_{hip} and z_{cg}, the vertical distance of the hip and the trunk mass center from the ground, can be expressed as follows:

$$\mathrm{z_{hip}} = \mathrm{z_{cg}} - \mathrm{l'_3}\cos\varphi, \tag{B.4}$$

and thus,

$$\ddot{\mathrm{z}}_{\mathrm{hip}} = \ddot{\mathrm{z}}_{\mathrm{cg}} + \mathrm{l'_3}(\dot{\varphi}^2\cos\varphi + \ddot{\varphi}\sin\varphi). \tag{B.5}$$

Based on the study in [133], $\dot{\varphi}^2$ is much smaller than $\ddot{\varphi}$ ($\dot{\varphi}^2 < 0.01|\ddot{\varphi}|$) and therefore the effective mass can be defined by combining Eqs. (B.1), (B.2), (B.3) and (B.5),

$$\mathrm{M_{effective}} = \frac{\mathrm{I_3m_3}}{\mathrm{I_3+l'_3dm_3}\sin\varphi}. \tag{B.6}$$

In Eq. (B.6), d defines the horizontal distance between the hip and the trunk mass center in the plane passing through the upper trunk and z-axis which can be determined as

$$d = l'_3 \sin \varphi, \tag{B.7}$$

where φ is the angle between the vertical and the trunk that can be calculated as

$$\varphi = \arccos(\cos \gamma \cos \kappa). \tag{B.8}$$

In Eq. (B.8), γ is the angle between the vertical and the projection of the trunk segment on the y-z plane and κ is the angle between the trunk and the line through the hinge at the floor and the hip joint (Figure 4.2).

The same procedure is used for calculating the lower extremity effective mass. As the lower extremity configuration does not have any considerable change during the impact, and there is no abduction/adduction DoF for the knee joint [133], the shank and the thigh segments can be considered rigidly interconnected during the impact for the purpose of calculating the effective mass. As shown in Figure B.2, Link 1 (the shank) and Link 2 (the thigh) are treated as a single link [133] in derivations of the lower extremity effective mass.

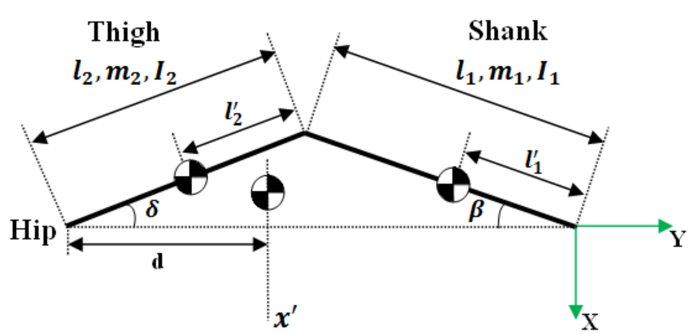

Figure B.2. Top view of the shank (Link 1) and the thigh (Link 2) at the impact moment

Eq. (B.9) defines the lateral distance between the hip and the mass center of the lower extremity,

$$\mathrm{d} = \frac{(1-\mathrm{Q})\mathrm{l}_2\mathrm{m}_2\cos\delta + \mathrm{m}_1\big((1-\mathrm{P})\mathrm{l}_1\cos\beta + \mathrm{l}_2\cos\delta\big)}{\mathrm{m}_1+\mathrm{m}_2}, \tag{B.9}$$

where $P = \frac{l_1'}{l_1}$ and $Q = \frac{l_2'}{l_2}$. The lower extremity mass moment of inertia about x′-axis, parallel to the x-axis and passing through the total leg center of mass, is calculated using the parallel-axis theorem:

$$\mathrm{I}_{\mathrm{total}} = \mathrm{I}_{1\ \mathrm{transfered}} + \mathrm{I}_{2\ \mathrm{transfered}} \tag{B.10}$$

$$\begin{aligned}\mathrm{I}_{1\ \mathrm{transfered}} = {} & \mathrm{I}_1(\cos\beta)^2 \\ & + \mathrm{m}_1\Bigg((1-\mathrm{P})\mathrm{l}_1\cos\beta + \mathrm{l}_2\cos\delta \\ & - \frac{\mathrm{m}_2(1-\mathrm{Q})\mathrm{l}_2\cos\delta + \mathrm{m}_1\big((1-\mathrm{P})\mathrm{l}_1\cos\beta + \mathrm{l}_2\cos\delta\big)}{\mathrm{m}_1+\mathrm{m}_2}\Bigg)^2\end{aligned} \tag{B.11}$$

$$\begin{aligned}\mathrm{I}_{2\ \mathrm{transfered}} = {} & \mathrm{I}_2(\cos\delta)^2 \\ & + \mathrm{m}_2\Bigg(\frac{\mathrm{m}_2(1-\mathrm{Q})\mathrm{l}_2\cos\delta + \mathrm{m}_1\big((1-\mathrm{P})\mathrm{l}_1\cos\beta + \mathrm{l}_2\cos\delta\big)}{\mathrm{m}_1+\mathrm{m}_2} \\ & - (1-\mathrm{Q})\mathrm{l}_2\cos\delta\Bigg)^2\end{aligned} \tag{B.12}$$

where $I_1(cos\,\beta)^2$ and $I_2(cos\,\delta)^2$ are respectively I_1 and I_2 about the x-axis. The effective mass of the lower extremity is obtained using Eq. (B.6) where m_3 and I_3 are respectively substituted by $(m_1 + m_2)$ and I_{total} and considering that $\varphi = 90^o$:

$$M_{\text{effective (lower extremity)}} = \frac{I_{\text{total}}}{d^2 + \frac{I_{\text{total}}}{m_1 + m_2}} \tag{B.13}$$

The total effective mass is then calculated as follows:

$$M_{\text{effective (total)}} = M_{\text{effective (lower extremity)}} + M_{\text{effective (upper extremity)}} \tag{B.14}$$

List of Publications

Journal Papers

[1] Masoud Nasiri Sarvi, Yunhua Luo, 2015, "Gender Differences in the Association between Hip Fracture Risk and Body Parameters", *Bone*, Under review

[2] Masoud Nasiri Sarvi, Yunhua Luo, 2015, "A Two-Level Subject-Specific Biomechanical Model for Improving Prediction of Hip Fracture Risk", *Clinical Biomechanics*, vol. 30, no. 8, pp. 881-887

[3] Masoud Nasiri Sarvi, Yunhua Luo, Peidong Sun, Jun Ouyang, 2014, "Experimental Validation of Subject-Specific Dynamics Model for Predicting Impact Force in Sideways Fall", *Journal of Biomedical Science and Engineering*, vol. 7, no. 7, pp. 405-418

[4] Yunhua Luo, Masoud Nasiri Sarvi, 2015, "A Subject-Specific Inverse-Dynamics Approach for Estimating Joint Stiffness in Sideways Fall", *International Journal of Experimental and Computational Biomechanics*, vol. 3, no. 2, pp. 137-160

[5] Yunhua Luo, Masoud Nasiri Sarvi, Peidong Sun, William D. Leslie, Jun Ouyang, 2014, "Prediction of Impact Force in Sideways Fall by Image-Based Subject-Specific Dynamics Model", *International Biomechanics*, DOI: 10.1080/23310472.2014.975745

[6] Yunhua Luo, Masoud Nasiri Sarvi, Peidong Sun, Jun Ouyang, 2013, "A Subject-Specific Dynamics Model for Predicting Impact Force in Elderly Lateral Fall", *Applied Mechanics and Materials*, vol. 446-447, pp. 339-343

Conference Papers

[1] Masoud Nasiri Sarvi, Yunua Luo, "Estimation of Body Segment Masses Using Whole Body DXA Image", Canadian Congress of Applied Mechanics, Saskatoon, SK, Canada, CANCAM 2013

[2] Masoud Nasiri Sarvi, Yunhua Luo, "Development of an Image-Based Biomechanical Model for Assessment of Hip Fracture Risk", ASME 2015 International Design Engineering Technical Conference & Computers and Information in Engineering Conference, IDETC/CIE 2015, August 2-5, 2015, Boston, Massachusetts, USA

[3] Masoud Nasiri Sarvi, Yunhua Luo, "A Compound Risk Indicator for Subject-Specific Prediction of Hip Fracture in Sideways Falls", ASME 2015 International Design Engineering Technical Conference & Computers and Information in Engineering Conference, IDETC/CIE 2015, August 2-5, 2015, Boston, Massachusetts, USA